Kaunas University of Technology

Faculty of Mathematics and Natural Sciences

Investigation of Isomeric Derivatives of Triphenylamine and Dibenzothiophen-2-yl(phenyl)methanone with Different Emission Behaviors for Electronic Devices and Optical Sensors of Oxygen

Master's Final Degree Project

Melika Ghasemi

Project author

Dr. Dmytro Volyniuk

Supervisor

Kaunas, 2022

Kaunas University of Technology

Faculty of Mathematics and Natural Sciences

Investigation of Isomeric Derivatives of Triphenylamine and Dibenzothiophen-2-yl(phenyl)methanone with Different Emission Behaviors for Electronic Devices and Optical Sensors of Oxygen

Master's Final Degree Project

Materials Physics (6213CX001)

Melika Ghasemi

Project author

Dr. Dmytro Volyniuk

Supervisor

Prof. Dr. Liutauras Marcinauskas

Reviewer

Kaunas, 2022

Kaunas University of Technology

Faculty of Mathematics and Natural Sciences

Melika Ghasemi

Investigation of Isomeric Derivatives of Triphenylamine and Dibenzothiophen-2-yl(phenyl)methanone with Different Emission Behaviors for Electronic Devices and Optical Sensors of Oxygen

Declaration of Academic Integrity

I confirm the following:

1. I have prepared the final degree project independently and honestly without any violations of the copyrights or other rights of others, following the provisions of the Law on Copyrights and Related Rights of the Republic of Lithuania, the Regulations on the Management and Transfer of Intellectual Property of Kaunas University of Technology (hereinafter – University) and the ethical requirements stipulated by the Code of Academic Ethics of the University;
2. All the data and research results provided in the final degree project are correct and obtained legally; none of the parts of this project are plagiarised from any printed or electronic sources; all the quotations and references provided in the text of the final degree project are indicated in the list of references;
3. I have not paid anyone any monetary funds for the final degree project or the parts thereof unless required by the law;
4. I understand that in the case of any discovery of the fact of dishonesty or violation of any rights of others, the academic penalties will be imposed on me under the procedure applied at the University; I will be expelled from the University and my final degree project can be submitted to the Office of the Ombudsperson for Academic Ethics and Procedures in the examination of a possible violation of academic ethics.

Melika Ghasemi
Confirmed electronically

Ghasemi, Melika. Investigation of Isomeric Derivatives of Triphenylamine and Dibenzothiophen-2-yl(phenyl)methanone with Different Emission Behaviours for Electronic Devices and Optical Sensors of Oxygen. Master's Final Degree Project / supervisor Dr. Dmytro Volyniuk; Faculty of Mathematics and Natural Sciences, Kaunas University of Technology.

Study field and area (study field group): Physics, Physical Sciences

Keywords: Organic light emitting diode; room temperature phosphorescence; thermally activated delayed fluorescence; long persistent luminescence; optical oxygen sensors.

Kaunas, 2022. 67 pages.

Summary

Organic semiconductors showed great potential in many real-life applications including organic light-emitting diodes (OLEDs) and optical sensors. Despite previous achievements for organic semiconductors in the field of organic electronics, there are still no such ideal semiconductors, but scientific community is looking for them. The aim of this work is to discover the potential of isomeric compounds in electronic devices and optical oxygen sensors. Different properties of the compounds were investigated, devices were fabricated, and their performances in potential applications were determined. Competition of room-temperature phosphorescence (RTP) and thermally activated delayed fluorescence (TADF) was investigated on four newly synthesized organic isomeric compounds, **TPA23DBT**, **TPA24DBT**, **TPA26DBT**, and **TPA35DBT**, containing two electron-donating triphenylamine moieties and single electron-accepting dibenzothiophene-2-yl(phenyl)methanone unit by numerous theoretical and experimental approaches. Diversity of the emission origin (RTP or TADF) of the isomeric compounds was caused by different energy gaps (0.09-0.39 eV) between the lowest singlet and triplet states that are locally exited and charge transfer in nature. The effect of the competition of RTP and TADF on the performance of electronic devices and optical sensors of oxygen is demonstrated and discussed. Very different external quantum efficiencies, ranging from 2.8 to 13.9%, were observed for green phosphorescent organic light-emitting diodes which were fabricated using the isomeric compounds as hosts. Such differences in device efficiency were partly related to the different hole mobility values. The hole mobilities of ca. 1×10^{-3} $cm^2V^{-1}s^{-1}$ were observed at electric field of 6.4×10^5 V/cm for the derivatives having triphenylamine moieties at C-2, C-4 (**TPA24DBT**) and at C-3, C-5 (**TPA35DBT**) positions of the central benzene ring**.** Considerably lower hole mobilities of ca. 1×10^{-5} cm^2 V^{-1} s^{-1} were recorded at the same electric field for the compounds with triphenylamine groups at C-2, C-3 (**TPA23DBT**) and at C-2, C-6 (**TPA26DBT**) positions. Depending on the great extent on RTP and TADF processes, different efficiencies of long persistent luminescence (LPL) of the exciplex-forming solid-state mixtures of the isomers and bis[2-(diphenylphosphino)phenyl] ether oxide (DPEPO) were detected. The compound with triphenylamine groups at C-3, C-5 (**TPA35DBT**) positions as RTP emitter and its molecular mixture with DPEPO as LPL emitter for the active layers of optical sensors of oxygen were prepared. They showed the Stern–Volmer constant of 4.55×10^{-4} ppm in the range of oxygen concentrations of up to 10000 ppm.

Ghasemi, Melika. Trifenilamino ir dibenzotiofen-2-il(fenil)metanono izomerinių darinių, turinčių skirtingą emisiją elektroniniams įrenginiams ir optiniams deguonies jutikliams, tyrimas. Magistro studijų baigiamasis projektas / vadovas Dr. Dmytro Volyniuk; Kauno technologijos universitetas, Matematikos ir gamtos mokslų fakultetas.

Studijų kryptis ir sritis (studijų krypčių grupė): Fizika, Fiziniai mokslai

Reikšminiai žodžiai: Organiniai šviesos diodai; fosforescencija kambario temperatūroje; termiškai aktyvuota uždelsta fluorescencija; ilgalaikė liuminescencija; optiniai deguonies jutikliai.

Kaunas, 2022. 67 p.

Santrauka

Organiniai puslaidininkiai parodė didelį potencialą daugelyje praktinių pritaikymų, įskaitant organinius šviesos diodus (OLED) ir optinius jutiklius. Nepaisant ankstesnių pasiekimų organinių puslaidininkių tyrimuose organinės elektronikos srityje, idealių organinių puslaidininkių vis dar nėra, tačiau mokslo bendruomenė siekia juos sukurti. Šio darbo tikslas – nustatyti izomerinių junginių potencialius taikymus elektroniniuose prietaisuose ir optiniuose deguonies jutikliuose. Ištirtos skirtingos junginių savybės, pagaminti prietaisai, nustatyti jų veiksmingumas galimuose panaudojimuose. Kambario temperatūros fosforescencija (RTP) ir termiškai aktyvinta uždelsta fluorescencija (*angl.* TADF) buvo ištirta naudojant keturis naujai susintetintus organinius izomerinius junginius **TPA23DBT**, **TPA24DBT**, **TPA26DBT** ir **TPA35DBT**, turinčius du trifinelamino fragmentus – elektronų donorus ir vieną elektronų akceptorių – dibenzotiofeną-2-yl(fenil)metanoną skirtingais teoriniais ir eksperimentiniais metodais. Izomerinių junginių emisijos kilmės (RTP arba TADF) įvairovę lėmė skirtingi energiniai skirtumai (0,09-0,39 eV) tarp žemiausio singleto ir tripleto būsenų, kurios yra lokaliai sužadinamos ir pernešančios krūvį. Tyrime parodytas ir aptartas RTP ir TADF procesų vienalaikis veikimas elektroniniuose prietaisuose ir optiniuose deguonies jutikliuose. Buvo pastebėtas labai skirtingas išorinis kvantinis efektyvumas, svyruojantis nuo 2,8 iki 13,9%, naudojant žalius fosforescuojančius organinius šviesos diodus, kurie buvo pagaminti naudojant izomerinius junginius kaip pagrindinius. Tokie prietaiso efektyvumo skirtumai iš dalies buvo susiję su skirtingomis skylių mobilumo vertėmis. Bandiniams turintiems trifenilamino fragmentus ties C-2 ir C-4 (**TPA24DBT**) ir ties C-3, C-5 (**TPA35DBT**) padėtimis centriniame benzeno žiede, skylių mobilumas buvo $1 \cdot 10^{-3}$ $cm^3V^{-1}s^{-1}$, kai kai elektrinis laukas $6{,}4 \cdot 10^5$ V/cm. Junginių turinčių trifenilamino grupes ties C-2, C-3 (**TPA23DBT**) ir ties C-2, C-6 (**TPA26DBT**) skylių mobilumas buvo ženkliai mažesnis ir siekė $1 \cdot 10^{-5}$ $cm^3V^{-1}s^{-1}$ esant tokiam pačiam elektriniam laukui. Priklausomai nuo RTP ir TADF procesų, buvo aptiktas skirtingas eksciplekską formuojančių kietojo kūno izomerų mišinių ir bis[2-(difenilfosfino)fenil] eterio oksido (DPEPO) ilgalaikės liuminescencijos (LPL) efektyvumas. Buvo paruoštas junginys su trifenilamino grupėmis C-3, C-5 (**TPA35DBT**) padėtyse kaip RTP emiteris ir jo molekulinis mišinys su DPEPO kaip LPL emiteris, deguonies optinių jutiklių aktyviems sluoksniams. Šie bandiniai pasižymėjo Stern-Volmer konstantos verte - $4{,}55 \cdot 10^{-4}$ ppm deguonies koncentracijos diapazone iki 10 000 ppm.

Table of contents

List of figures

List of tables

List of abbreviations and terms

A – acceptor
ACEL – alternative current electroluminescence
Al – aluminum
Alq_3 – 8-hydroxyquinoline aluminum
cd – candela
CE – current efficiency
CFL – compact fluorescence lamp
CIE – Commission Internationale de l'Eclairage
CT – charge transfer
CTE – charge transfer exciton
CV – cyclic voltammetry
D – donor
DBT – dibenzothiophene-2-yl(phenyl)methanone
DPEPO – Bis[2-(diphenylphosphino)phenyl]ether oxide
DSC – differential scanning calorimetry
EA – electron affinity
EBL – electron blocking layer
EIL – electron injection layer
EL – electroluminescence
ELD – electroluminescent display
EML – emission layer
E_{ox} – oxidation potential
EPA – exciton-polaron annihilation
EPQ – exciton-polaron quenching
EQE – external quantum efficiency
EQM – electric quadrupole moment
E_{red} – reduction potential
ETL – electron transport layer
eV – electron volt
Fc – ferrocene
FL – fluorescence
HBL – hole blocking layer
HIL – hole injection layer
HOMO – highest occupied molecular orbital
HTL – hole transport layer
IC – internal conversion
IP – ionization potential
IQE – internal quantum efficiency
$Ir(ppy)_3$ – tris(2-phenylpyridine)iridium(III)
ISC – intersystem crossing
ITO – indium tin oxide
K_{sv} – Stern-Volmer constant
L – luminescence
LCD – liquid crystal display
LE – luminous efficiency
Li – lithium
LiF – lithium fluoride
lm – lumen
LPL – long persistent luminescent
LUMO – lowest unoccupied molecular orbital
M – Mole
mCBP – 1,3-bis(9-carbazolyl)benzene
ML – mechanoluminescence
MO – molecular orbital
MoO_3 – molybdenum trioxide
n – index of refraction
nm – nanometer
OLED – organic light emitting diode
OLPL – organic long persistence luminescence
PH – phosphorescence
PL – photoluminescence
PLQY – photoluminescence quantum yield
R2R – roll-to-roll
RGB – red, green, blue
RISC – reverse intersystem crossing
rpm – revs per minute
RTP – room temperature phosphorescence
S_0 – singlet ground state
S_1 – singlet excited state
SE – singlet exciton
SiC – silicon carbide
SOC – spin orbital coupling
SPA – singlet-polar annihilation
sr – steradian
SSA – singlet-singlet annihilation
STA – singlet-triplet annihilation
T_1 – triplet excited state
TADF – thermally activated delayed fluorescence
TAPC – Cyclohexylidenebis[N,N-bis(4 methylphenyl)benzenamine]
T_{cr} – crystallization temperature
TD – time decay

$T_{d\text{-}5\%}$ – decomposition temperature
TE – triplet exciton
TFEL – thin film electroluminescent
TFOLED – thin film organic light emitting diode
T_g – glass transition temperature
TGA – thermogravimetric analysis
T_m – melting temperature
TOF – time of flight
TOF – time of flight
TPA – Triphenylamine
TPA – triplet-polaron annihilation
TPBi – 2,2',2''-(1,3,5-benzinetriyl)-tris(1-phenyl-1-H-benzimi-dazole)
TSPO – diphenyl-4-triphenylsilyl-phenylphosphineoxide
TTA – triplet-triplet annihilation
TTA – triplet-triplet annihilation
ttr – transit time
UV – ultraviolet
Vis – visible light
ZnS – zinc sulfide
ZnS:Mn^{2+} – zinc sulfide manganese

.

Introduction

Almost 14 billion years ago after The Big Bang, the first light rays were created followed by stars (light source) where one such star, the Sun, became an important factor for ecosystem in which plants thrive on it and provide food for other living organisms. Since the invention of artificial light and after centuries the discovery of electroluminescence (EL) phenomena scientists have been trying to invent new materials and developing processes to broaden not only our knowledge but also the efficiency of the light sources used in different devices or apparatus. With the development and advancement of technology and material science, different types of light sources are implemented in our everyday life such as television or monitor screen, light bulbs, smart watches, phones, etc. However, some of the light sources such as incandescent, halogen, fluorescence tube, and compact fluorescent lamp (CFL) are inefficient, fragile, short lifespan, and even toxic, hence the invention of light emitting diode (LED) and organic light emitting diode (OLED) [1–6].

Both LED and OLED are semiconductors where, LED is made from inorganic materials, has long service life, very good efficiency, resistance to impact and temperature however, it is rigid and cannot be used in certain applications [7]. On the other hand, OLED is comprised from organic compounds, is light, thin, fast emission response, self-emission, long lifetime, flexible, etc. [2, 8–10]. Nowadays, such technology is advanced enough that it is used in gaming industries, for example, the new virtual reality headset or even the bendable phone where they contain OLED display [10–12].

Even with such great properties, OLED technology needs to overcome some critical challenges. For example, high cost, challenging manufacturing process, susceptibility to water, degradation (black spot phenomenon). Critical problems are, low efficiency, performance, and lifetime of blue OLED compared to red and green device as well as producing white OLEDs [9, 13–18]. All of these issues could be solved by creation of new materials, innovation of different device structure, as well as new manufacturing processes [17].

OLED can be implemented in variety of applications such as electronic devices and optical oxygen sensor. In order for the material to be qualified for such usage they need to meet the necessary requirements. In this work, four newly synthesized compounds were investigated to discover their properties and their potential for such applications.

The aim of this work is to discover the potential of four new isomeric luminophore compounds for electronic devices and optical sensors of oxygen.

The objectives performed to achieve the aim:

1. Investigate isomerization effects on photophysical, electrochemical, thermal, and charge transport properties of the studied compounds.
2. Design, fabricate, and examine organic light emitting devices based on the studied compounds.
3. Develop active probes for optical sensor of oxygen.

1. Literature Review

1.1. Electroluminescence

The origin of artificial light goes back to 500 BC, where after centuries of advancement in technology different light sources were discovered or invented [19]. Light can be produced by two methods: incandescence and luminescence. Incandescence involves the vibration of atoms which is a simple way of producing light by passing an electric current through a filament that has enough resistance to heat up and produce light (continuous spectrum). In this case the higher is the resistance of conductor the brighter is the emitted light [5, 20, 21].

Luminescence is a cold body radiation where the electrons are mainly involved. The emitted light could be in ultra-violet (UV), visible (Vis), or infrared region. In luminescence, based on band theory of solids, after the excitation of luminescent materials or in another word phosphors, the electrons of the materials would get excited to higher energy levels, followed by a decay back to ground state, in which photon/light is emitted where its wavelength is only specific to the material (fingerprint of element) and not the excitation source. The produced spectra is a line spectrum [5, 20–22].

There are different types of luminescence, for example, chemiluminescence where light with a specific wavelength is produced due to chemical reaction that causes the excited radicals go from higher to lower energy levels, photoluminescence in which a photoluminescence material generates light after getting exposed to intense light, mechanoluminescence (ML) where visible light is emitted when ML material is exposed to mechanical stress (friction, tension, and compression), and EL, where it is when EL material is subjected to electric field or current where visible light is emitted without generation of thermal energy, etc. [20, 23–26].

1.1.1. History of Electroluminescence

Captain Henry Joseph Round was the first person to observe electroluminescent phenomena in 1907. By passing a current through silicon carbide (SiC) detector, he witnessed a yellow light. In 1936 Georges Destriau was the person who coined the word “electroluminescent” and discovered that by applying electrical current to zinc sulfide (ZnS) phosphor powder light can be produced. In 1950s the first alternative current EL (ACEL) ceramic lamps were created by GTE Sylvania which contained two conductive surface layers sandwiching light emitting phosphor layer and the dielectric layer. The commercialization of such technology failed due to insufficient lifetime [5, 20, 22, 27–33].

However, by the advancement in science the first thin film EL (TFEL) device (green light emission) was fabricated from powdered ZnS doped with manganese ($ZnS:Mn^{2+}$) a semiconductor by Popkov and Vlasenko in 1960. Such discovery led to interesting combination of crystalline and amorphous materials (properties) and their interfaces to obtain phenomenon such as electrical, optical, optoelectrical, etc. [5, 20, 22, 27–32].

In electroluminescence, luminescent materials or simply phosphors such as a mix of cubic ZnS with lead or copper made into a thin plate capacitor is used to create low level illumination by passing electrical current through it, in which photons are generated from radiative recombination of holes and electrons [5, 21, 22]. In EL light is generated by electrical excitation instead of black body radiation [29]. The TFEL devices were fabricated using methods such as electron beam deposition, atomic layer epitaxy, sputtering deposition, and thermal evaporation on glass or ceramic substrates

[32, 34]. In 1978 and 1985 TFEL became commercially available to be used in monochromatic televisions and computer displays and laptops respectively [32].

A generic term for light emitting devices is EL displays (ELD). There are different types of ELD; TFEL, thick dielectric EL, powder phosphor devices, and LED (inorganic and organic) devices [32]. OLED has become one the main research area in the last decades due to its interesting and promising properties.

1.2. History of Organic Light Emitting Diode

Most EL devices were made from inorganic materials until mid-1920s, where Bernanose and his coworkers witnessed the first organic EL phenomena by applying voltage (400 V) to both sides of a piece of single crystal organic anthracene. In 1963 when the first OLED was invented by Martin Pope and his coworkers from anthracene compound. Since the device had high driving voltage and low quantum efficiency, such organic EL was not researched further. However, in 1987 a breakthrough was made by Stephan Van Slyke and Ching Tang, from Eastman Kodak's R & D group, by fabricating OLED from tris 8-hydroxyquinoline aluminum (Alq_3) and hole transporting aromatic diamine. They managed to create a thin film OLED containing double layers with higher external quantum efficiency (EQE) of 1% and better properties. This discovery triggered a worldwide interest in this technology. By 1990s, the main focus of research was on thin film organic light emitting diode (TFOLED) instead of color EL devices due to advantages of organic materials [21, 26, 29, 33, 35–41]. Since 1990 there have been continuous discoveries and improvements in OLED industry.

In 1990 Burroughs and his coworkers managed to incorporate polymers into EL devices which opened new possibilities and discoveries in OLED fabrication. By using small molecule materials and vacuum evaporation technique, scientists managed to fabricate devices with low concentration of contaminants and better properties such as band gaps and electron affinities. In organics charge transport occurs by hopping between molecules or polymer chains [32].

In 1998 Forrest and Baldo managed to create OLED devices with phosphorescent emitting materials (platinum octaethylporphyrin (PtOEP)) as emitters, where compared to fluorescent guest had higher efficiency since it harvests both singlet and triplet excitons. The first OLED display became commercially available by Tohoku Pioneer Corp. and Pioneer Corp. for an automotive audio system in 1997 and by 2000 they were implemented in mobile phones and other gadgets [4, 32, 33, 41–43]. Since then, many advancements have been made in OLED technology. Current research on OLED mostly focuses on increasing the efficiency and lifetime of the device by creating and incorporating organic materials with different structures and new fabrication techniques [33].

1.3. Organic Materials

Materials can be made from inorganic or organic elements or compounds. Organic materials are part of a massive class of compounds, where they are mainly composed of carbon and other elements, such as hydrogen, oxygen, nitrogen, etc. Organic materials can have small molecules with low molecular weight. However, polymers are made up from long repeated chains of smaller molecules called monomers, as a result they are larger molecules that have higher molecular weight. Homopolymer and copolymer are names given to polymers that are made from a repeated unit of only one type of monomer or different monomers (more than one type) connecting together respectively [33]. Polymers can be naturally occurring, where some examples include silk, hair,

protein, DNA, etc., or they are synthetically made in laboratories or factories, such as nylon, Teflon, epoxy, synthetic drugs, and so on [44]. When the molecule in organic materials have alternating single and double bonds they are considered semi-conducting which are called conjugated hydrocarbons and are used in organic electronics [33].

1.4. Organic Semiconductor

Organic semiconductors are organic materials that have the ability to generate electrons and holes and transport them from one electrode to another one, along with emission of a photon after electrical excitation or light absorption respectively [45]. In another word, organic materials have the properties of a semiconductor which are electrical conductivity of insulators and that of metals [46]. Chemical engineering can be used to change some properties of organic semiconductors which include optical, electrical, and chemical structure in order to have the desired effect/s for specific applications [43].

A carbon (C) atom has four valence electrons, which enable it to form molecular bonds with the same or different elements/atoms. sp^2 -hybridization is responsible for the charge transporting properties in organic molecules. When two organic atoms such as two carbons (C-C) get close to one another, due to their conjugated doubles bonds, one sp^2 -orbital and two p_z -orbitals for each atom are formed. When sp^2 -orbitals of the atoms overlap they form a bond called sigma-bond (σ) on the other hand, when the p_z -orbitals of carbons merge together they form a degenerate π-bond [33, 43]. A molecule of ethene (C_2H_4) is shown in Figure 1 where the carbons are connected through a double bond which is comprised of one sigma and one pi bond. Even though, both bonds are considered covalent bonds the π-bond is weaker than that of the σ-bond [43, 47].

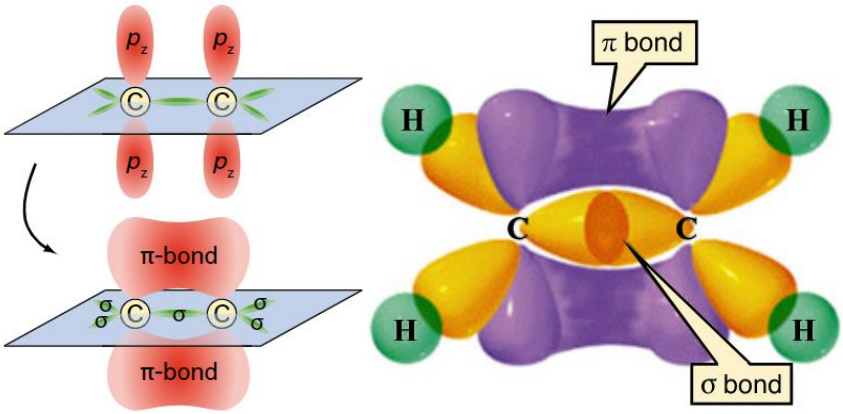

Fig. 1. Diagram of ethene molecule with a double bond composed of pi (π) and sigma (σ) bonds [33, 43]

Unlike metals that have free electrons due to their metallic bond, in organic semiconductors they are shared through a conjugated system where charges travel through the material by hopping between shared electron orbitals [41]. In conjugated double bonded molecules, the electrons are classified into two groups which consist of π and σ electrons. Compared to σ-electrons which are strongly bound to the molecule, the π-electrons are delocalized and mobile where they can easily hop from one molecule to another. Based on this, organic materials that have delocalized π-electrons are highly conductive and have semiconducting properties [32, 45].

Molecular orbital theory (MO theory) uses quantum mechanics (wave function ψ) to describe the behavior of delocalized electrons throughout a molecule which is similar to the distribution of

electrons in atoms [48]. Based on MO theory, semi-continuous bands are bonding (lower energy) at valance bands and anti-bonding (higher energy) at conduction bands [33, 48].

Electrons behave in particular ways. For example, electrons fill lower-energy atomic orbitals before the higher-energy atomic orbitals. The same concept is also true for lower and higher-energy bonding orbitals [48]. An atom contains different energy states, where each one can only be occupied with two electrons in which one electron has spin up and the other spin down. Therefore, only half of the energy states are filled in ground state [43].

Highest occupied molecular orbital (HOMO) is considered as the top of the valence band fully filled with electrons (π-bonding), stable, and promotes bonding. On the other hand, the lowest unoccupied molecular orbital (LUMO) energy level is fully unoccupied with electrons (π*-antibonding) and is considered as the bottom of the conduction band with less stability, and when occupied, electrons do not contribute to bond formation. In such materials delocalized electrons can be excited from HOMO to LUMO orbitals through a process called π- π* transition [32, 48–50]. Based on this, in organic solids the π-system is saturated and instead of forming covalent bonds its molecules are weakly bound by van der Waals forces [43]. Figure 2 shows the diagram of full and empty HOMO and LUMO energy levels of polyene series.

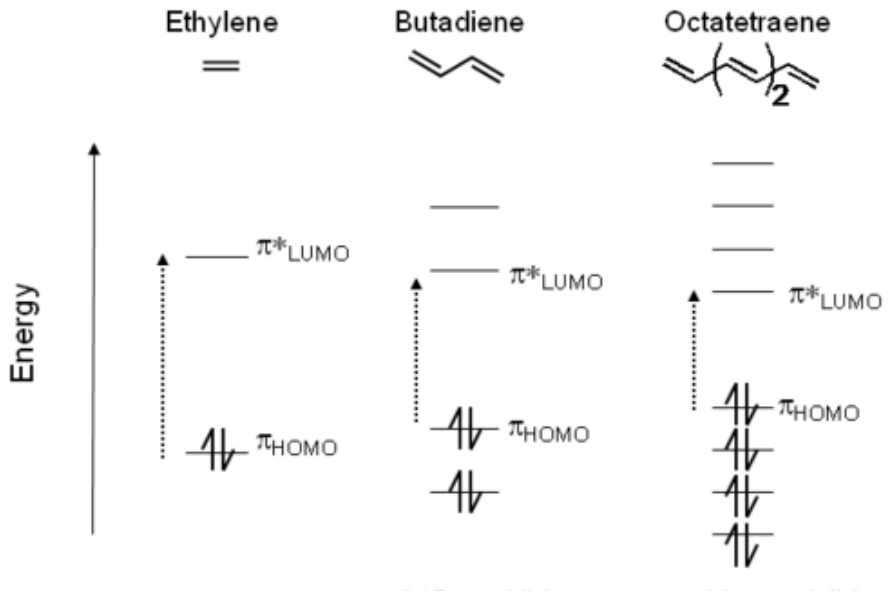

Fig. 2. Diagram of full and empty HOMO and LUMO energy levels of polyene series with decreasing bandgaps [51]

Koopman's theorem states that in a molecular system HOMO energy is equal to ionization potential (IP) and LUMO energy is the electron affinity (EA) (Figure 3). Aside from this, HOMO LUMO orbitals are responsible for the molecule's photo-physical and chemical properties. The HOLO-LUMO energy gap or the band gap, indicated by $\Delta E_g = E_{HOMO} - E_{LUMO}$ (1.5-3.5 eV in most organic materials), depends on the molecule's size where larger one has extended π-system resulting in a smaller gap. As shown in Figure 2, as the molecules in the polyene series increases in size the band gap decreases. It is possible to adjust the gap size by altering the number of aromatic rings or incorporation of other atoms (oxygen, nitrogen, and sulfur). ΔE_g is responsible for optical properties of the molecule such as absorption and emission [33, 43, 49].

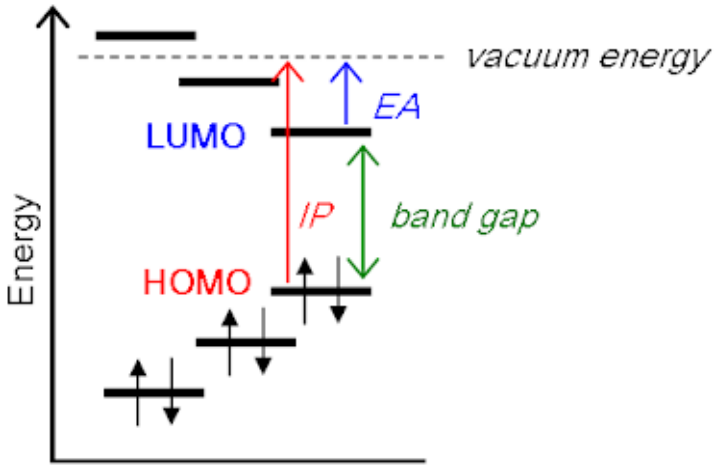

Fig. 3. Schematic representation of HOMO, LUMO, bandgap, electron affinity (EA), and ionization potential (IP) [52]

1.5. Charge Transport

As mentioned before, compared to inorganic semiconductors where the charge transition happens through band transport, in organics delocalized charges move from one molecule to another or between π-conjugation discontinuities by hopping to adjacent energy levels (localized states) (Figure 4). In different materials or even within the same type of substance the energy levels vary based on molecular interactions and disorder. As a result, the energy difference of sites and their distance directly effects the transfer rate of charges. Due to bent or kinked chain in polymers the π-conjugation is disrupted and causes a decrease in charge mobility [33, 53, 54].

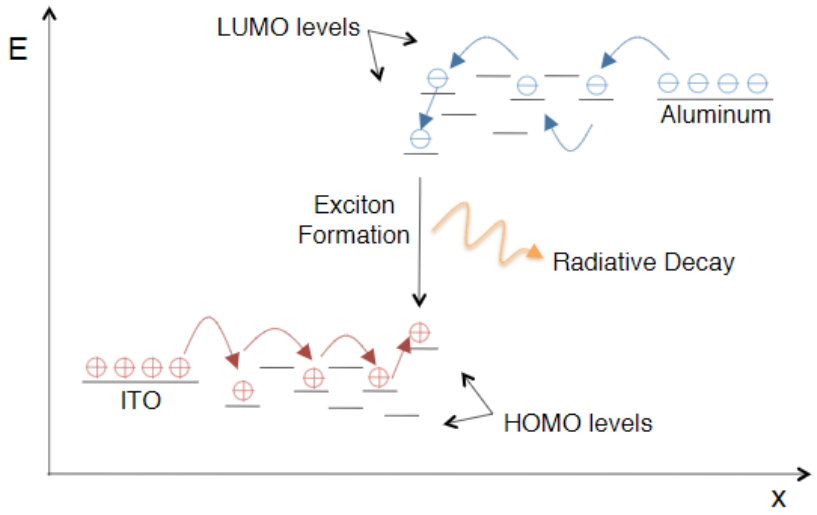

Fig. 4. Diagram of hopping transport in an organic semiconducting device [33]

Since in a device injection with the low current regime limits the charge transport, characteristics and properties of the metal-injection and injection-organic interface greatly influence the charge mobility. Because at the interface the charges can overcome the barrier by hopping over using gap states or tunneling through the barrier [33, 53, 54].

The carriers can hop to higher energy sites only when a photon with an appropriate energy is absorbed. As a result, the probability of moving to a higher energy localized state decreases. And due to localized length the energetic charges can only hop to a site within certain distances. Charge mobility

in specific materials is determined by various methods which include Hall effect, delayed EL, and the method used in this work time-of-flight (TOF) [33, 53].

1.6. Exciton Formation and Recombination

A traveling mobile charge which carries a lattice distortion or phonons with itself is called a polaron. Low energy and stable polarons are formed when electrons and holes are injected into the organic layer. Compared to inorganic crystals that have delocalized phonons, in organic materials phonons are localized vibrations on a molecular or conjugated segment. A bipolaron is formed when two polarons with the same charge are paired and is stabilized by a counter charge of opposite sign [33, 54].

Hole is a positively and electrons is a negatively charged polaron (in an organic molecule) in which when excited electrically or optically (Coulomb-bound pair) an exciton is formed. The nature of the exciton in optoelectronic devices determines the difference between inorganic and organic ones. There are three types of excitons: Frenkel, charge transfer (CT), and Wannier-Mott shown in Figure 5 as (a), (b), and (c) respectively [33, 55].

In organic semiconductors the most common type of exciton is called Frenkel exciton where the electron and hole are localized on a single molecule with high binding energy of $E_b \sim 0.5$ eV and a small radius of < 5 Å (binding energy is inversely proportional to the exciton radius). On the other hand, CT excitons are located on neighboring molecules and have slightly larger and smaller radius and binding energy respectively. Similar to inorganic semiconductors where Wannier-Mott excitons are found, in organic ones such pair form a charge transfer exciton in which the hole and electron are on neighboring molecules and have a large intermolecular distance of r ~ 10 Å (r- effective radius) where they are still able to correlate, along with low binding energy of few meV. Since the relative dielectric constant in organic materials is low (~ 3-5) compared to inorganic semiconductors (> 10), and the exciton binding energies are between 0.1-1 eV they result in the presence of a stable Frenkel state at room temperature [33, 55].

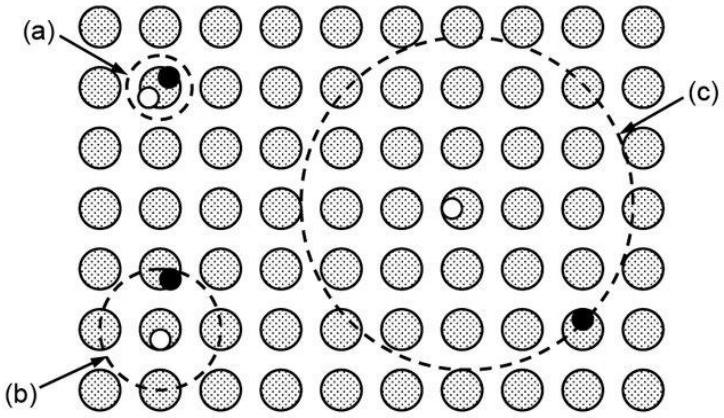

Fig. 5. Schematic representation of the three types of excitons. (a) Frenkel, (b) charge transfer, and (c) Wannier-Mott [55]

As mentioned before, electrons can get excited by absorbing light and move from the HOMO, which is the ground state denoted by S_0, to the LUMO considered an excited state and denoted by S_n. During such excitation the electron spin is preserved and since the transition of excitons to triplet state is forbidden, they end up as singlet exciton (SE) state. In another word, based on quantum mechanics

the probability of occurrence of singlet state with preserved spin is higher than that of the triplets with forbidden spin. In organics the singlet to triplet ratio is $10^9 – 10^{10}$ to [49, 54].

In singlet ground state (S_0) the paired electrons have opposite spin, where after excitation by light (UV or visible light with particular wavelengths) they move to a higher energy state in which if the electrons keep opposite spin (compared to each other), they are called singlet excited state denoted by S_1. However, if the excited electron has the same spin orientation (parallel spin) as the unpaired one in excited state, it is called triplet excited state shown by T_1. Figure 6 shows the spin orientation in ground and excited states [46, 56, 57].

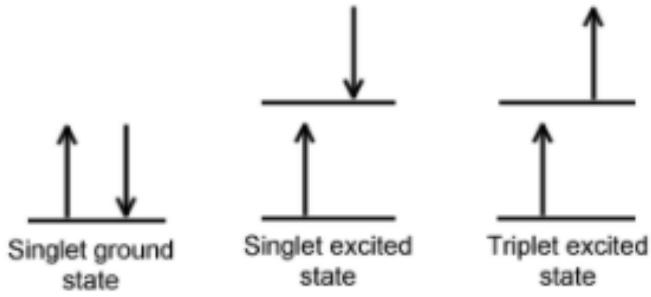

Fig. 6. Spin orientation of the ground state (S_0) and excites singlet (S_1) and triplet (T_1) states [57]

In order to describe S_0, S_1, and T_1 equation of multiplicity is used which is, 2S+1, where S is the total spin angular momentum (sum of all the electron spins). As mentioned before, spins can be spin up (s = +1/2) or spin down (S = -1/2) (Figure 7). Since the electrons in excited singlet state have opposite spins the equation would be, 2 (+1/2 -1/2) +1= 1. And the spin multiplicity for excited triplet state is 2 (+1/2 +1/2) +1= 3 [49, 57].

Overall, in total electrons can have four different spin combinations which are antiparallel spins or opposite spins that results in singlet and three combinations of parallel or same spin where gives triplet. Hence, based on statistics only 25% of the excitons represent singlets and 75% depict triplets [58, 59].

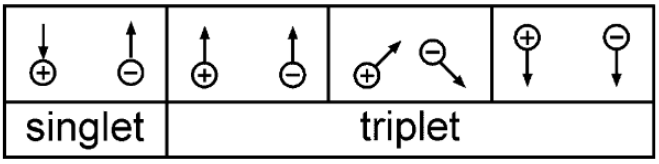

Fig. 7. Schematic representation of spin combinations of one singlet and one triplet state [59]

A molecule in a ground state is different than in excited state, due to the fact that electrons in ground state are diamagnetic and in excited state are paramagnetic. The spin state makes transition from singlet to singlet more probable than singlet to triple (or triplet to singlet). Due to change in electronic state (after singlet to triplet (or reverse)), the lifetime of the triplet is longer by ~ 10^4 seconds fold compared to the singlet state [57].

1.7. Jablonski Diagram

Jablonski diagram (Figure 8) was created by Aleksander Jablonski. In this diagram the thick black horizontal lines indicate the limit of energy state for electrons and each line represents particular

energy state (eigenstate) for a specific molecule. Thin lines represent vibrational state. The value of the energy increases along the vertical axis. Overall, this diagram is used to show the possible excited states along with radiative and non-radiative relaxations. In Figure 8, S_0, S_1, and T_1 represent first singlet ground, singlet excited, and triplet excited state respectively. Internal conversion by IC, intersystem crossing by ISC, and reverse intersystem crossing with RISC. [46, 56, 57].

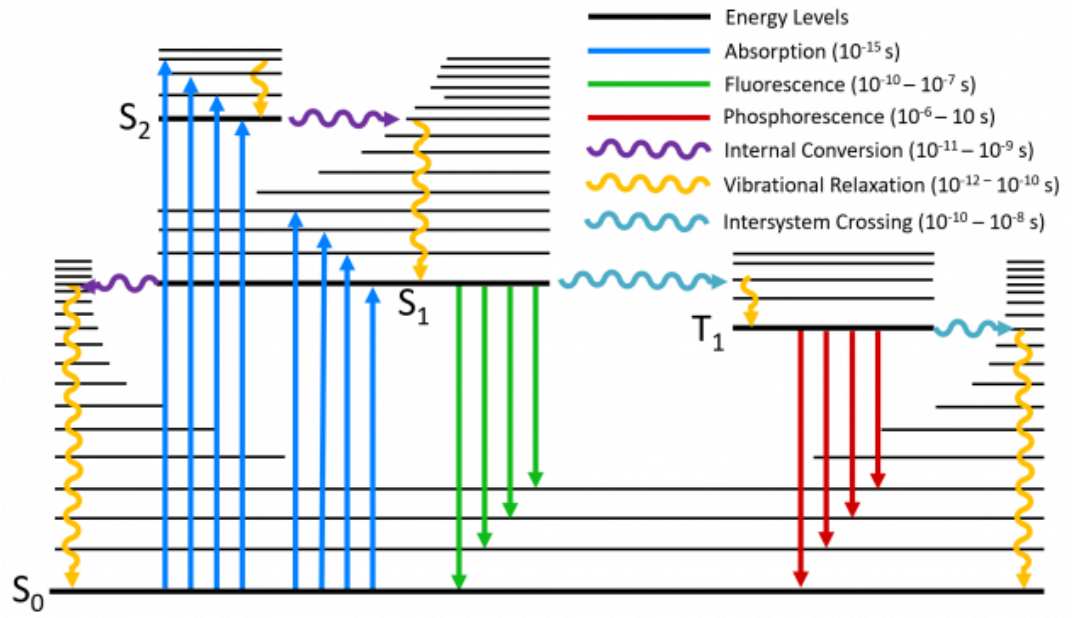

Fig. 8. Schematic representation of Jablonski diagram showing the possible radiative and non-radiative transitions [60]

When a luminescent molecule absorbs a photon its energy is converted to internal energy of the molecule which allows the electron to go from ground state (S_0) to higher vibrational level (Blue arrows) of first or second electronic state (S_1 or S_2) in about 10^{-15} s (fastest transition). Since most molecules are in the lowest vibrational level of ground state at room temperature, in the diagram the absorption starts from S_0 to singlet excited states. Due to conversion of angular momentum a direct transition to triplet energy levels is not possible [41, 60, 61]. In order to reach a stable state, it decays back to the ground state either non-radiatively or radiatively (results in emission of light).

1.7.1. Non-radiative Relaxation

As shown in Jablonski diagram (Figure 8), two types of non-radiative relaxation are possible after photon absorption and excitation. In vibrational relaxation depicted by orange arrow the excited electron is in a non-equilibrium state, in order to reach equilibrium and go back to the lowest vibrational level of the electronic state, the gained excess energy is lost through vibrational mode within the same (intramolecular) or surrounding (intermolecular) molecules. This process takes around 10^{-12} to 10^{-10} s [60].

The other process is internal conversion (IC) shown by purple arrow. In this process the excited electron is located on the higher energy singlet state where through internal conversion and immediately after by vibrational relaxation goes to lower energy singlet state and lowest vibrational level of the electronic state ($S_3 \rightarrow S_2$, $S_2 \rightarrow S_1$, etc.) respectively. Timescale of this process is 10^{-11} to 10^{-9} s [60].

1.7.2. Fluorescence (Radiative relaxation)

Radiative recombination is only possible when interaction between orbital and spin angular momentum is small. The process of photon emission after excitation, which is the result of light and matter interaction, is called photoluminescence [41, 61].

Fluorescence (FL) (green arrow) occurs between two electronic states with the same spin multiplicity. In this process after absorption the excited electron moves from $S_0 \rightarrow S_1$ (Figure 8, 9). In order to reach its stable state, the electron moves from singlet excites state to the singlet ground state ($S_1 \rightarrow S_0$) and releases the energy through emission of a photon which in this case is fluorescence. singlets have spin conserving properties which results in a faster emission of fluorescence [62]. Timescale of this process is 10^{-10} to 10^{-7} s [60]. In this process only singlets are harvested, and the remaining triplets are converted into heat or are absorbed through the material. Since the ratio of singlets to triplets is 1:3 the internal quantum efficiency (IQE) of fluorescence is only 25%.

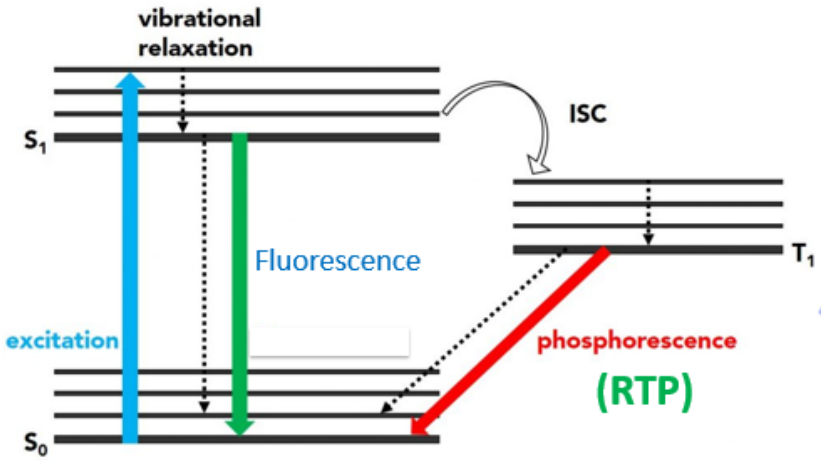

Fig. 9. Schematic representation of fluorescence and room temperature phosphorescence (RTP through Intersystem crossing (ISC)) emission [63]

1.7.3. Phosphorescence

Transition from singlet to triplet excited state is forbidden (quantum physics) due to conversion of spin angular momentum. However, the spin orbit coupling (SOC) between the spin and orbital angular momentum allows the electron to make such transition ($S_1 \rightarrow T_1$) through a process called intersystem crossing (ISC) (Figure 8, 9). Rate of ISC can increase by incorporating heavy atoms (carbonyl or sulfone groups) which increases SOC strength. When the electron moves from $T_1 \rightarrow S_0$ the energy is released via a photon known as phosphorescence (PH) shown with red arrow [60]. Unlike singlet that has a spin conserving transitions which results in FL emission, the triplet induces a slower process for PH emission because it does not conserve spin [62]. The timescale value is in the 10^{-6} to 10 s range [60]. The long lifetime of PH heavy metals (microsecond scale) can cause domination of triplet-triplet annihilation (TTA) which can cause long range of exciton diffusion to quench in neighboring layers of materials in OLED [64].

In this case, singlets (25%) are converted to triplets (75%) where both are harvested. As a result, the IQE of this process is 100%. Even though maximum IQE is obtained, due to high cost, poor stability, and toxicity of noble metals, PH is not desirable [64–66].

Due to toxicity and growing costs of heavy metals (Iridium (III), Platinum (II), and Osmium (II)) in PH materials, scientists developed materials that are free of any heavy metals, have long lived (triplet-active) emission, and can be used in technologies such as OLEDs and optical sensors [67, 68].

Room temperature phosphorescence (RTP), as the name suggests, is a PH process that occurs at room temperature and does not require very cold temperature (77K) to be present and emit light. It is rare to see RTP properties in organic materials. Organic emitters which exhibit RTP properties can compete with and are better than conventional noble metals-based PH emitters that are commonly used as indicators (luminescent probes) of optical oxygen sensors [61]. RTP is influenced by oxygen quenching, molecular vibration and packing, along with intermolecular interactions. To obtain an efficient and ultralong RTP, smallest ΔE_{ST} (ISC) and $\pi\,\pi^*$ configuration (ultralong phosphorescence) of T_1 is required [66].

1.7.4. Thermally Activated Delayed Fluorescence

In thermally activated delayed fluorescence (TADF) the electrons go back from the lowest triplet state to the lowest singlet excited state ($T_1 \rightarrow S_1$) through a process called reverse intersystem crossing (RISC) as shown in Figure 10. For relaxation the electron transition from $S_1 \rightarrow S_0$ and releases a delayed fluorescence with a long emission. In order for the RISC to occur the molecule must have enough thermal energy to overcome the ΔE_{ST} [60, 64].

In order to have an efficient RISC a small ΔE_{ST}, charge transfer (CT) character, and a very small HOMO-LUMO overlap is required. To obtain such characteristics the configuration of the implemented compounds can be donor-acceptor or donor-acceptor-donor.

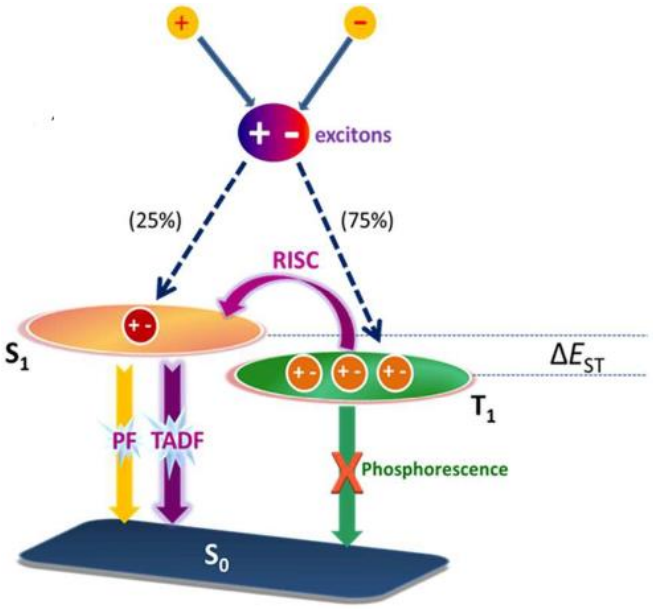

Fig. 10. Schematic representation of thermally activated delayed fluorescence (TADF) mechanism [64]

Due to toxicity and growing costs of rare-earth metals in PH materials, scientists developed materials that are free of any heavy metals, have long lived (triplet-active) emission, and can be used in technologies such as OLEDs and optical sensors [67, 69].

In OLED when electrons and holes react and combine with each other they give rise to S_1 and T_1 excitons with 1:3 ratio. In order to have a fluorescent OLED with high efficiency, both singlets and triplets need to be harvested (100% exciton utilization). Such phenomenon is possible by using materials with TADF properties. For such results, triplets are converted to singlets through RISC process in which upon relaxation, photon is emitted. In theory, through such mechanism device efficiency of up to 100% is reached [70].

By carefully designing the organic molecules it is possible to get small singlet-triplet band gap (ΔE_{ST}) which enhances RISC process (overcome non-radiative decay pathway) and leads to a more efficient TADF material with radiative decay rate of $> 10^6$ 1/s . Intermolecular charge transfer in a system that contains spatially separated donor and acceptor moieties enable this process [71].

The long delay in a TADF system is the result of triplet excitons that have undergone many ISC processes. In these type of materials tightly packed molecules can cause quenching of the excitons due to strong intermolecular collisions in which, molecule capsulation can reduce such effect and result in a long decay curve [72].

In the past few years many discoveries and innovations have been made by scientists with regards to OLEDs. By using phosphorescent (PH) or TADF emitters, the internal and external quantum efficiency of OLED has increased to 100% and 62.5% respectively (theoretically) since both singlets and triplets are harvested [66, 73].

Based on the latest research done by Ren Sheng and his colleagues, it is possible to obtain external quantum efficiency (EQE) of 20.4%, which shows low efficiency roll-off (18.7% at 1000 cd/m^2), by using TADF materials as sensitizer in OLED devices (ultrathin orange emissive layer) in order to induce a double RISC process, improve the performance of the device, and achieve color stability [74].

1.7.5. Long Persistent Luminescence

When some materials absorb light (UV or visible light) they get excited and through relaxation they release the energy (as a photon) quickly like FL or slowly such as PH. Long persistent luminescence (LPL) is another mechanism with slow emissions (long afterglow) where in the dark the emitted light from the excited material can last for several seconds, minutes, or even days [75, 76].

Most efficient LPL materials are rare-earth based metals. However, in order for this process to takes place and achieve long loved charge separated state in an organic LPL (OLPL), the structure of the compound needs to be donor-acceptor or donor-acceptor-donor [76].

The emission of organic LPL contains multiple processes as shown in Figure 11. In the first step (i) the electron (black circle) gets excited by absorbing a photon (photo-excited) and move to higher energy state (HOMO to LUMO) in the acceptor which results in a hole. In the next step (ii) an electron from the HOMO of the donor is transferred to the HOMO of the acceptor (charge transfer). Meanwhile, the excited electron moves through the energy levels of the acceptor without any emission of light (charge separation). In the 4rth step (iv) the excited electron from the acceptor would move back to the HOMO level of the donor where the electron and a hole are recombined (charge recombination) and result in emission of a photon (exciplex emission (v)). By using light to make

ionized states and charge-separated state, which are photo-induced, a very long lifetime can be achieved in LPL [76].

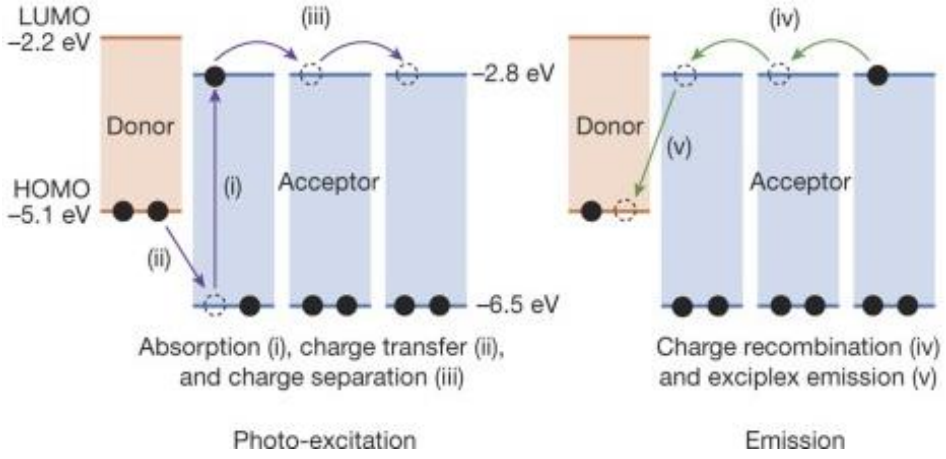

Fig. 11. Schematic diagram of the Emission mechanism of long persistent luminescence [76]

1.8. Organic Light Emitting Diode

In the last few years, the performance of organic semiconductor devices has improved to the point of being a replacement option for conventional ones. As a result of this they have been implemented in areas such as thin film transistors (TFTs), flexible photo diodes, solar cell, memory devices, and organic light emitting diodes [46, 77]. Compared to inorganic LEDs, OLEDs are not impacted as much by the ambient temperature which results in cooler temperature and safe to the touch while operating [78].

OLED is an innate surface emitting light source, where unlike liquid crystal display (LCDs) does not require backlight nor chemical shutters and has been the main focus of research in artificial lighting due to its interesting and attractive properties. For example, they have high efficiency, good brightness and response time, very flexible, can be made in larger sizes, wide view angle, light emission of entire visible spectra, etc. In addition, it is possible to use glass, plastic, metal, or ceramic substrate and fabricate the devices by depositing or printing the organic materials on them [6, 26, 37, 38, 42, 43, 79–82].

In glass substrate the fabricated device is protected by a glass lid or a deposited metal layer however, even though the plastic substrate enables us to have a lighter and thinner OLED device, it still requires a protective layer (thin passivation film) from moisture and oxygen since OLED has high sensitivity to both [6, 41, 42, 83].

OLEDs are semiconductor light sources. There is n-type semiconductor which has excess electrons and as a result is negatively charged. On the other hand, the p-type has electron deficiency where instead contains holes which makes it positively charged after DC is applied. At the p-n junction the electrons and holes combine with one another which results in emission of photons. OLEDs are good light sources in general lighting application, because they can operate at a very low voltage (3-5V) [21].

Compared to incandescent lamps which turn around 90% of the energy into heat, fluorescent converts 70% of the energy into light, with the luminous efficiency of 13-20 lm/W and 90 lm/W respectively.

In order to use the energy resources properly and reduce the efficiency loss, researchers have been focusing on inventing and improving the novel organic semiconductors [38].

In the past few decades, the solid-state light technology of OLED has become one of the main research topics due to its potential of becoming more energy efficient light source [43, 84]. Photophysical properties of organic compounds are the most important features in OLED since its usefulness and application depends on them. For example, π-electrons of the compound is responsible for light generation determine its optical and electrical properties based on its small HOMO-LUMO energy gap [84].

1.8.1. Generations of Organic Light Emitting Diode

OLED is classified into three different generations: 1st, 2nd, and 3rd OLED generations (Figure 12). In the 1st generation the implemented organic materials were pure which made the exciton transition from triplet state to singlet ground state ($T_1 \rightarrow S_0$) forbidden (based on quantum mechanics). As a result, only singlet excited state to singlet ground state ($S_1 \rightarrow S_0$) are possible which comprised of only 25% of the excitons. Hence 75% (belong to T_1) are wasted through heat and non-radiative transitions. 1st generation of OLED has 25% maximum internal efficiency. 1st generation produces fluorescence and is suitable for producing blue colored pixels (consumes too much energy and has low efficiency so far) [85].

In 2nd generation of OLED, instead pure organic compounds heavy metals were incorporated with the material. Due to this, the spin orbital coupling (SOC) of the molecules increases and enabled the transition of $T_1 \rightarrow S_0$ where the process is $S_0 \rightarrow S_1 \rightarrow T_1 \rightarrow S_0$ through ISC. Since singlet is converted to triplet, both of them are harvested which makes the OLED to have internal efficiency of 100%. 2nd generation produces phosphorescence where red and green pixels are obtained from it. It is recommended to not use heavy metals since they are expensive and most importantly toxic [85]. Phosphorescence can lead to quenching problems.

In order to have internal quantum efficiency of 100% without the heavy metals, 3rd generation of OLED was invented. The material has TADF properties and can be used to produce stable blue pixels. In this process the triplets are converted to singlets ($S_0 \rightarrow T_1 \rightarrow S_1 \rightarrow S_0$) and both are harvested hence, the 100% efficiency [85]. Another possible method for obtaining delayed fluorescence is triplet-triplet-annihilation (TTA) which will be explain in detail in upcoming chapter. In short, two triplet excitons collide, one gain the energy and the other loses it and returns back to ground state. in this process maximum internal quantum efficiency is 62.5% (25% (singlet) +1/2*75% (triplet state)) [49].

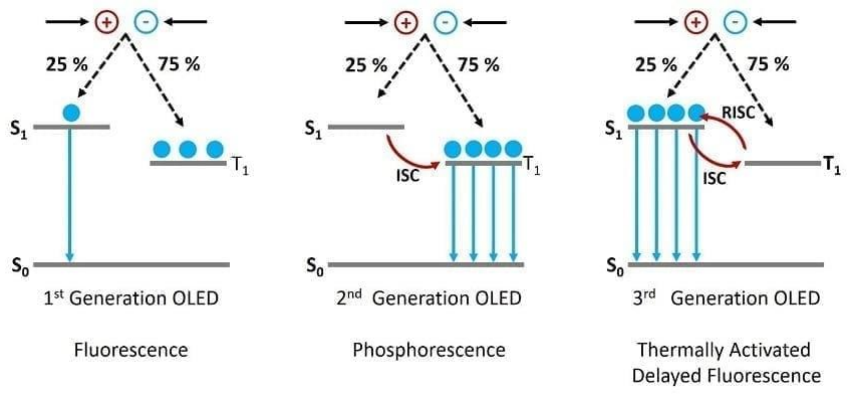

Fig. 12. Operating principle of 1st, 2nd, and 3rd generation of OLEDs [85]

1.9. Device Fabrication

Current OLED device fabrication processes, on a lab scale, include vacuum sputtering, spin coating, and the most efficient methods, such as solution processing (wet processes), and thermal evaporation in high vacuum. The mentioned methods are not readily applicable for low-cost manufacturing. Some suggested methods for a cost effective OLED device fabrication are roll-to-roll printing techniques [82, 86].

1.9.1. Spin Coating

Compared to other techniques, solution technique is low cost and enables production of large areas. It is considered one of the easiest ways to deposit different layers of materials in a solution from. However, this method has its own problems and limitations. For example, it is not suitable for mass production due to material waste, the solubility of organic materials for different layers in similar solvents makes it difficult to fabricate a multilayered device since the sequential layer can dissolve the previous ones. Also, in this technique parameters such as rotation speed, applied temperature, concentration of the solution, and types of solvents makes it challenging to control the morphology of each layer. Spin coating is used for fabrication of thin films (micrometer to nanometer) that do not require fine patterning. This technique makes it possible to create uniform layers on flat surfaces [41, 87–90].

The first step in this process is to place a clean substrate on the holder, which can be held by a suction mechanism (Figure 13). In the next step, a prepared solution is dispensed carefully onto the center of the substrate, which then is rotated by turning on the spinning mechanism. The high spinning speed (1000-3000 rpm (revs per minute)) creates centrifugal force which distributes the solution (outward) on the substrate, dries the remaining solution, and results in a very thin and uniform layer [87–90]. It is also possible to dry the layer/s by soft baking at low temperature (~100°C) to rid the films of residual solvent [33, 90]. This method was used in this work for fabrication of thin films.

The thickness of the deposited layer can be change based on the viscosity of the solution, the higher is the viscosity of the solution the thicker is the deposited layer and vice versa. It is the same for the speed of the rotation, the higher is the speed of the rotation the thinner is the thickness of the final layer and vice versa [33, 88–90]. For example, to obtain a film with a thickness of 1.5-1 µm, the rotational speed needs to be between 2000-6000 rpm which is rotated for about 30-60 s [90].

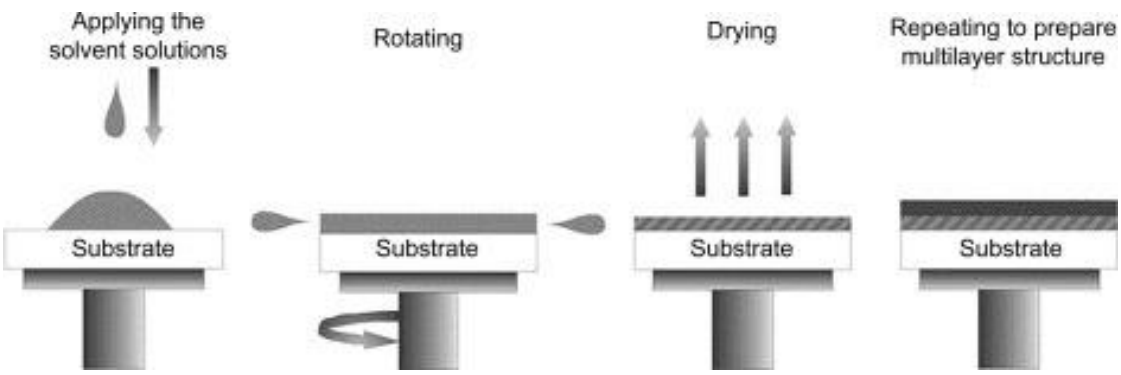

Fig. 13. Schematic diagram of spin coating diagram [89]

1.9.2. Thermal Vacuum Evaporation

One the most popular and low risk methods for a homogeneous OLED fabrication (film), both in research and mass production, is thermal vacuum evaporation. Even though compared to alternative processes this method is elaborated and expensive, it enables the construction of a very precise, complex, and multilayered device structure with higher efficiency [41].

At first, cleaned glass or plastic substrates are placed in holder positioned above the heating coil. In the next step (Figure 14), organic material for each layer is placed separately in a quartz crucible in which the crucible is then placed on top of the tungsten coil. On the other hand, the inorganic or metals are placed directly on the tungsten wire basket. The vacuum chamber (inert atmosphere glove box (nitrogen or argon)) is vacuumed until the pressure reaches 10^{-6} to 10^{-7} mbar. The tungsten coil heats the organic materials to the point of their sublimation (solid to gas phase). Due to the lower temperature of the substrate, upon contact, the deposited material transforms from gas phase to solid phase. In order to control the thickness of the deposited layer shutters are used on top of the crucibles, the temperature is controlled, and the distance between the source and the substrate is several cm. For the deposition shutters are opened and the substrate holder rotates to ensure and even deposited layer. Rate of deposition is controlled by a quartz crystal resonator monitor [33, 87].

Even though such process produces multilayer OLED devices with good efficiency, polymers cannot be used as deposited materials since at high temperatures they chemically degrade. Only materials with small molecules can be evaporated. Another limitation is that it is not possible to use this method for large scale production due to the fact that, it will be expensive, requires large vacuum chamber, and the deposited layers might not be evenly distributed [33, 41]. In this work this method was used for device fabrication.

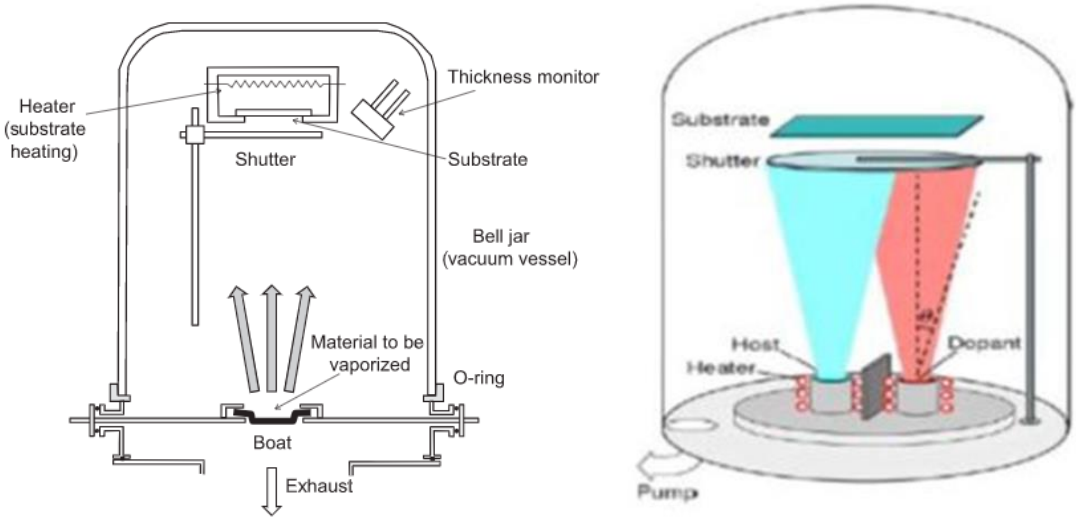

Fig. 14. Schematic representation of vacuum thermal evaporation [17, 91]

1.10. Principle of Operation

OLED devices are made from multiple layers. The simplest OLED was made from one or more organic thin film layers sandwiched between two electrodes an anode and a cathode. On the other hand, the new OLED devices could have 3 to 8 layers based on their applications with a thickness of few 100 nm. In such structure at least one of the electrodes needs to be transparent, for example, indium tin oxide (ITO) is the most frequently used transparent anode (substrate) in device fabrication due to its high work function (~4.8 eV), low sheet resistance of around 20 Ω/sq, wide bandgap, easy patterning, and stable chemical properties which are important factors for device performance (charge injection) [43, 78, 80, 92–94]. The work function of the anode must be compatible with the HOMO energy of the organic material (emissive compound) in order to have ohmic contact [41]. On the other hand, the other electrode, or in another word, the cathode is made from metals that have low work function such as Ca, Mg, Li, or most frequently Aluminum (Al) because of its high oxygen resistance and environmentally more stable structure [38, 94–96]. The work function of Al is between 4.0-4.28 eV, it is reported that when in contact with lithium fluoride (LiF) its work function decreases to 3.4 eV which results in a lower onset voltage and an increase in efficiency of the device [81, 97, 98]. Overall, substrates must have high tolerance to coating solvents, low oxygen and water permeability, as well as good thermal and scratch resistance [82].

In some cases the work function of ITO and cathode layer could be low or high respectively for energy levels of some organic compounds used in the emission layer (EML) where the energy difference makes the carrier transport from both electrodes to the EML difficult therefore, limits the hole and electron injection at their interface, increases operating voltage, and decreases the efficiency of the OLED device [41, 81, 93, 94]. In organic materials there is a possibility for the electrons to get trapped by impurities with higher electronegativity, such as oxygen or aldehyde-like chains, which can reduce the electron mobility and shift the exciton recombination towards the cathode and cause quenching of the luminescence [32].

In order to improve or overcome such problems multiple layers of organic thin film is used. Such layers include, hole injection layer (HIL), hole transport layer (HTL), electron blocking layer (EBL), hole blocking layer (HBL), electron transport layer (ETL), electron injection layer (EIL), along with a very thin layer (1 nm) of lithium fluoride (LiF) (as injection barrier at organic and metal/cathode interface) which are sandwiched between two inorganic electrodes, anode as hole injector and cathode as electron injector [93–95]. A standard multilayered OLED device is shown in Figure 15.

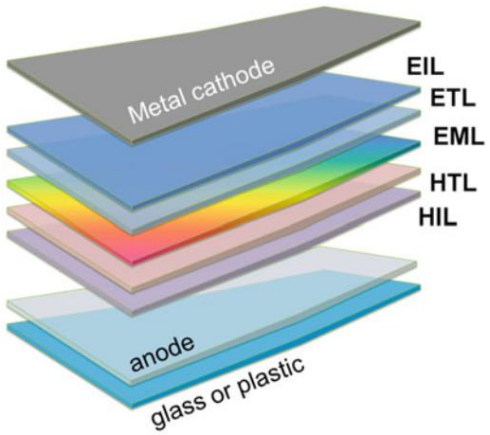

Fig. 15. Schematic representation of multilayered OLED device [41]

The role of HIL and EIL, as their name suggests, is to enhance and improve the injection of holes and electrons from the anode and cathode to the EML by choosing a suitable HOMO and LUMO energy levels in relation to the emissive compounds respectively in order to guarantee an ohmic contact with the electrodes [41, 81]. In this word MoO_3 (molybdenum trioxide) was used as HIL and TPBi (2,2',2''-(1,3,5-benzinetriyl)-tris(1-phenyl-1-H-benzimi-dazole)) was used as EIL in relation to the energy levels of other layers.

The next layers are HTL and ETL where these layers help with the injection and transportation of holes and electrons from ITO and the metal cathode through the device respectively [39, 94]. In this work TAPC (4,4′-Cyclohexylidenebis[N,N-bis(4 methylphenyl)benzenamine]) and TPBi (2,2',2''-(1,3,5-benzinetriyl)-tris(1-phenyl-1-H-benzimi-dazole)) were used as HTL and ETL respectively based on their properties and compatibility with the other layers in the device.

The results of studies done by other scientists suggests that, by including the blocking layers in OLED devices not only the energy barrier between the TL and EML decreases, and the carriers are confined in the emissive layer (higher recombination), but it also improves the overall color purity and quantum efficiency of the devices. In order to achieve such results, the HBL is required to have low HOMO level and/or low hole mobility. On the other hand, EBL needs to have high LUMO and/or low electron mobility [39, 81, 94, 99]. In this work mCBP (1,3-bis(9-carbazolyl)benzene) and TSPO1 (diphenyl-4-triphenylsilyl-phenylphosphineoxide) were used as EBL and HBL respectively.

The EML is located in the center of the device and can be comprised from pure organic compound (non-doped). However, in order to avoid concentration quenching and at the same time increase the emission efficiency of the EML, the organic compounds are doped with very low concentration of dopants (<10%) in which they act as guest and host (in our study respectively) or vice versa. Dopants are chosen based on their HOMO and LUMO levels, carrier mobility, and triplet levels in relation to the organic compounds. A desirable OLED emitter has a high thermal and oxidative stability, good film forming properties, suitable HOMO and LUMO energy levels for easier hole and electron injection [39, 41, 81, 82, 94, 100]. In this work $Ir(ppy)_3$ (tris(2-phenylpyridine)iridium(III)) was used as a dopant (host) in device fabrication. Example of other dopants include DPEPO (Bis[2-(diphenylphosphino)phenyl]ether oxide) and ZEONEX. Organic chemistry makes it possible to create emissive compounds with specific structures and properties in order to obtain desired colors [82, 100].

As mentioned before each layer has a specific roll/function in the device which results in the emission of light. The energy diagram and working principle of a multilayered OLED device is shown in Figure 16. The height of each box represents the HOMO and LUMO of each layer (material) which are chosen based on their relation to other materials' energy levels. From anode and cathode layers holes (white circles) and electrons (black circles) are injected through HIL and EIL respectively indicated by step (a). In the second step (b) holes and electrons are transported by HTL and ETL respectively. EBL and HBL are implemented in the device in order to block electrons and holes from entering other layers and contain them in EML indicated by (c). The last step (d) is electrons and holes (excitons) recombination in EML followed by the emission of a photon in which its wavelength is directly related to the type of relaxation [41, 96].

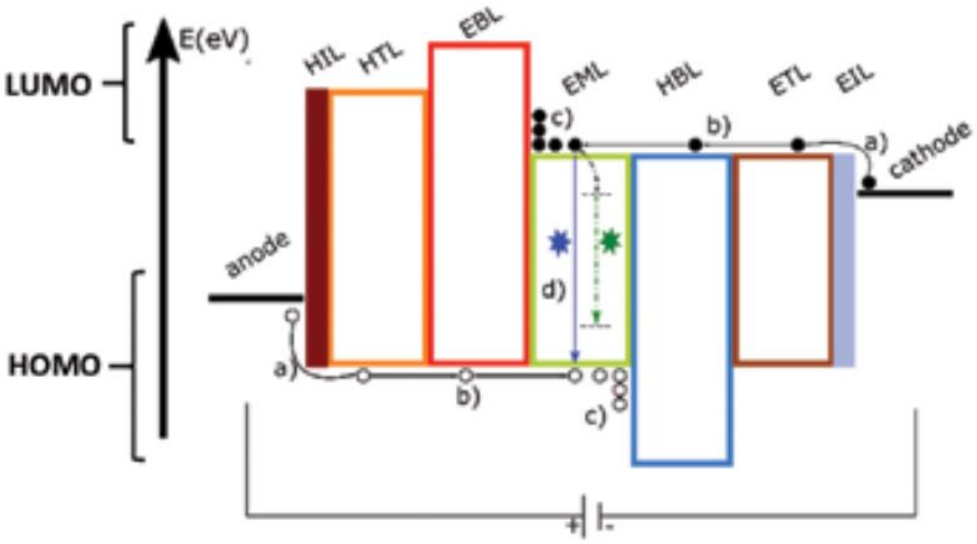

Fig. 16. Energy diagram and working principle of a typical multilayer OLED [96]

Based on the organic material and its potential application a careful design strategy is required since it can significantly affect the properties of the device such as efficiency, generation of heat, emission wavelength, lifetime, etc. [78, 96]. Some requirements need to be met regarding the materials used in OLED fabrication:

- Chosen materials need to be morphologically stable and form a uniform vacuum-sublimed films;
- Based on the function of each layer in the device they were chosen to align ideally, with respect to one another, by considering their HOMO-LUMO energy levels;
- To avoid exciton quenching effects the triplet energy of the layers should be analyzed;
- The thickness of each layer should be adjusted in order for the carrier mobility of the layers to be suitable for a good charge carrier [94].

1.11. Device Efficiency

The efficiency of an OLED device is characterized by quantum, power, and luminous efficiency. The quantum efficiency of a device consists of internal quantum efficiency (IQE), external quantum efficiency (EQE), luminous efficiency (LE), etc. [38, 82].

1.11.1. Internal Quantum Efficiency

Internal quantum efficiency is the total number of photons which are generated from each pair of electron-hole that are injected inside of the device. Most of the generated photons are trapped and absorbed inside the device. IQE is represented by η_{int} in which for fluorescent materials it is obtained from the following Equation (1):

$$\eta_{int} = \gamma\, \eta_s \phi_f, \tag{1}$$

where γ is the charge balance factor in which ideally is equal to 1 (equal amount of holes and electrons injected), η_s is the singlet exciton efficiency (fraction of singlet excitons), and $\phi_f$is quantum efficiency of fluorescent (fraction of energy released as light by the material or in another word ratio

of number of emitted photons to number of optically absorbed photons which is ideally close to 1) [38, 41, 82].

As mentioned before for fluorescent the maximum value of IQE used to be 25% where only singlets were excited, relaxed, and harvested as photons. On the other hand, OLEDs that contain phosphorescence emitters harvest both singlets through ISC and triplets which result in IQE of near 100% [82]. Some fundamental phenomena such as exciton-exciton quenching, polaron-exciton quenching, and exciton dissociation can reduce internal quantum efficiency for both FL and PH [62, 82].

The exciton-exciton quenching or in another word, triplet-triplet annihilation (TTA) is a mechanism (related to dexter energy transfer) where, the energy is transferred from one molecule to another while in their triplet state. In this process the excited molecule transfers its energy and returns to grown state while the other excited molecule goes to higher energy states (singlet, triplet, or quintet) [101].

1.11.2. External Quantum Efficiency

External quantum efficiency is the total number of emitted photons from the device per electron-hole pair injected into the device. EQE is denoted by η_{ext} and is related to IQE as shown in Equation (2):

$$\eta_{ext} = \eta_{OUT}\, \eta_{int}, \tag{2}$$

where η_{OUT} is the number of emitted photons from the device per number of generated photons inside the OLED also known as outcoupling or extraction efficiency. Because of the way OLED device is designed, only a small fraction of generated photons can escape the device into the air. The outcoupling efficiency of a device can be obtained from the following simplified Equation (3):

$$\eta_{OUT} = \frac{1}{2n^2} \tag{3}$$

where *n* is the index of refraction of each matter. For example, if theoretically IQE of a device is 100% and the substrate is glass where its index of refraction is equal to *n*=1.5, the value of η_{OUT} is only around 20% which means only 1/5 of the generated photons get to escape to the outside. In a simple planar OLED device (Figure 17) 80% of photons are lost because of light reflection (internal reflection) at the layer interfaces, due to different refractive indices, and getting absorbed by the device. It is possible to improve outcoupling efficiency by reducing the thickness of the external scattering layer, adding surface texture, adding one or array of lenses, using substrates with low *n* value [38, 41, 82].

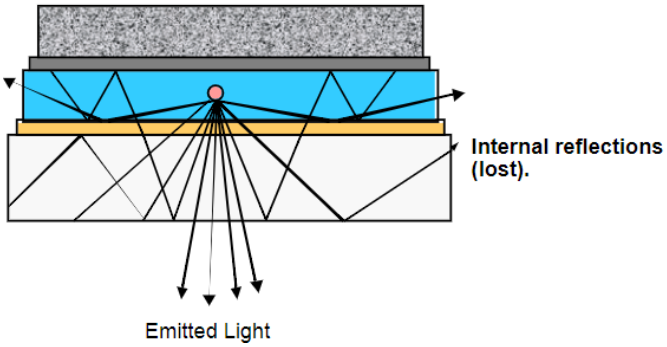

Fig. 17. Schematic representation of photon loss in a device due to internal reflections [82]

1.11.3. Luminous Efficiency

Luminous efficiency (LE) is a measure of brightness in relation to sensitivity of the human eye (standardized model) which is denoted by η_p and can also be described as the ratio of lumen output per input electrical watts of the device. LE is measured in candela per ampere (*cd/A*). Power efficiency (PE) is the total photometric power emitted in all directions from a light source. PE is described as the luminous flux per unit power of the device which is measured in lumen per watt (*lm/W*). [21, 38, 41, 82]. Candela (cd) is a unit of luminous intensity and Lumen (lm) is a unit of luminous flux [41, 82]. "Luminous efficiency function or luminosity function is the visual efficiency of detecting lights of different wavelengths" [21]. Luminous flux/power (lm) is the perceived power of light which is different from the radiant flux since it is the total power of emitted light [21].

1.11.4. Luminous Efficacy

Luminous efficacy is denoted by η_v and it is described as the ratio of the lumen output to the optical watts (radiative power), or in another word it is a measure of brightness in relation to the sensitivity of the human eyes. Both luminous efficiency and efficacy indicate the sensitivity of the human eye to certain spectra. For example, if two OLED devices have similar quantum efficiencies they can have different spectra of emitted light which affects the luminous property of the device [21, 82].

Both luminous efficiency and luminous efficacy are related to one another which is described by the following Equation (4):

$$\eta_p = \eta_\gamma\left(\frac{P_{in}}{\phi}\right) \tag{4}$$

where P_{in} is input (watts) and ϕ is lumen output [82].

1.11.5. Luminous Intensity

Luminous intensity of a point source is the amount of emitted visible light in unit of time per unit solid angle, which should not be confused with the total emitted light by an object. Lumen is the unit used for describing the quantity of light generated and discharged from a source in any one second. It is highly dependent on visual sensation (perceived by the human eyes). Human eye has high sensitivity to light with wavelength of 555 nm (green/yellow), to which there is 685 lumens per watt of radiant power/flux (luminous efficiency). Standard candle or candela (cd), which is one lumen per

steradian (1 cd = 1 lm/sr), is the given SI base unit for luminous intensity (monochromatic radiation) [21, 78, 102].

1.12. Challenges In Organic Light Emitting Diode Technology

1.12.1. Efficiency Roll-off

Due to recent demands for OLEDs that have high brightness, the efficiency roll-off has become a major problem in this field, because by increasing the brightness of the device the efficiency decreases due to quenching [41]. A related parameter is current efficiency (CE) which is the ratio of photometric measure luminance (L) to the applied current (j) as shown in Equation (5):

$$CE = \frac{L}{j} \tag{5}$$

It is suggested that this problem is caused by various annihilation processes, such as singlet-triplet annihilation (STA), singlet-polaron annihilation (SPA), triplet-polaron annihilation (TPA), and loss of charge carrier balance [43, 73, 74, 81, 103].

Figure 18 provides a summary of all the quenching processes using illustrated lines where electrons, holes, as well as triplet and singlet excitons are shown by e^-, h^+, T, and S respectively. Empty and full circles indicate the destruction and creation of particles respectively. processes that can quench or in another word quench singlets include, SPA, singlet-singlet annihilation (SSA), or STA. On the other hand, triples are quenched by TPA or triplet-triplet annihilation (TTA). Heat or applied electric field can cause the excitons to dissociate. Generated photons move out of the stacked layers [43]. In the following section couple of such quenching processes are explain.

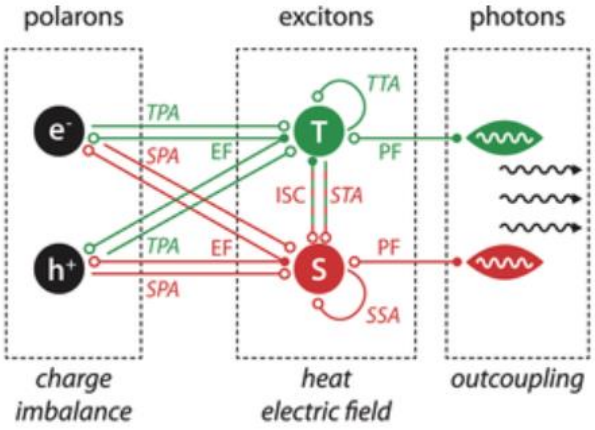

Fig. 18. Schematic illustration of quenching processes causing efficiency roll-off in OLEDs [43]

The exciton-exciton quenching, such as triplet-triplet annihilation (TTA) is a mechanism (related to dexter energy transfer) where, the energy is transferred from one molecule to another while in their triplet state. In this process the excited molecule transfers its energy and returns to ground state while the other excited molecule goes to higher energy states (singlet, triplet, or quintet) [101]. Total amount of triplets converting to singlets through multiple TTA processes is 15% which would increase the efficiency of the device [43, 94]. In an OLED device TTA and TPA quenching processes are considered to be a severe energy leakage pathway [72].

Annihilation process can also happen between two excited singlets (SSA) however, the spin is conserved during the process which indicates that no triples are formed. In STA the excited singlet state (from donor) transfers its energy to the first excited triplet (in acceptor), which then leaves the acceptor with higher energy level. The singlet-polar annihilation occurs when the concentration of trapped charge is higher than that of free charge [43].

Exciton-polaron quenching (EPQ), also known as exciton-polaron annihilation (EPA) in OLED devices with high exciton densities are the cause of IQE loss. In this process in order for the exciton in a donor to go back to ground state transfers its energy to the acceptor's polaron, which can have positive or negative charge. After such exchange, the acceptor molecule would promptly loose its excess energy through vibrational relaxation processes [43, 103].

It is known that the intermolecular interaction depends on the intermolecular distance due to the fact that the molecular force is inversely proportional to intermolecular distance. Based upon this rule, one way to reduce quenching effect is to increase the distance between the molecule by using steric bulky unit. In a non-doped OLED device, such effect in PH and TADF material can be reduced by molecular encapsulation [72].
OLED technology has been developing throughout years of research for different applications in various fields. For example, in medical field it can be used as light sources such as photodynamic therapy, organic lasers, and biosensors for environment and clinical monitoring like oxygen sensor [40, 43].

1.13. Organic Sensor

Nowadays, sensors are implemented in almost every electronic device such as TVs, smartphones and watches, and even cars. A sensor is an interface which converts physical process or signal into usable data [104]. Even though, majority of sensors are made from inorganic materials, sensors which contain organic material, especially pure organic phosphorescent (RTP), have been the main focus of research in the past few years. Because compared to inorganic sensors they can be deposited at room temperature, on a flexible substrate, larger areas, is inexpensive, noninvasive, etc, [61, 69, 105]. "The technical criteria that characterize a sensor are generally its measurement range, sensitivity, resolution, accuracy, reproducibility, fidelity, linearity, response time, bandwidth, hysteresis and functional temperature range" [104].

Since oxygen is essential for life it is by far considered one of the most important chemicals on earth. One of very important application areas of RTP materials (usually mixed with a donor) is oxygen sensing which is used in various fields such as biotechnology, chemistry, environmental and marine analysis, medicine, and food packaging [69]. Radiative decay occurs on comparable timescale to dynamic quenching which is influenced by oxygen (O_2) diffusion rate in a material. In order for the material to be used as "turn on" sensors, it needs to have weak/negligible FL and strong PH so it can emit light in an anaerobic or a low oxygen environment [67]. In this work, organic materials with RTP properties are examined for potential application in optical oxygen sensor.

All in all, compared to the existing inorganic light sources, organic luminophores are much more promising due to their valuable properties such as flexibility, good lifetime, color purity, good efficiency etc. Even with such characteristics, OLED technology still requires further research and discovery to improve or even eliminate its limitations like efficiency roll-off for applications in optoelectronic devices and optical sensors. Therefore, In this work, four newly synthesized isomeric luminophores **TPA23DBT**, **TPA24DBT**, **TPA26DBT**, and **TPA35DBT** containing triphenylamine moieties as and dibenzothiophene-2-yl(phenyl)methanone with a potential of having TADF and RTP properties were selected as emitters for electronic OLED devices and/or optical sensors. To do so, Photophysical, electrochemical, thermal, and charge transport properties of the compounds were characterized in different solvents, along with polymers (dopants), and under different conditions and forms (film or solid). Electroluminescent properties of fabricated devices using the compounds as emitters for OLED were investigated. Possible use of compounds in optical oxygen sensor was also explored.

2. Materials and Experimental Methods

2.1. Materials

In this work four organic luminophore compounds, containing triphenylamine and dibenzothiophen-2-yl(phenyl)methanone fragments, were investigated (Figure 19b). The compounds were synthesized by Dr. Dalius Gudeika in Department of Polymer Chemistry and Technology at Kaunas University of Technology [106]. Given name and the IUPAC name of the four materials are as following:

- **TPA23DBT** (4,4"-bis(diphenylamino)-[1,1':2',1"-terphenyl]-3'-yl)(dibenzo[b,d]thiophen-2-yl)methanone,
- **TPA24DBT** (4,4"-bis(diphenylamino)-[1,1':3',1"-terphenyl]-4'-yl)(dibenzo[b,d]thiophen-2-yl)methanone,
- **TPA26DBT** (4,4"-bis(diphenylamino)-[1,1':3',1"-terphenyl]-2'-yl)(dibenzo[b,d]thiophen-2-yl)methanone,
- **TPA35DBT** (4,4"-bis(diphenylamino)-[1,1':4',1"-terphenyl]-2'-yl)(dibenzo[b,d]thiophen-2-yl)methanone.

The chemical structure and synthesis process of the samples are shown in Figure 19.

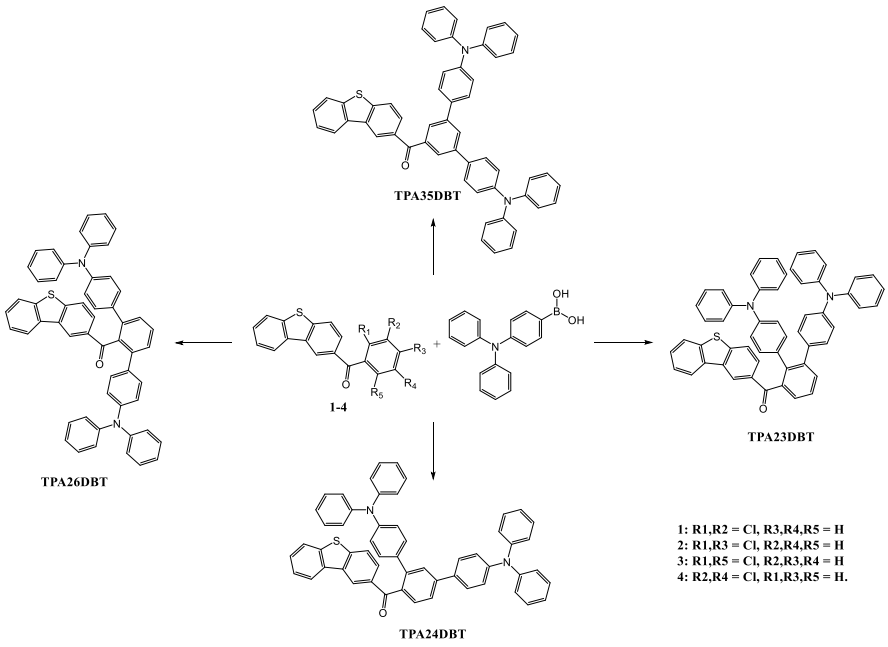

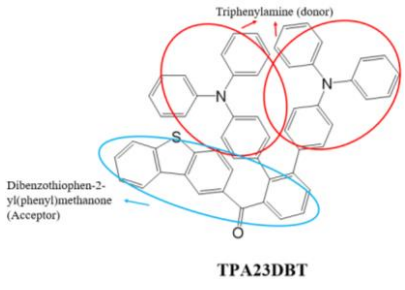

Fig. 19. Schematic representation of synthesis process for the isomeric compounds (a) and positions of triphenylamine and dibenzothiophen-2-yl(phenyl)methanone fragments (b) [107]

The following information is provided by Dr. Dalius Gudeika [106]. Schematic representation of synthesis process for all four isomers, **TPA23DBT**, **TPA24DBT**, **TPA26DBT**, and **TPA35DBT**, are shown in Figure 19a. Friedel-Crafts Alkylation reactions [108] of dibenzo[b,d]thiophene with 2,3-dichlorobenzoyl chloride, 2,4-dichlorobenzoyl chloride, 2,6-dichlorobenzoyl chloride or 3,5-dichlorobenzoyl chloride gave the intermediate compounds 1-4 respectively. The next step Suzuki-Miyaura cross-coupling reactions [109] of 4-(diphenylamino)phenylboronic acid with dichloro derivatives of dibenzo[b,d]thiophene compounds 1-4 catalyzed by Pd(OAc)2/XPhos in dimethylformamide gave the target derivatives. For indebt explanation of synthesis process please refer to the reference [107].

Materials used in device fabrications, molybdenum trioxide (MoO_3), 4,4′-cyclohexylidenebis[N,N-bis(4 methylphenyl)benzenamine] (TAPC), 1,3-bis(9-carbazolyl)benzene (mCBP), diphenyl-4-triphenylsilyl-phenylphosphineoxide (TSPO1), 2,2’,2’’-(1,3,5-benzinetriyl)-tris(1-phenyl-1-H-benzimi-dazole) (TPBi), and tris(2-phenylpyridine)iridium(III) ($Ir(ppy)_3$) were purchased from *Sigma Aldrich* or *Lumtec* and were used as received [110]. The chemical structures of the compounds are along with their HOMO and LUMO energy levels are depicted in Figure 20 and Table 1.

Table 1. HOMO and LUMO energy levels of organic compounds used in device fabrication

Materials	HOMO (eV)	LUMO (eV)	Reference
MoO_3	5.4	2.3	[1]
TAPC	5.5	2.0	[111]
mCBP	6.0	2.4	[112]
$Ir(ppy)_3$	5.6	3.0	[113]
TSPO	6.7	2.5	[114]
TPBi	6.2	2.7	[115]

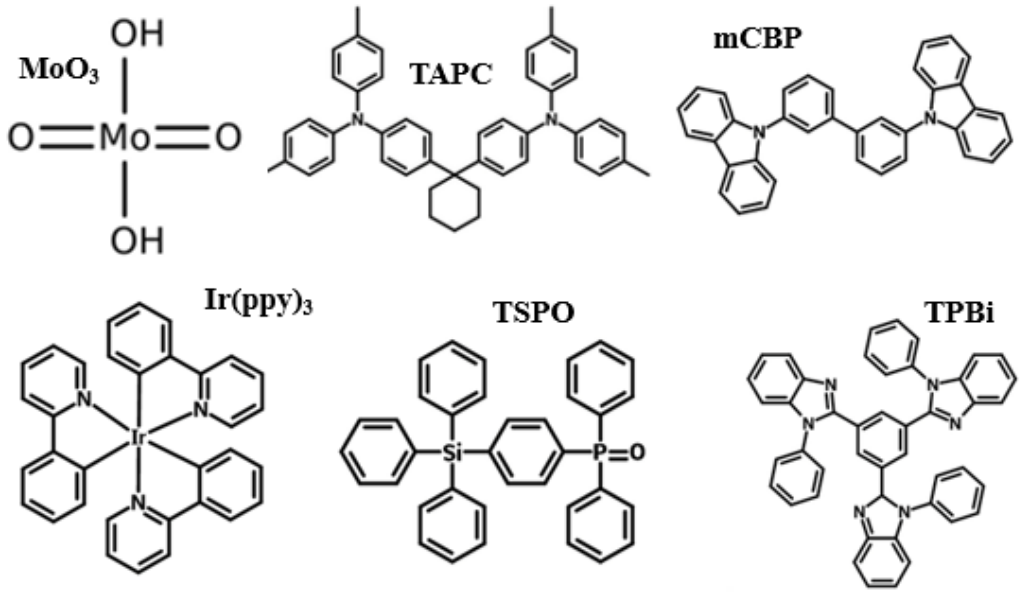

Fig. 20. Chemical structure of organic compounds used in device fabrication [111–116]

2.2. Experimental Methods

In this section applied methods and used apparatus for investigation of the compounds under different conditions are discussed.

2.2.1. Absorption

Absorption spectra of the compounds were recorded using *Avantes Avalight-DHc* UV-Vis spectrometer (Figure 21). Dilute solutions (toluene or THF) containing 10^{-4}-10^{-5} M of compounds were measured using standard quartz cuvettes. Thin film samples were prepared from a solution on a glass/quartz substrate by spin coating, under normal atmosphere and at room temperature.

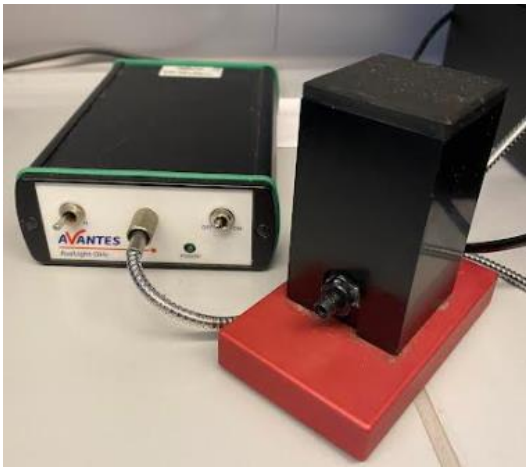

Fig. 21. *Avantes Avalight-DHc* UV-Vis spectrometer

2.2.2. Photoluminescence Spectra, Decay Curve, Quantum Yield

Photoluminescence (emission) spectra of the compounds were recorded using *Edinburgh Instruments FLS980 Fluorescence Spectrometer* (Figure 22), where samples were excited by xenon lamp at wavelength of 350 nm. Dilute solutions containing 10^{-4}-10^{-5} M of compounds were measured using standard quartz cuvettes. Thin film samples were prepared from a solution or solids (compounds) on a glass/quartz substrate by spin coating or drop casting in air, as well as melt casting in vacuum respectively. Photoluminescence decay curves were measured by exciting sample with a *PicoQuant LDH-D-C-375* diode laser (excitation wavelength of 374 nm), coupled to *FLS980* using time-correlated single photon counting technique. The photoluminescence spectra and decay curves of toluene, THF solutions (air, degassed, oxygenated), and solid films (air, vacuum) of the compounds were recorded at room temperature under different conditions. To distinguish the photoluminescence spectra and phosphorescence spectra a diluted solution of samples in THF at 77K were used during the measurement. PLQY of the solid and solution samples were measured by using integrated sphere accessory to *Edinburgh Instruments FLS980* spectrometer [49, 110, 117].

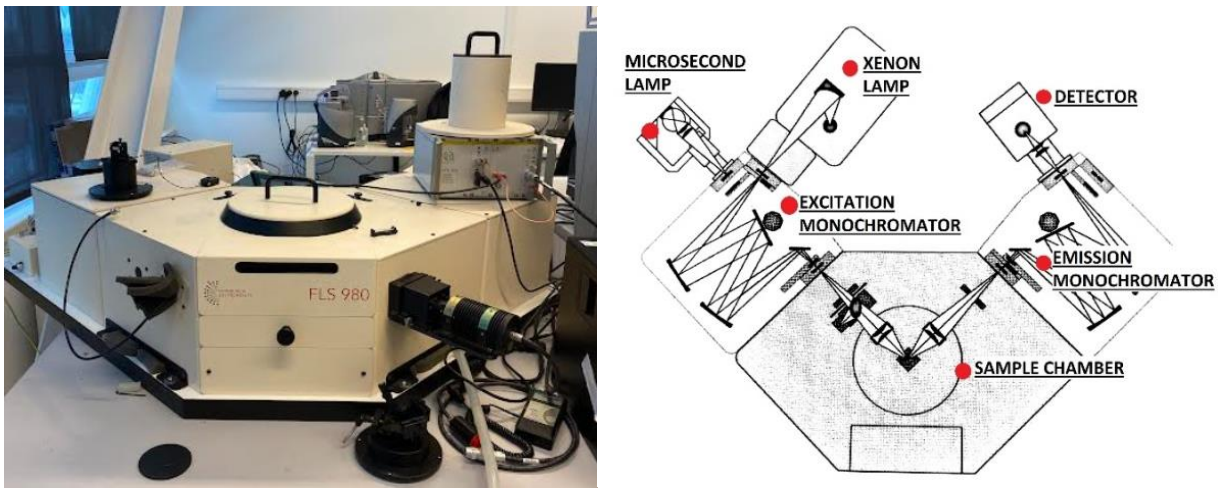

a) b)

Fig. 22. *Edinburgh Instruments FLS980* photoluminescence spectrometer (a) scheme of spectrometer (based on user's manual of *FLS980*) (b)

2.2.3. Cyclic Voltammetry

Electrochemical properties of the solutions of the compounds were studied by cyclic voltammetry (CV) using a *μ-Autolab III* (Metrohm Autolab) potentiostat-galvanostat equipped with a standard three-electrode configuration. A three-electrode cell equipped with a glassy carbon working electrode, an Ag/Ag^+ (0.01 M in anhydrous DMF) reference electrode, and a Platinum wire counter electrode was used. CV measurements were performed with 0.1 M of tetrabutylammonium hexafluorophosphate as the supporting electrolyte under nitrogen atmosphere at a scan rate of 0.1 V/s at room temperature. The measurements were calibrated using ferrocene/ferrocenium (Fc) system as an internal reference. Ionization potential (I_p^{CV}) was estimated from the onset oxidation potential using the following relationship (Equation (6)):

$$I_p^{CV} = 4.8 + E_{ox} \text{ vs. Fc}, \quad (6)$$

where E_{ox} vs. Fc is the onset first oxidation potential versus the Fc reference [99, 110].

2.2.4. Ionization Potential of Solid State

Ionization potentials (I_P^{PE}) of solid samples were estimated by electron photoemission spectrometry in air. Samples were vacuum deposited (2×10^{-6} mbar) onto fluorine doped tin oxide (FTO) coated glass slides (substrates) using *Kurt J. Lesker* vacuum equipment in glove box. Exploiting setup consists of deep UV deuterium lamp (*ASBN-D130-CM*) as light source, monochromator (*CM110 1/8m*), and electrometer (*6517B Keithley*). Photoelectron emission spectra was recorded exciting the samples from low energy to high energy with the step of 1 nm and recording electron photoemission current at different excitation energies. The values of I_P^{PE} are obtained from the intersection of x-axis and the low energy linear part of measured photoelectron emission spectra.

The following Equation (7) is used to estimate the electron affinities (E_A^{PE}) of thin films:

$$E_A^{PE} = I_p^{PE} - E_g, \quad (7)$$

where E_g is the optical band gap, obtained from onset of lowest energy absorption band (Tauc relation, [118]) [99, 110].

2.2.5. Thermal Properties

Thermal properties of the compounds were characterized by differential scanning calorimetry (DSC) measurements performed with *Perkin Elmer DSC 8500* equipment at heating and cooling rates of 10°C/min under nitrogen atmosphere. Thermogravimetric analysis (TGA) was performed using *Perkin Elmer TGA 4000* apparatus at a heating rate of 20°C/min under nitrogen atmosphere. Melting points were measured by MEL-TEMP (Electrothermal) melting point apparatus (Figure 23) [15].

a) b)

Fig. 23. DSC and (a) TGA apparatus (b)

2.2.6. Charge Mobility Measurement

For hole and electron mobilities of vacuum-deposited layers of ITO/ compounds /Al, time of flight (TOF) method was used. The TOF setup contains a laser (*EKSPLA NL300*, 355 nm wavelength) used for excitation. For electron and hole transport in deposited layers at different electric fields, variety of negative and positive external voltages (U) were applied. *TDS 3032C* oscilloscope (*Tektronix*) was used to record the photocurrent transients of holes or electrons [99, 110].

2.2.7. Device Fabrication

Vacuum processed OLEDs were fabricated using *Kurt J. Lesker* vacuum equipment, which is mounted in *MB EcoVap4G* glove box with an inert atmosphere of nitrogen (Figure 24a, b). electroluminescent devices were fabricated by deposition organic and metal layers onto a pre-cleaned indium tin oxide (ITO) coated glass substrate under vacuum (2×10^{-6} mbar). ITO coated glass substrates with a sheet resistance of 15 Ω/sq were pre-patterned for getting four independent devices with area of 6 mm^2 [99, 110].

a) b)

Fig. 24. *MB EcoVap4G* glove box containing (a) *Kurt J. Lesker* vacuum deposition chamber (b)

2.2.8. Device Characterization

Density-voltage and luminance-voltage characteristics were recorded using photodiode *PH100-Si-HA-D0* together with PC-based power and energy Monitor *11S-LINK* and *Keithley 2400C* source meter. Electroluminescence (EL) spectra were recorded by *Avantes AvaSpec-2048XL* spectrometer. The efficiency of the devices was calculated using all the data from luminance, current density, and EL spectra in MATLAB program [99, 110].

3. Results and Discussion

In this work RTP and TADF properties of four newly synthesized organic isomeric compounds (**TPA23DBT**, **TPA24DBT**, **TPA26DBT**, and **TPA35DBT**) having a donor-acceptor-donor structure containing two electron-donating triphenylamine (TPA) moieties as donors and single electron-accepting dibenzothiophene-2-yl(phenyl)methanone (DBT) unit as acceptor were studied on their own and in a polymeric host by numerous theoretical and experimental approaches. Emitters were investigated by photophysical (steady-state and time-resolved spectroscopy), thermal (DSC and TGA), electrochemical (cyclic voltammetry) and photoelectrical (electron photoemission spectroscopy) methods. The obtained results were used to develop OLED devices and study their potential as electronic devices and optical sensors.

3.1. Photophysical Properties

The effect of the molecular structure of isomers **TPA23DBT**, **TPA24DBT**, **TPA26DBT**, and **TPA35DBT** on their photophysical properties were studied by recording absorption and steady-state photoluminescence (PL) spectra of their dilute solutions in toluene and THF as well as of neat films (Figure 25a, b). Comparison of the absorption spectra of compounds in solutions and as neat films, revealed only slight differences that could be caused by aggregation effects. It is known that the electron-accepting unit dibenzothiophene is characterized by the low-energy absorption band at ca. 275-295 nm ($\pi \rightarrow \pi^*$) [119]. The TPA-based compounds are typically characterized by the 2-fold shape of absorption spectra with bands peaking at ca. 300 nm and ca. 360 nm [120].

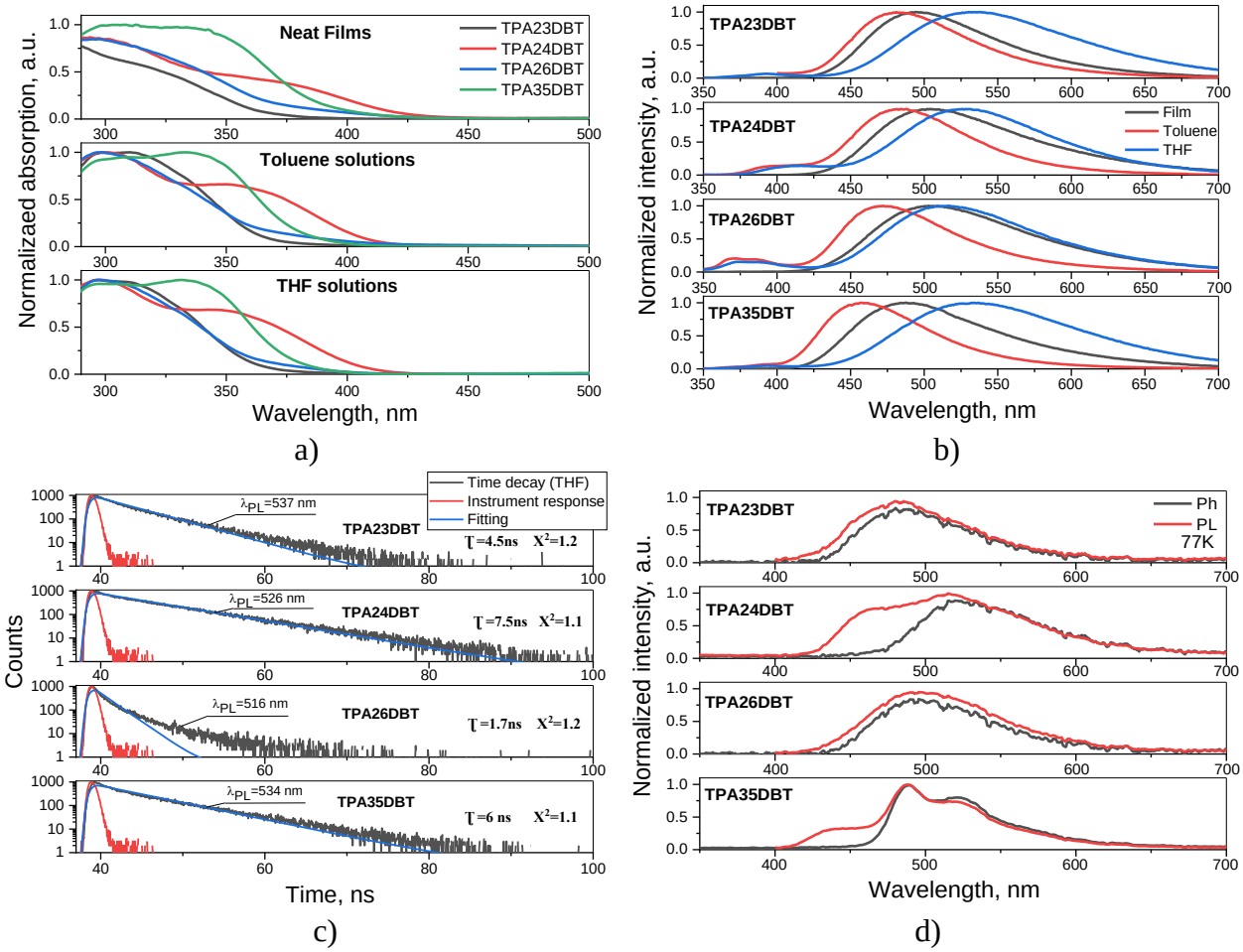

Fig. 25. Absorption (a) and PL (b) spectra of toluene, THF solutions and neat films of the compounds. PL decay curves of toluene solutions (c). PL and phosphorescence spectra of THF solutions recorded at 77K (d). Phosphorescence spectra were recorded using delay of 1 ms after excitation

It is evident that absorption spectra of **TPA23DBT**, **TPA24DBT**, **TPA26DBT**, and **TPA35DBT** are mainly characterized by bands attributable to TPA segments at wavelengths higher than 300 nm. The low-energy absorption bands of **TPA24DBT** and **TPA35DBT** are red-shifted compared to the bands of **TPA23DBT** and **TPA26DBT** (Figure 25a, Table 2). The tails of the absorption spectrum of the film of **TPA24DBT** have reach even 430 nm. This observation can be explained either by a more extended π–conjugation systems of **TPA24DBT** and **TPA35DBT** than those of **TPA23DBT** and **TPA26DBT** or by strong intramolecular charge transfer (CT) transitions between the involved donor and acceptor moieties.

The contribution of intramolecular CT of **TPA23DBT**, **TPA24DBT**, **TPA26DBT**, and **TPA35DBT** is also evidenced by the red-shifted PL spectra of the solutions of the compounds in a more polar solvent THF compared to that of their solutions in a less polar one toluene (Figure 25b). Relaxation of intramolecular CT states of the studied isomers in toluene solutions resulted in blue fluorescence with the spectra peaked in the range from 457 to 484 nm and the fluorescence lifetimes of 1.7 to 6 ns (Figure 25c). The intensity of fluorescence is practically not sensitive to oxygen excluding triplet harvesting processes in solutions (Figure 26a, b). In contrast, the triplet harvesting processes via TADF or RTP were detected for the compounds in solid-state. They are discussed below. High-energy emission bands were observed for toluene and THF solutions of **TPA23DBT**, **TPA24DBT**, **TPA26DBT**, and **TPA35DBT** indicating the contribution of relaxation of locally excited (LE) and mixed states.

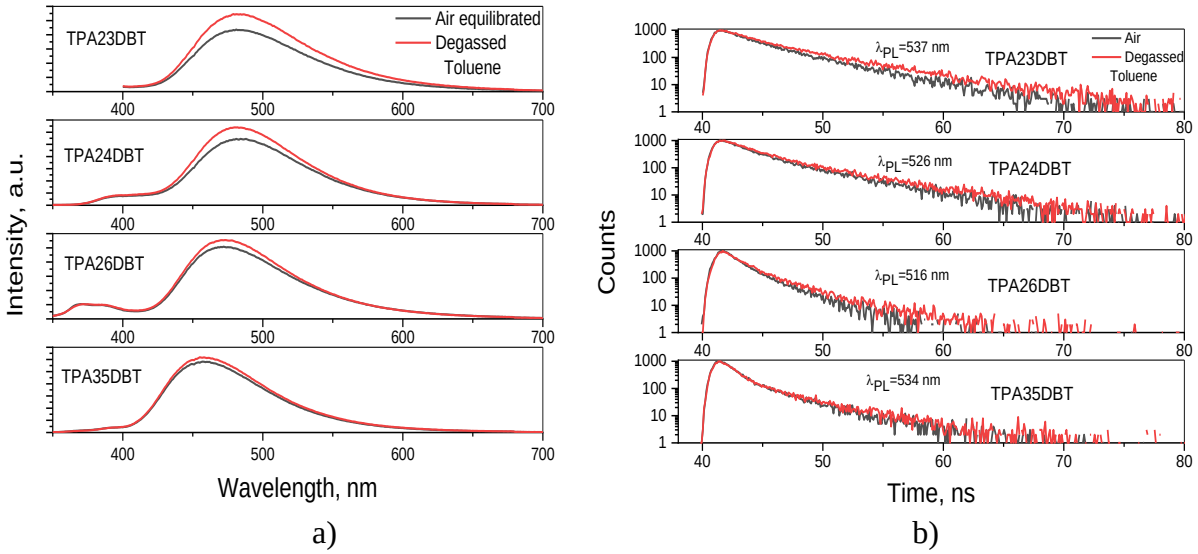

Fig. 26. PL spectra and time decay curves of degassed and air equilibrated dilute toluene solutions of compounds recorded at room temperature

Bluish-green emissions of neat films of **TPA23DBT**, **TPA24DBT**, **TPA26DBT**, and **TPA35DBT** were characterized by PL spectra with the single unstructured band. The films of compounds **TPA23DBT** and **TPA26DBT** were characterized by long-lived fluorescence which was TADF in nature (Figure 27a). This claim is in good agreement with the small ΔE_{ST} of 0.09 eV observed for **TPA23DBT** and 0.011 eV for **TPA26DBT** (Figure 25d, Table 2) obtained from the measurements

results. Only prompt fluorescence was detected for the films of **TPA24DBT** and **TPA35DBT** due to experimental ΔE_{ST} values of 0.27 and 0.32 eV respectively.

Table 2. Isomer-dependent photophysical parameters of the compounds

Parameters↓	Samples→	**TPA23DBT**	**TPA24DBT**	**TPA26DBT**	**TPA35DBT**
PLQY(%)	Toluene /THF/Neat Film	0.9/1.2/7.7	12.3/19.7/3.6	0.1/0.1/2.5	2.7/5.1/6
τ, ns	THF	4.5	7.5	1.7	6
S_1, eV		2.94	2.93	2.93	3.00
T_1, eV		2.85	2.66	2.82	2.68
ΔE_{ST}, eV		0.09	0.27	0.11	0.32

* Singlet and triplet energies (E) were calculated using set-on wavelengths ($\lambda_{set\text{-}on}$) of fluorescence and phosphorescence spectra respectively (Figure 25d) by empiric formula $E=1240/\lambda_{set\text{-}on}$.

It should be noted that non-structured fluorescence and phosphorescence spectra of THF solutions of **TPA23DBT** and **TPA26DBT** were recorded at 77K indicating light-emitting relaxation of triplet CT states. For the frozen THF solutions of **TPA24DBT** and **TPA35DBT**, the structured phosphorescence spectra were observed indicating light-emitting relaxation of triplet LE states. This observation indicates that the triplet CT states of the studied compounds are of higher energy than their triplet LE states. The triplet LE states are the same for all four isomers since the same moieties are present in their molecular structure. The singlet and triplet CT states are not the same causing different triplet harvesting mechanisms of the compounds, i.e., TADF in **TPA23DBT** and **TPA26DBT** and RTP in **TPA24DBT** and **TPA35DBT** (Figure 27b, c). To explain why the TADF was observed for **TPA23DBT** and **TPA26DBT** and not for **TPA24DBT** and **TPA35DBT**, schematic energy diagrams shown in Figure 28 are used. These diagrams show that the energies of triplet ^{3}LE states which are by ca. 0.3 eV are lower than those of triplet ^{1}CT states. These values were taken from the phosphorescence and fluorescence spectra of the solution in THF at 77 K respectively (Figure 25d). For **TPA23DBT** and **TPA26DBT**, the energies of triplet ^{3}CT states are slightly lower than those of ^{1}CT states resulting in small ΔE_{ST} values mentioned above (see Figure 25d, Table 2). The TADF observed for **TPA23DBT** and **TPA26DBT** occurred via RISC of exciton energy from ^{3}LE to ^{1}CT. The RISC process is efficient due to the vibronic mixing of ^{3}LE and ^{3}CT as it is described elsewhere [121]. Internal conversion (IC) and reverse internal conversion (RIC) are also shown in the schematic energy diagram (Figure 28). In the case of **TPA24DBT** and **TPA35DBT** the energies of triplet ^{3}CT states are significantly lower than those of ^{1}CT states. The vibronic mixing of ^{3}CT and ^{3}LE did not sufficiently decrease the gap between the lowest singlet and triplet states in order to get an efficient RISC. However, efficient ISC from ^{1}CT to ^{3}LE, and light-emitting relaxation of ^{3}LE, even at room temperature, can be expected for **TPA24DBT** and **TPA35DBT** in the appropriate media [122].

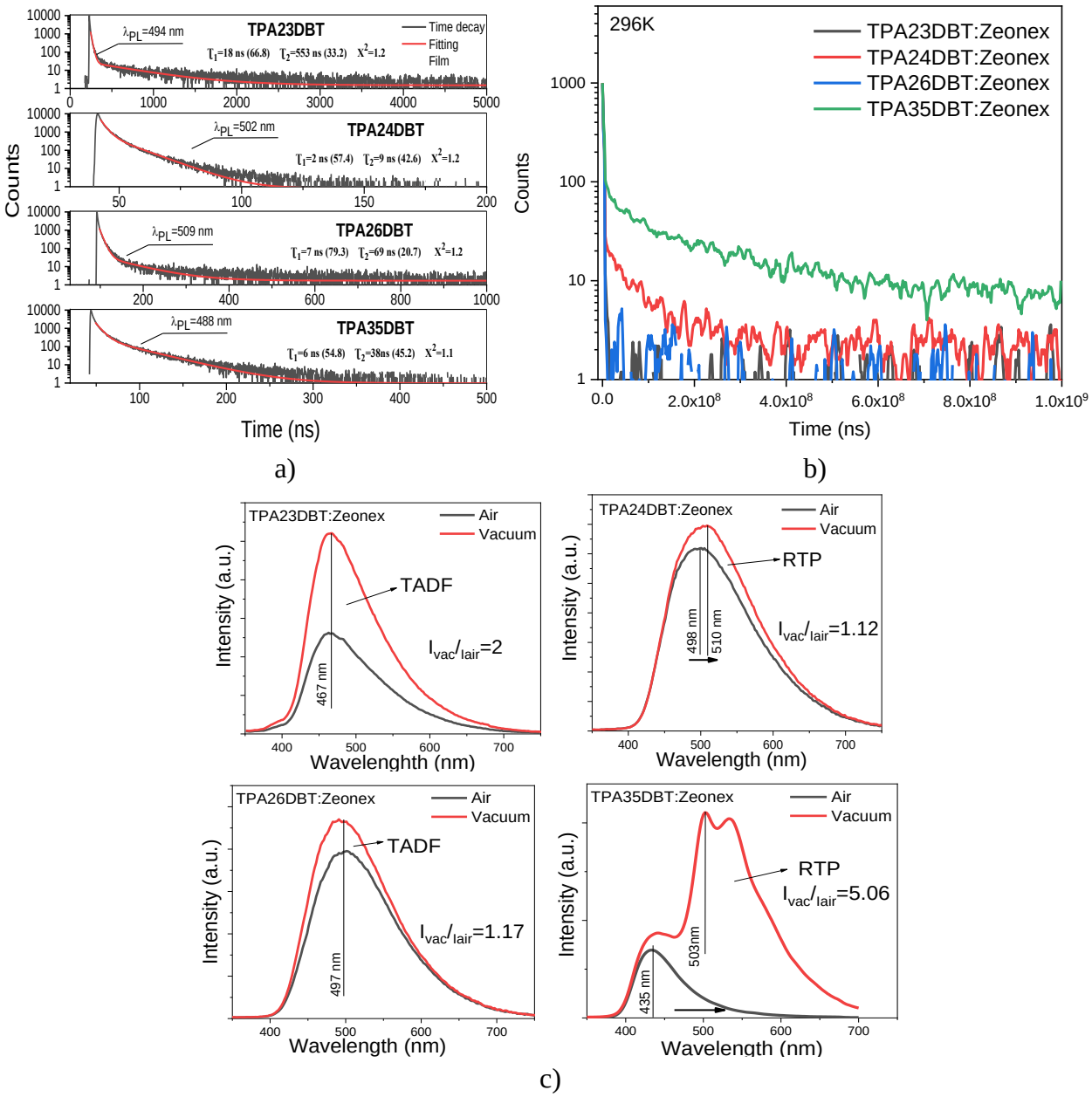

Fig. 27. PL decay curves of neat films (a) and of the films of 5 wt.% solid solutions of the compounds in ZEONEX matrix (b) and PL spectra (c) of the films of the compounds doped in in ZEONEX under air and vacuum

To support the above presumption of RTP of **TPA24DBT** and **TPA35DBT**, the compounds were molecularly dispersed (5wt.%) in an inert polymer called ZEONEX. This allows minimization of the effects of vibration and intermolecular interactions [123]. PL spectra of the solid samples of the molecular dispersions are shown in Figure 27c. Indeed, when triplets are not quenched by triplet oxygen, in an inert atmosphere compounds **TPA24DBT** and **TPA35DBT** demonstrated red-shifted PL spectra compared to the fluorescence spectra recorded in air (Figure 27c). These shifts were caused by RTP relaxation time. The samples were excited a second after the excitation pulse (Figure 27b). The samples of the molecular dispersions of **TPA23DBT** and **TPA26DBT** in ZEONEX demonstrated increased PL intensity after deoxygenation. This increase is attributed to TADF for which the shifts are not expected due to the same spectra of prompt and delayed fluorescence. PL decay measurements did not show the contribution of RTP (Figure 27b). According to the different ratios of PL intensity

in air (I_{air}) and vacuum (I_{vac}), varied TADF and RTP efficiencies were detected. Compound **TPA23DBT** (I_{vac}/I_{air}=2) showed the best TADF properties due to the smallest gap of 0.09 eV between the energies of ^{1}CT and ^{3}CT states (Figure 28a, Table 2). On the other hand, compound **TPA35DBT** (I_{vac}/I_{air}=5.06) indicated the best RTP properties due to the biggest gap of 0.32 eV between the energies of ^{1}CT and ^{3}LE states (Figure 28b, Table 2).

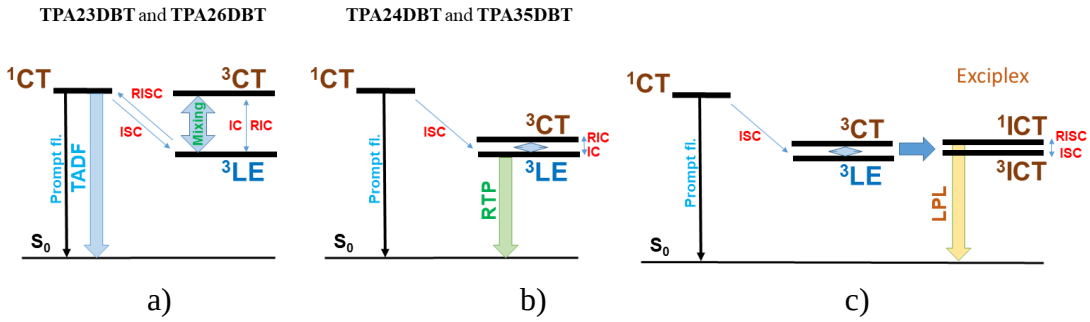

Fig. 28. Schematic energy diagrams representing different triplet harvesting abilities, i.e., either TADF (a), RTP (b), or LPL (c) of **TPA23DBT**, **TPA24DBT**, **TPA26DBT**, and **TPA35DBT** based solid-state samples

The schemes shown in Figure 28 are useful for classification, but they are simplified. The explicit discrimination between CT and LE states on the ground of experimental analysis and assignment (Figure 28) seems to be a kind of oversimplification from the theoretical point of view. In fact, the T_1 state of the molecules represents a large mixture of configurations and differs from that of the S_1 state. Expansions of the T_1 state wavefunctions are much more complicated and longer than those for the singlet excited S1 states and definitely include some LE configurations. However, the later correspond mostly to excitations inside donor TPA moieties and include charge transfer between donors. Thus, the simple assignments in Figure 28 for the T_1 state to LE type is an oversimplification. The detailed analysis shows that the T_1 state wavefunctions of the molecules of **TPA24DBT** and **TPA35DBT** have large configurations which represent mixtures of CT and LE excitations. This provides spin orbital coupling (SOC) enhancement between T_1 and S_1 states which is caused by the C=O group involvement through the SOC integral. The T_1 and S_1 states of these two molecules differ in occupation numbers just of these two MOs. Such SOC enhancement leads to an increase of the ISC and subsequently RTP rate constants.

To develop LPL emitters for optical sensors, 5 wt.% solid solutions of the compounds in bis[2-(diphenylphosphino)phenyl] ether oxide (DPEPO) as exciplex-forming acceptor were prepared. The reason of selection of DPEPO was its high triplet level of 3.52 eV which is required for efficient LPL [124]. The samples were fabricated by co-melting method of exciplex-forming donor (**TPA23DBT**, **TPA24DBT**, **TPA26DBT**, or **TPA35DBT**) and acceptor DPEPO. Their PL spectra were recorded under air and vacuum. They are shown in Figure 29a. The red-shifts of PL spectra of the films of the molecular mixtures of the studied compounds with DPEPO relative to those of neat films of the individual compounds are the evidences of the formation of exciplexes (Figure 29c). No shifts of PL spectra after deoxygenation were observed. Thus, RTP was not detected for the samples. This observation was supported by the different shapes and timescales of PL decay curves compared to those of RTP compounds (Figure 29b). The most efficient LPL (I_{vac}/I_{air}=4.57) was observed for the molecular mixture of **TPA35DBT** and DPEPO. The mechanism of LPL is schematically presented in Figure 28c. In the case of the system of **TPA35DBT** and DPEPO, intermolecular singlet (^{1}ICT)

and triplet (^{3}ICT) exciplex states are very close to ^{3}CT and ^{3}LE states of **TPA35DBT**. As a result, ^{3}ICT exciplex states are very efficiently populated by energy transfer from ^{3}CT and ^{3}LE states of **TPA35DBT** which leads to an efficient LPL, i.e. emission from the exciplex with prolonged life-time due to the electron migration in the host DPEPO before relaxation [125]. For the other compounds, ^{3}CT states are slightly higher than ^{3}LE, thus they are higher than corresponding ^{1}ICT and ^{3}ICT exciplex states. These differences prevent very efficient energy transfer from donors to exciplex. Taking into account the LPL efficiency, the layer of molecular mixture of **TPA35DBT** and DPEPO was selected as an active layer for oxygen sensors (see section Oxygen sensing).

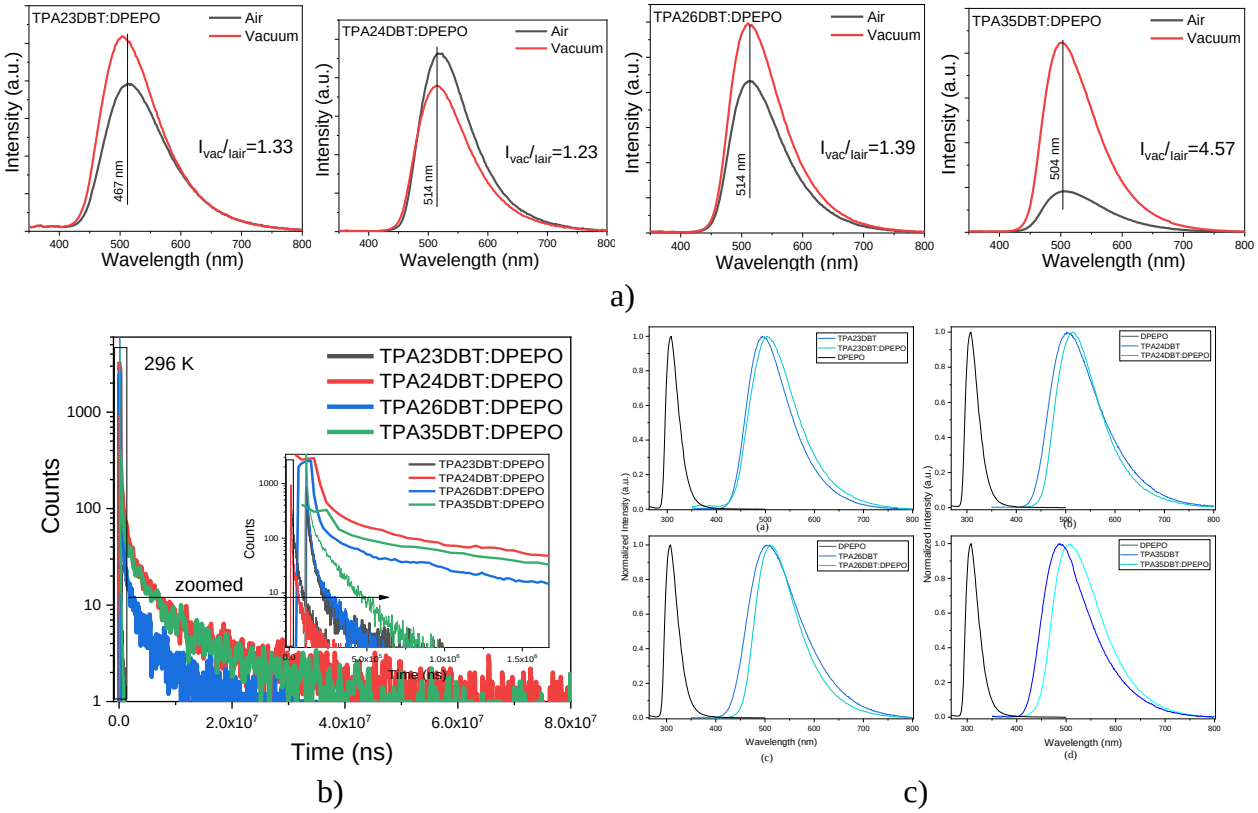

Fig. 29. PL spectra (a) and PL decay curves (b) of co-melted samples of the molecular mixtures of the compounds (5wt.%) and DPEPO. PL spectra (c) of the spin-coated film of the molecular mixture of **TPA23DBT**, **TPA24DBT**, **TPA26DBT**, **TPA35DBT** (50wt.%) and DPEPO (50wt.%) and of neat films of compounds and DPEPO

3.2. Thermal Properties

Before usage isomeric derivatives of triphenylamine and dibenzothiophene-2-yl(phenyl)methanone in solid optoelectronic devices, examination of their thermal properties was performed. Analysis of their thermal properties allows to estimate the possibility to use thermo-vacuum deposition for the fabrication of the solid layers. In addition, conditions (co-melting temperature) of the preparation of active layers of oxygen sensors based on the developed LPL emitters can be accurately selected. Thermogravimetric (TG) analysis and differential scanning calorimetry (DSC) measurements were performed for the isomeric compounds. The thermal characteristics are collected in Table 3. The TG and DSC curves are shown in Figure 30a, b. Isomers **TPA23DBT** and **TPA26DBT** start to lose their mass at visibly lower temperatures than **TPA24DBT** and **TPA35DBT**. The highest 5 % weight-loss temperature ($T_{d\text{-}5\%}$) of 447ºC was observed for compound **TPA35DBT**. This weight loss can be attributed rather to sublimation than to thermal degradation. DSC curves of the compounds showed

the single-stage drop of mass to zero. All the compounds were found to form molecular glasses. The highest glass transition temperatures (T_g) of 125ºC and 123ºC were observed for compounds **TPA24DBT** and **TPA35DBT** respectively (Table 3). As a result, high morphological stability can be expected for compounds **TPA24DBT** and **TPA35DBT**. Higher $T_{d\text{-}5\%}$ and T_g values of **TPA24DBT** and **TPA35DBT** can be attributed to either more rigid molecular structures or stronger molecular interaction/packing in solid-state [75]. Apparently, because of such structural peculiarities, the studied isomers demonstrated different photophysical properties as it was discussed above. The peaks corresponding to the crystallization were not observed in their DSC curves suggesting high morphological stability of the solid amorphous samples of the compounds.

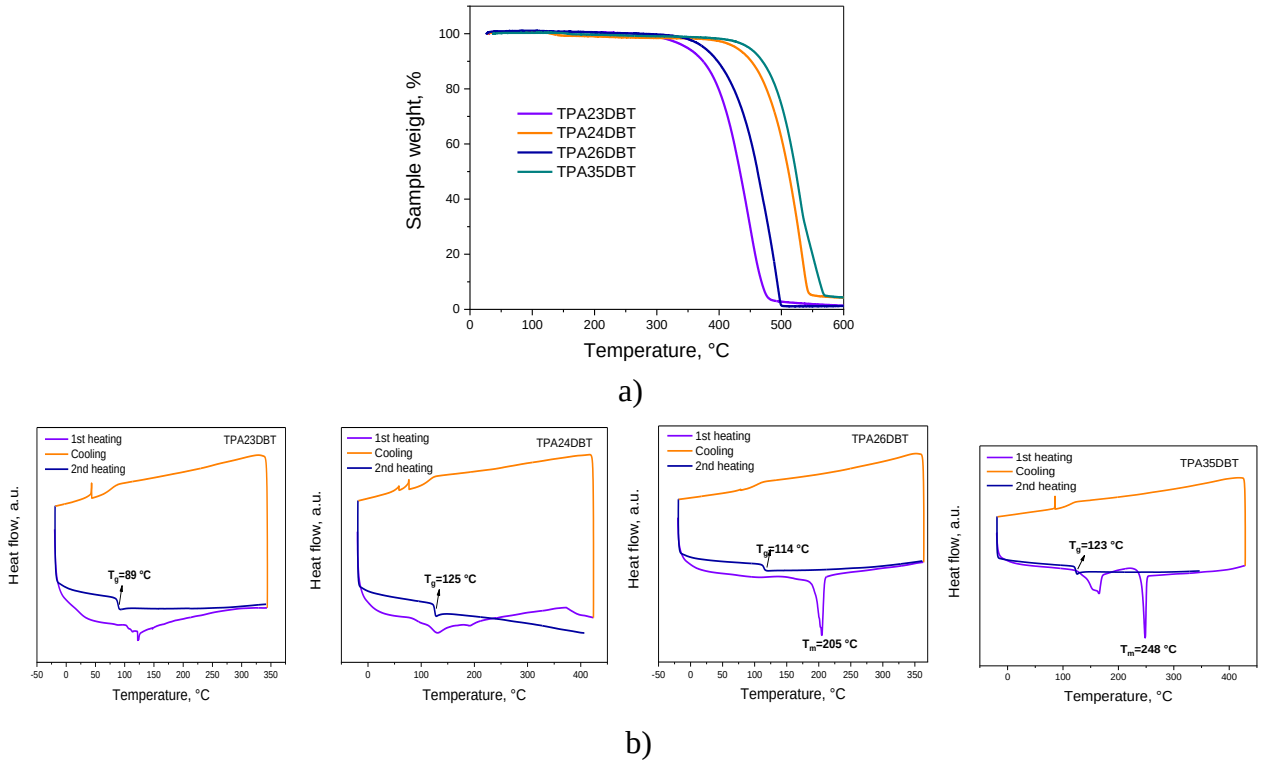

Fig. 30. TGA (a) and DSC (a) curves of studied compounds

3.3. Electrochemical, Photoelectron emission, and Charge-transporting Properties

For optoelectronic applications of organic semiconductors, their ionization potentials (IP) and electron affinities (EA) are required. As a starting point, their oxidation (E_{ox}) and reduction (E_{red}) potentials were obtained from cyclic voltammetry (CV) measurements (Figure 31, Table 3). These potentials can be used for the calculation of IP_{CV} and EA_{CV} (Table 3). The IP_{CV} and EA_{CV} values of the isomeric compounds were found to be close the corresponding values ranging from 5.27 eV to 5.49 eV and -3.1 eV to -3.0 eV. In principle, by using certain correlations, it is a possibility to transform IP_{CV} and EA_{CV} values estimated for solutions to the corresponding IP and EA values of the solid-state [126].

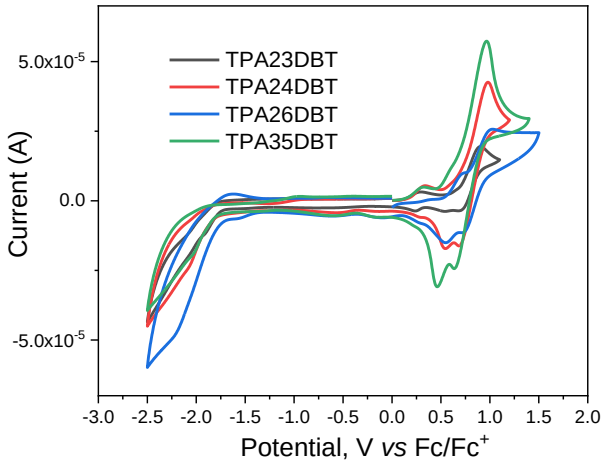

Fig. 31. Cyclic voltammetry curve (CV) of the studied compounds

To avoid errors which may appear using correlations, photoelectron emission (PE) spectroscopy was employed for the estimation of ionization potential (IP_{PE}) of the solid films of the compounds (Figure 32). They showed moderate IP_{PE} values in the close range of 5.5-5.62 eV which are appropriate for injection of holes from electrodes without the usage of several additional layers. The IP_{PE} values of the films were found to be different from the corresponding IP_{CV} values [126]. Considering some errors of the common procedure the optical gap (E_g^{opt}) was used instead of the transport gap in the determination of electron affinity $EA_{EP} = IP_{EP} - E_g^{opt}$ [126]. EA_{EP} values were obtained in the range of 2.31-2.66 eV which should be suitable for electron injection in a real OLED (Table 3).

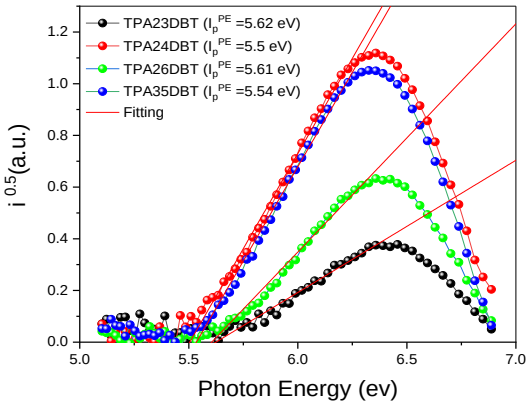

Fig. 32. Photoelectron emission spectra of studied compounds

Exploiting time of flight (TOF) technique, the effect of the isomerization of **TPA23DBT**, **TPA24DBT**, **TPA26DBT** and **TPA35DBT** on their charge-transporting properties in vacuum-deposited films was investigated. The diode-type indium tin oxide (ITO)/thick film/Al TOF samples were deposited where the thickness of the films range from 2.35 to 4.60 micrometres. For electrons, transit times (ttr) were observed neither in linear scales nor in log-log scales. For holes, transit times were observed when TOF current transients plotted in log-log scales (see Figure 33b). Such shapes of TOF transients are typically attributed to dispersive charge transport [127, 128].

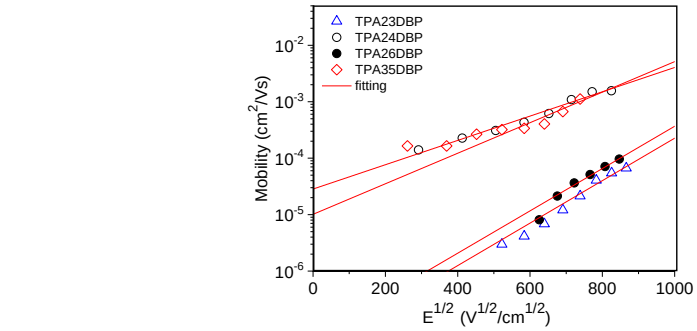

a)

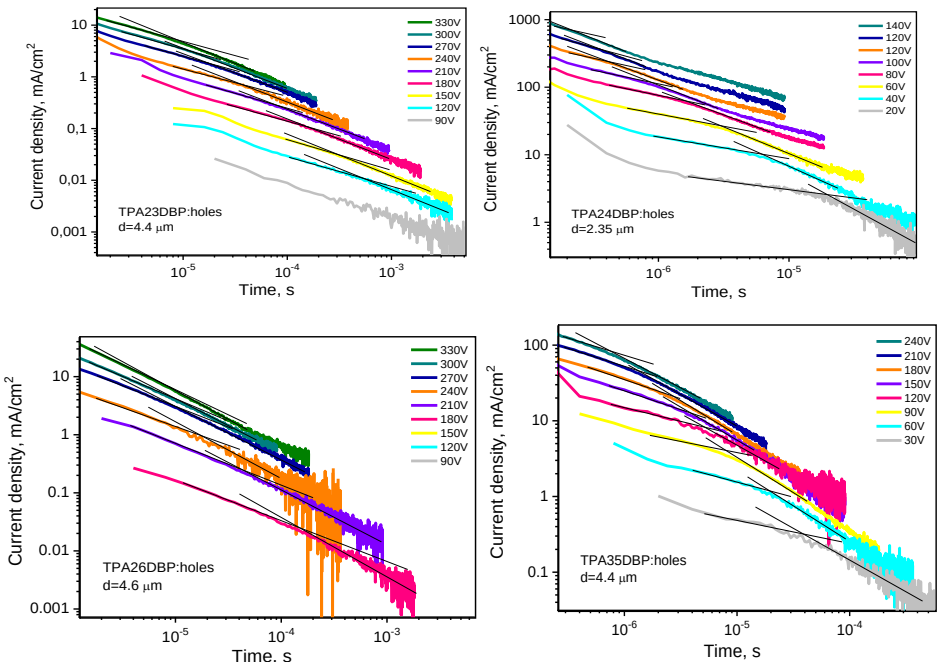

b)

Fig. 33. Hole mobility versus electric field (a) and time of flight (TOF) current transients of holes (b) for the deposited layers of **TPA23DBT**, **TPA24DBT**, **TPA26DBT** and **TPA35DBT**

Hole mobilities were estimated at different electric fields (Figure 33a). Compounds **TPA23DBT** and **TPA26DBT** showed clearly different hole-transporting properties than **TPA24DBT** and **TPA35DBT**. For example, at electric field of 5×10^5 V/cm, hole mobility (μ_h) of 1.6×10^{-5} and 3.3×10^{-5} cm^2 V^{-1} s^{-1} were obtained for **TPA23DBT** and **TPA26DBT** respectively (Figure 33a, Table 3). Meanwhile, at the same electric field, isomers **TPA24DBT** and **TPA35DBT** showed by ca. two orders of magnitude higher hole mobilities. They were found to be of 1×10^{-3} cm^2 V^{-1} s^{-1} and 8.2×10^{-4} cm^2 V^{-1} s^{-1} for compounds **TPA24DBT** and **TPA35DBT** respectively. Such big differences in hole mobilities of the isomeric compounds containing the same donor and acceptor moieties can be apparently attributed to the differences in their molecular packing in solid-state, consequently to the different HOMO-HOMO overlapping. The electric field dependences of hole mobilities of the isomeric compounds were additionally analysed by the Poole–Frenkel relationship ($\mu_h = \mu_0 e^{\beta E^{1/2}}$). Even higher differences were observed between the values of zero-field mobilities (μ_0) of the compounds. In addition, the relatively high field dependence parameters (β) from 5×10^{-3} to 8.7×10^{-3} cm$^{-1/2}$ V$^{-1/2}$ were obtained. Such hole mobility parameters can be attributed to the relatively strongly dispersive hole transport. The highest μ_0 value of 2.84×10^{-5} cm^{2}V^{-1}s^{-1} and the lowest β

value of 5 $cm^{-1/2}V^{-1/2}$ were obtained for compound **TPA24DBT** with the weakest hole dispersity (Figure 33b, Table 3).

Table 3. Isomer-dependent/independent physical parameters of the isomeric derivatives of triphenylamine and dibenzothiophene-2-yl(phenyl)methanone

Parameter	Sample	**TPA23DBT**	**TPA24DBT**	**TPA26DBT**	**TPA35DBT**
DSC and TGA measurements					
T_m, °C	Powder	-	-	205	248
T_g, °C		89	125	114	123
T_{cr}, °C		-	-	-	-
$T_{d\text{-}5\ \%}$, °C		348	427	375	447
Photoelectron emission spectroscopy					
IP_{PE}	Film	5.62 (4.90)	5.5 (4.96)	5.6 (4.89)	5.53 (4.95)
[a] E_g^{opt}, eV		3.31 (3.32)	2.89 (3.33)	3.23 (3.30)	3.13 (3.27)
EA_{EA}		2.31 (1.58)	2.66 (1.63)	2.37 (1.59)	2.4 (1.68)
CV properties					
[a] E_{ox} *vs* Fc/Fc^+, V	DCM solution with $TBAPF_6$	0.69	0.57	0.52	0.47
[b] E_{red}, V		-1.74	-1.78	-1.7	-1.8
[c] IP_{CV}, eV		5.49	5.37	5.32	5.27
[d] EA_{CV}, eV		-3.06	-3.02	-3.1	-3.0
Time of flight study					
[e] μ_{holes}, $cm^2/(V\cdot s)$	Film	1.6×10^{-5}	1×10^{-3}	3.3×10^{-5}	0.82×10^{-3}
μ_0, $cm^2\ V^{-1}\ s^{-1}$		3.9×10^{-8}	2.84×10^{-5}	6.6×10^{-8}	1×10^{-5}
β, $cm^{-1/2}\ V^{-1/2}$		8.7×10^{-3}	5×10^{-3}	8.7×10^{-3}	6.2×10^{-3}

[a] $E_g^{opt}=1240/\lambda_{abs}$, where wavelengths λ_{abs} were taken from onset of low-energy bands of absorption spectra of films (Figure 25a); [b] potential *vs.* Fc/Fc^+; [c] calculated according to equation: $EA = e(E_{red.onset} + 4.8)$ [eV]; [d] calculated according to equation: $IP = -e(E_{ox.onset} + 4.8)$ [eV]. [a] at $E = 5 \times 10^5$ V/cm.

3.4. Electroluminescent Properties

To demonstrate the isomerization effect on electroluminescent (EL) properties of the compounds, they were used as hosts for green phosphorescent OLEDs. Such role for the developed compounds was based on our expectations that their IP_{EP} and EA_{EP} values ensure hole and electron recombination within the layer of emitter tris[2-phenylpyridinato-C2,N]iridium(III) ($Ir(ppy)_3$) (Figure 34a, Table 4). In addition, the lowest triplet states of hosts are higher than the corresponding triplet state of $Ir(ppy)_3$. Therefore, efficient singlet and triplet harvesting by $Ir(ppy)_3$ was expected [129]. The OLED structure of ITO/MoO_3 (1 nm)/TAPC (40 nm)/mCBP (8 nm)/ guest (10 wt. %): host light-emitting layer (24 nm)/TSPO1 (8 nm)/TPBi (40 nm)/LiF (1 nm):Al (80nm) was used. The devices containing hosts **TPA23DBT**, **TPA24DBT**, **TPA26DBT**, or **TPA35DBT** were named as h1-h4. In the devices, hole and electron injection was performed by the layers of MoO_3 and LiF respectively. Typical hole and electron transporting layers of TAPC and TPBi respectively were used in OLEDs (Figure 34b). According to the equilibrium diagram, recombination of hole-electron pairs with the following exciton formation occurs on the host or emitter. To increase the probability of exciton relaxation within the light-emitting layer, widely known exciton blocking layers of mCBP and TSPO1 were used (Figure 34b).

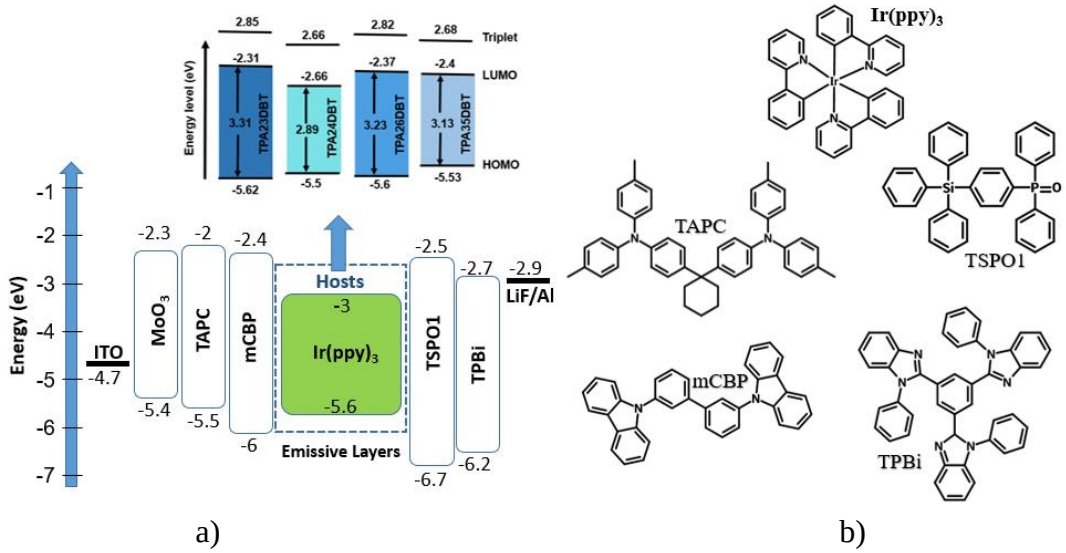

Fig. 34. Equilibrium energy diagram (a) and the molecular structures (b) of the compounds used for the charge-transporting and exciton-blocking layers

The EL spectra of the fabricated devices were related to the emitter used, i.e., $Ir(ppy)_3$ (Figure 35c) [130]. The emissions of additional functional layers in the near-UV/blue region were not observed in EL spectra of the devices h1-h4. The EL of the devices h1-h4 was relatively stable at different external voltages. However, the low-energy shoulders could be recognized especially for device h2 at high voltages. This observation can be attributed to the formation of electroplex of TAPC the emission of which peaked at 580 nm [131]. Less probable reasons of the shoulders could be the contribution of RTP of compound **TPA24DBT.** Since the exciton blocking layers were used in the OLED structure, reasons of the shoulders cannot be attributed to interface exciplexes between the neighbouring functional layers (TAPC or TPBi) and light-emitting layer (Figure 27c).

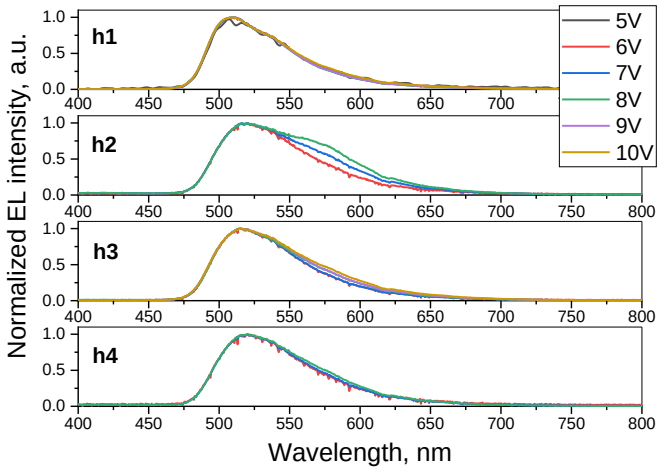

Fig. 35. Normalized EL spectra under different applied voltages

Despite the fact that the same device structure (additional functional layers were deposited for all the devices at the same procedure) and the same emitter ($Ir(ppy)_3$) was used, output EL parameters were very different (Figure 36, Table 4). For example, turn-on voltages of devices h1-h4 at a luminance of 10 cd m-1 were in the wide range of 4.1-6.3 V, PE_{max} values were in the range of 6.2-26.8 lm/W, and EQE_{max} values were between 2.8-13.9 %. Taking into account the highest hole mobilities of

compounds **TPA24DBT** and **TPA35DBT** (Figure 28a), the best output EL parameters were expected for devices h2 and h4. Indeed, the highest EQE_{max} value of 13.9 % was obtained for device h2, but device h4 showed the lowest EQE_{max} (Figure 36). Such low EQE_{max} of device h4 can be related to the very strong contribution of RTP (Figure 27c). The long-lived triplet excitons can be a source of different energy loss processes (e.g. exciton-exciton or exciton-polaron annihilation) [132, 133]. Considering the difference in ISC rates, the contribution of RTP in case of **TPA24DBT** is much smaller than that of the **TPA35DBT**.

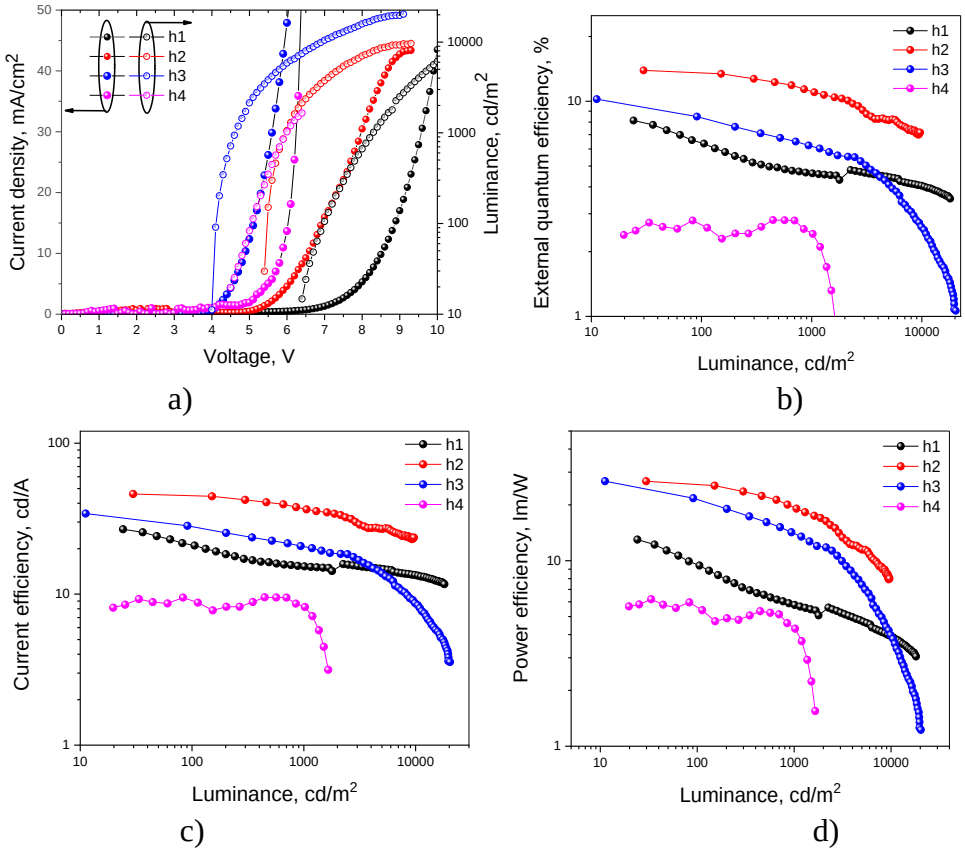

Fig. 36. Current density and luminance as the function of applied voltages (a), external quantum efficiency (EQE) (b), current efficiency (c) and power efficiency (d) versus luminance curves of the fabricated OLEDs

TADF compounds **TPA23DBT** and **TPA26DBT** did not suffer from strong RTP as it was observed for **TPA35DBT** or for previously published 4-(9,9-dimethylacridan-10-yl)-4‘-(thianthrene-1-yl)diphenylsulfone [134]. Even better triplet harvesting properties can be expected for devices h1 and h3 than for phosphorescent OLEDs with the conventional hosts because of the usage of the molecular systems phosphorescent emitter and TADF host [135]. However, devices h1 and h3 showed moderate EQE values (Figure 36b). This result is attributed to a lower charge balance factor than unity caused by the low hole mobilities of the hosts (Figure 33a). Since precise optimization (e.g., optimization of thickness of functional layers or concentration of emitter $Ir(ppy)_3$) of devices was not performed, the fabricated devices did not demonstrate state-of-art EQE values, but it is clearly seen isomerization effects on hosting performances of the compounds.

Table 4. Parameters of OLEDs

Device	Light emitting layer	V_{on},[a] V	Max brightness,[b] cd/m^2	$PE_{1000}/CE_{1000}/EQE_{1000}$ (lm W^{-1}/cd A^{-1}/%) [c]	$PE_{max}/CE_{max}/EQE_{max}$ (lm W^{-1}/cd A^{-1}/%) [d]
Hosting properties for green emitters					
h1	Ir(ppy_3)(10 wt%): **TPA23DBT**	6.3	18100	5.8/15.3/4.6	13/26.8/8.1
h2	Ir(ppy_3)(10 wt%): **TPA24DBT**	5.3	9660	19.1/36.5/11.1	26.7/46/13.9
h3	Ir(ppy_3)(10 wt%): **TPA26DBT**	4.1	20310	14.1/20.3/6.1	26.8/34.1/10.2
h4	Ir(ppy_3)(10 wt%): **TPA35DBT**	4.5	1650	4.3/8.3/2.4	6.2/9.5/2.8

[a] Turn-on voltage at a luminance of 10 cd m^{-1}, [b] Maximum brightness, [c] Power efficiency (PE_{1000}), current efficiency (CE_{1000}) and external quantum efficiency (EQE_{1000}) at 1000 cd m^{-2}, [d] Maximum power efficiency (PE_{max}), maximum current efficiency (CE_{max}) and maximum external quantum efficiency (EQE_{max}).

3.5. Oxygen Sensing

Compound **TPA35DBT** has high potential for oxygen sensing applications due to the efficient and long-living RTP and LPL. PL properties of **TPA35DBT** containing samples were additionally studied under different oxygen and nitrogen mixtures (Figure 37b). In contrast to the strong RTP in vacuum (Figure 27c), phosphorescence of the sample of the solid solution of **TPA35DBT**(5wt.%) in Zeonex practically did not show RTP under purge of nitrogen (Nitrogen Instrument 5.0 ≥ 99.999%) (Figure 37a). This observation shows that RTP of **TPA35DBT** was quenched even by the smallest traces of oxygen.

The reason is the complicated orbital nature of T_1 state of **TPA35DBT** and a relatively large electric quadrupole moment (EQM) of 24.52 Debye·Å. Its interaction with EQM of the triplet oxygen molecule (0.35 Debye Å) provides additional contribution to the RTP quenching. The largest components of the EQM tensor are given [45-47]. Spin density (ρ) in the optimized T_1 state is localized in the carbonyl group (ρ_O=0.77, ρ_C=0.38). The rest is distributed in the π-systems of the nearest phenyl rings. This supports the ^{3}LE nature of the optimized phosphorescent state.

Thus, compound **TPA35DBT** can be used as an oxygen-sensing probe when extremely high sensitivity is needed in the range of oxygen concentrations of up to ca. 5 ppm. Unfortunately, oxygen sensing parameters (e.g., the Stern–Volmer constants) for the oxygen-sensing probes working at such concentrations of oxygen could not be provided in the present work due to the testing setup limitations i.e., due to the implemented flowmeters of oxygen and nitrogen working at a not appropriate range, small concentration of oxygen present in nitrogen used, etc. In the case of LPL sample i.e., solid solution of **TPA35DBT** (5 wt.%) in DPEPO, different PL decays were recorded at different oxygen concentrations from ca. 0 up to 100 % (Figure 37c). Quenching of LPL of the probe by triplet oxygen could be related to the oxygen concentration with a relationship predicted by the Stern-Volmer equations (Equation (8)), the simplest of which is [138]:

$$\frac{\tau^0_{LPL}}{\tau_{LPL}} = 1 + K_{sv}[O_2] \quad (8)$$

where τ_{LPL} and τ^0_{LPL} are LPL lifetimes under presence and absence of oxygen, respectively; K_{sv} is the Stern–Volmer constant.

The τ_{LPL} values were obtained for the probe of the solid solution of **TPA35DBT** (5 wt.%) in DPEPO at different concentrations of oxygen by the exponential fitting of the corresponding PL decay curves (Figure 37c). The dependence of τ_{LPL} as a function of oxygen concentration was fitted by Equation (8) with high accuracy (R^2 higher than 0.998). As a result, the Stern–Volmer constant of 4.55×10^{-4} ppm was obtained at oxygen concentrations of up to 10000 ppm (Figure 37c). It should be noted that the probe of the solid solution of **TPA35DBT** (5 wt.%) in DPEPO can be used in a very wide range of concentrations of oxygen from 0 to 100% (Figure 37c). However, at oxygen concentrations higher than 10000 ppm, the non-linear fitting must be used. According to these data, compound **TPA35DBT** shows very promising properties as the probe for optical sensors of oxygen.

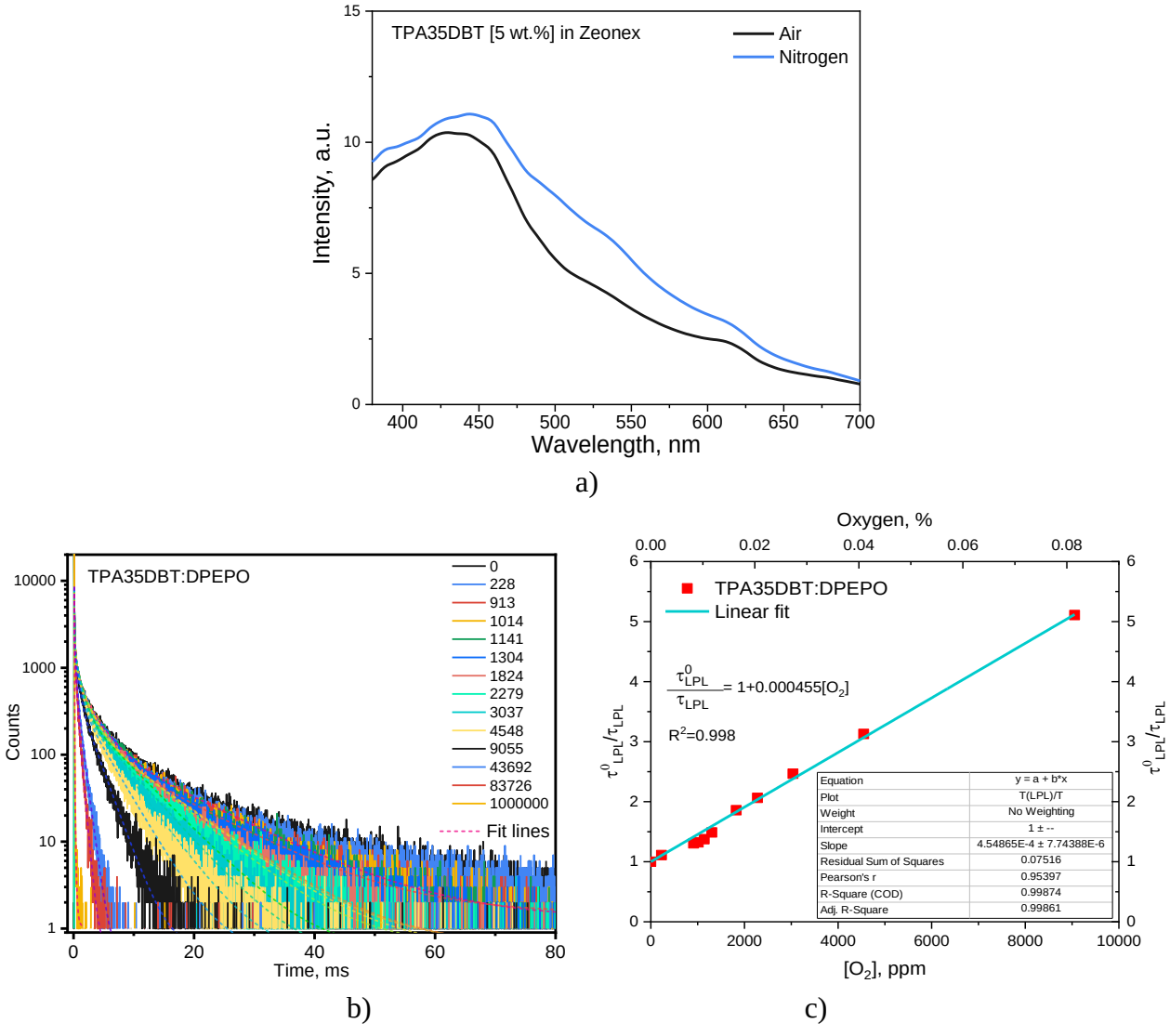

Fig. 37. PL spectra of the probe **TPA35DBT**:DPEPO at air and flow of nitrogen (a), LPL lifetimes of the probe of the solid solution of **TPA35DBT**(5 wt.%) in DPEPO at the different oxygen fractions in ppm (b) and the corresponding Stern-Volmer plot (c)

Conclusions

This work is on the isomeric compounds showing very different long-lived emissions with different potential applications in electroluminescent devices and optical sensors of oxygen. Four new derivatives of triphenylamine and dibenzothiophene-2-yl(phenyl)methanone demonstrated either room-temperature phosphorescence, thermally activated delayed fluorescence, or long persistent luminescence due to the different maps of their singlet and triplet excited states.

The main findings of this work are as following:

1. The potential of long persistent luminescence emitters as active probes for optical sensors was unclosed for the first time. Long persistent luminescence emitters were not previously used for optical sensors due to the best of our knowledge. In this study, we partly aimed to demonstrate for the first time the potential of long persistent luminescence emitters for the fabrication of optical sensors.
2. One isomer **TPA35DBT** exhibiting room temperature phosphorescence and long persistent luminescence was demonstrated to be a very good candidate for active layers of optical sensors of oxygen showing the Stern–Volmer constant of 4.55×10^{-4} ppm a in wide range of oxygen concentrations.
3. Isomerization effect on charge-transporting properties was demonstrated. The different by two orders of magnitude hole mobility values were obtained for the isomeric compounds at the same electric fields. The highest hole mobility belongs to **TPA24DBT** which reached 1×10^{-3} cm^2 V^{-1} s^{-1} at electric field of 5×10^5 V/cm.
4. The isomer **TPA24DBT** exhibiting room temperature phosphorescence and high hole-transporting mobility values was used as the host of green organic light emitting diode (h2) which showed external quantum efficiency of 13.9%.
5. The disclosed hints for the development of emitters exhibiting room temperature phosphorescence, thermally activated delayed fluorescent or long persistent luminescent.
6. The revealed effect of the positions of triphenylamine donor moieties of isomeric emitters on the nature of their emission (room temperature phosphorescence, thermally activated delayed fluorescent or long persistent luminescent). Schematic energy diagrams representing different triplet harvesting routes is proposed.
7. The detailed analysis of the triplet (T_1) state wavefunctions of the studied molecules representing mixtures of the charge transfer and locally excited excitations are provided by the theoretical calculations. This results in spin-orbit coupling enhancement between triplet (T_1) and singlet (S_1) states leading to the increase of the intersystem crossing and room temperature phosphorescence rate constants.

List of references

1. ZHONG, Jian Qiang, MAO, Hong Ying, WANG, Rui, LIN, Jia Dan, ZHAO, Yong Biao, ZHANG, Jia Lin, MA, Dong Ge and CHEN, Wei. Ionization potential dependent air exposure effect on the MoO 3/organic interface energy level alignment. *Organic Electronics*. 1 December 2012. Vol. 13, no. 12, p. 2793–2800. DOI 10.1016/j.orgel.2012.07.048.
2. GHASEMI, Melika. *MAIN Melika-Ghasemi-Semester Project 2-Report*. 2021. Kaunas.
3. MEI-YEE, Maggie Chan, TAO, Chi Hang and WING-WAH, Vivian Yam. Overview and highlights of WOLEDs and organic solar cells: From research to applications. *Green Energy and Technology* [online]. 2010. Vol. 43, p. 1–35. [Accessed 17 February 2022]. DOI 10.1007/978-3-642-14935-1_1. Available from: https://link.springer.com/chapter/10.1007/978-3-642-14935-1_1
4. MICHAEL, Vineeth. Fabrication of OLED on FTO and ITO coated Substrates A thesis submitted to De Montfort University in partial fulfillment of the requirements for the award of the Degree of Masters of Science (Msc) in Microelectronics and Nanotechnology. [online]. 2012. [Accessed 19 February 2022]. Available from: https://www.researchgate.net/publication/234037453_Fabrication_of_OLED_on_FTO_and_ITO_coated_Substrates_A_thesis_submitted_to_De_Montfort_University_in_partial_fulfillment_of_the_requirements_for_the_award_of_the_Degree_of_Masters_of_Science_Msc_in_Mi
5. NAIR, Govind B. and DHOBLE, S.J. Introduction to luminescence. In : *The Fundamentals and Applications of Light-Emitting Diodes*. Woodhead Publishing, 2021. p. 3–33. ISBN 978-0-12-819605-2.
6. ALEKSANDROVA, Mariya. *Specifics and Challenges to Flexible Organic Light-Emitting Devices*. 2016. Hindawi Limited.
7. GREENIE POLSKA. The advantages and disadvantages of LED lighting | Greenie-world.com. [online]. 2018. [Accessed 17 February 2022]. Available from: https://greenie-world.com/en/article/the-advantages-and-disadvantages-of-led-lighting/
8. JUAN, Chang Jung and TSAI, Ming Jong. Implementation of a novel system for measuring the lifetime of OLED panels. *IEEE Transactions on Consumer Electronics*. February 2003. Vol. 49, no. 1, p. 1–5. DOI 10.1109/TCE.2003.1205448.
9. HONG, Gloria, GAN, Xuemin, LEONHARDT, Céline, ZHANG, Zhen, SEIBERT, Jasmin, BUSCH, Jasmin M. and BRÄSE, Stefan. *A Brief History of OLEDs—Emitter Development and Industry Milestones* [online]. 1 March 2021. Wiley-VCH Verlag. [Accessed 18 February 2022]. Available from: https://www.researchgate.net/publication/348573850_A_Brief_History_of_OLEDs-Emitter_Development_and_Industry_Milestones
10. SANDANAYAKA, Atula S.D., MATSUSHIMA, Toshinori and ADACHI, Chihaya. Degradation Mechanisms of Organic Light-Emitting Diodes Based on Thermally Activated Delayed Fluorescence Molecules. *Journal of Physical Chemistry C* [online]. 2 October 2015. Vol. 119, no. 42, p. 23845–23851. [Accessed 18 February 2022]. DOI 10.1021/acs.jpcc.5b07084. Available from: https://www.researchgate.net/publication/282584107_Degradation_Mechanisms_of_Organic_Light-Emitting_Diodes_Based_on_Thermally_Activated_Delayed_Fluorescence_Molecules
11. PlayStation VR | Live the game with the PS VR headset | PlayStation. [online]. [Accessed 18 February 2022]. Available from: https://www.playstation.com/en-us/ps-vr/
12. VAN DE WEIJER, Peter, LU, Kangbo, JANSSEN, Richard R., DE WINTER, Suzanne H.P.M. and AKKERMAN, Hylke B. Mechanism of the operational effect of black spot growth in OLEDs. *Organic Electronics*. 1 October 2016. Vol. 37, p. 155–162. DOI 10.1016/j.orgel.2016.05.037.
13. BEN, Goncalves. *OLED Advantages and Disadvantages* [online]. 2015.

[Accessed 3 January 2021]. Available from: https://electronics.howstuffworks.com/oled5.htm
14. BAGHER, Askari Mohammad. Quantum Dot Display Technology and Comparison with OLED Display Technology. *International Journal of Advanced Research in Physical Science* [online]. 2017. Vol. 4, no. 1, p. 48–53. [Accessed 3 January 2021]. Available from: www.arcjournals.org
15. GHASEMI, Melika. *MAIN Melika-Ghasemi-Semester Project Report*. 2021. Kaunas.
16. OLED Screen Degradation Information – Cirrus Research Support. [online]. [Accessed 18 February 2022]. Available from: https://cirrusresearch.com/support/knowledge-base/knowledge-centre/optimus-and-optimus/oled-display-information/
17. CAI, Min. Organic Light-Emitting Diodes (OLEDs) and Optically-Detected Magnetic Resonance (ODMR) studies on organic materials. [online]. 2011. P. 134. [Accessed 18 February 2022]. DOI 10.31274/ETD-180810-2185. Available from: https://lib.dr.iastate.edu/etd/10388/
18. KULKARNI, Abhishek P., TONZOLA, Christopher J., BABEL, Amit and JENEKHE, Samson A. *Electron transport materials for organic light-emitting diodes*. 16 November 2004.
19. LED, Brilliance. Artificial Light Sources | History And Evolution Of Artificial Light. [online]. [Accessed 12 April 2022]. Available from: https://www.brillianceled.com/artificial-light-sources-a-history
20. HART, Jeffrey a, LENWAY, Stefanie Ann and MURTHA, Thomas. A History of Electroluminescent Displays. *academia.edu* [online]. 1999. P. 1–21. [Accessed 1 March 2022]. Available from: https://www.academia.edu/download/8455135/elds.pdf
21. CHOUDHURY, Asim Kumar Roy. Characteristics of light sources. In : *Principles of Colour and Appearance Measurement*. Woodhead Publishing, 2014. p. 1–52. ISBN 978-0-85709-229-8.
22. WITHNALL, Robert, SILVER, Jack, HARRIS, Paul G., IRELAND, Terry G. and MARSH, Paul J. AC powder electroluminescent displays. *Journal of the Society for Information Display*. 2011. Vol. 19, no. 11, p. 798. DOI 10.1889/jsid19.11.798.
23. KANAMARU, Kuniaki and UTSUNOMIYA, Hiroshi. In-situ observation of nonuniform deformation during tensile test of aluminum alloy sheet by means of screen-printed mechanoluminescence film. *Scripta Materialia*. 1 March 2022. Vol. 209, p. 114388. DOI 10.1016/j.scriptamat.2021.114388.
24. WANG, Wenxiang, WANG, Zhen Bin, ZHANG, Jiachi, ZHOU, Jinyu, DONG, Wenbo and WANG, Yuhua. Contact electrification induced mechanoluminescence. *Nano Energy*. 1 April 2022. Vol. 94, p. 106920. DOI 10.1016/j.nanoen.2022.106920.
25. SHEN, Wenkai, XING, Chang, LIU, Li, HU, Qiming, WU, Guohua, YANG, Yujia, WU, Shaohua, QIU, Penghua and WU, Jiangquan. Chemiluminescence-based characterization of heat release rate dynamic in a micro gas turbine combustion chamber. *Journal of the Energy Institute*. 1 June 2022. Vol. 102, p. 32–41. DOI 10.1016/j.joei.2022.01.006.
26. SU, Wenming. Printed Organic Light Emission and Display. In : *Printed Electronics* [online]. John Wiley & Sons, Ltd, 2016. p. 251–286. [Accessed 10 May 2022]. Available from: https://onlinelibrary.wiley.com/doi/full/10.1002/9781118920954.ch7
27. History of (EL) Electroluminescence | LightTapeUK. [online]. [Accessed 1 March 2022]. Available from: https://www.lighttape.co.uk/info/history-of-el/
28. Chapter 7 Current phosphor device technology. In : *Studies in Inorganic Chemistry*. Elsevier, 2004. p. 615–702.
29. PENG, Huisheng, SUN, Xuemei, WENG, Wei and FANG, Xin. Light Emitting Based on Polymer. In : *Polymer Materials for Energy and Electronic Applications*. Academic Press, 2017. p. 243–285. ISBN 978-0-12-811091-1.
30. LESKELÄ, Markku, LI, Wei Min, RITALA, Mikko and RAHMAN, Abu Zayed Mohammad Saliqur. Electroluminescent Phosphors. In : *Reference Module in Materials Science and Materials Engineering*. Elsevier, 2018.

31. GUENTHER, Bob D. and STEEL, Duncan G. *Encyclopedia of modern optics*. 2018. ISBN 9780128149829.
32. KRASNOV, Alexey N. Electroluminescent displays: History and lessons learned. *Displays*. 1 August 2003. Vol. 24, no. 2, p. 73–79. DOI 10.1016/S0141-9382(03)00015-5.
33. HELLERICH, Emily S. *Studies of solution-processed organic light-emitting diodes and their materials* [online]. Ames : Iowa State University, Digital Repository, 2013. [Accessed 18 April 2022]. Available from: https://lib.dr.iastate.edu/etd/13552/
34. LIN, Y. J., SU, Y. K. and YOKOYAMA, M. Crystallinity of ZnS: Tb,F thin films on green thin film electroluminescent devices prepared by RF-magnetron sputtering. *Applied Surface Science*. 2 March 1993. Vol. 65–66, no. C, p. 461–464. DOI 10.1016/0169-4332(93)90702-D.
35. POPE, M., KALLMANN, H. P. and MAGNANTE, P. *Electroluminescence in organic crystals [16]* [online]. 20 July 1963. American Institute of PhysicsAIP. [Accessed 1 March 2022]. Available from: https://aip.scitation.org/doi/abs/10.1063/1.1733929
36. TANG, C. W. and VANSLYKE, S. A. Organic electroluminescent diodes. *Applied Physics Letters* [online]. 4 June 1987. Vol. 51, no. 12, p. 913–915. [Accessed 1 March 2022]. DOI 10.1063/1.98799. Available from: https://aip.scitation.org/doi/abs/10.1063/1.98799
37. PARK, J. W., SHIN, D. C. and PARK, S. H. Large-area OLED lightings and their applications. *Semiconductor Science and Technology* [online]. 14 February 2011. Vol. 26, no. 3, p. 034002. [Accessed 23 March 2022]. DOI 10.1088/0268-1242/26/3/034002. Available from: https://iopscience.iop.org/article/10.1088/0268-1242/26/3/034002
38. MISRA, Aparna, KUMAR, Pankaj, KAMALASANAN, M. N. and CHANDRA, Subhas. *White organic LEDs and their recent advancements*. 1 July 2006.
39. REINEKE, Sebastian, THOMSCHKE, Michael, LÜSSEM, Björn and LEO, Karl. White organic light-emitting diodes: Status and perspective. *Reviews of Modern Physics* [online]. 30 July 2013. Vol. 85, no. 3, p. 1245–1293. [Accessed 14 April 2022]. DOI 10.1103/RevModPhys.85.1245. Available from: https://journals.aps.org/rmp/abstract/10.1103/RevModPhys.85.1245
40. SAMUEL, Ifor D.W. and TURNBULL, Graham A. *Organic semiconductor lasers* [online]. April 2007. American Chemical Society. [Accessed 28 April 2022]. Available from: https://pubs.acs.org/doi/full/10.1021/cr050152i
41. GIOVANELLA, Umberto, PASINI, Mariacecilia and BOTTA, Chiara. Organic Light-Emitting Diodes (OLEDs): Working Principles and Device Technology. In : . 2016. p. 145–196.
42. SUGIMOTO, Akira, OCHI, Hideo, FUJIMURA, Soh, YOSHIDA, Ayako, MIYADERA, Toshiyuki and TSUCHIDA, Masami. Flexible OLED displays using plastic substrates. *IEEE Journal on Selected Topics in Quantum Electronics*. January 2004. Vol. 10, no. 1, p. 107–114. DOI 10.1109/JSTQE.2004.824112.
43. MURAWSKI, Caroline, LEO, Karl and GATHER, Malte C. *Efficiency roll-off in organic light-emitting diodes* [online]. 1 December 2013. John Wiley & Sons, Ltd. [Accessed 21 April 2022]. Available from: https://onlinelibrary.wiley.com/doi/full/10.1002/adma.201301603
44. WATKINS, Scott and EVANS, Drew. Polymers: from DNA to rubber ducks. *Australian Academy of Science* [online]. 2020. [Accessed 11 May 2022]. Available from: https://www.science.org.au/curious/everything-else/polymers
45. THIYAGARAJAN, Manojkumar Dhanthala, BALIJAPALLI, Umamahesh, LEITONAS, Karolis, VOLYNIUK, Dmytro, SIMOKAITIENE, Jurate, KERUCKAS, Jonas, JATAUTIENĖ, Eglė, PATHAK, Madhvesh, IYER, Sathiyanarayanan Kulathu and GRAŽULEVIČIUS, Juozas Vidas. Human-eyes-friendly white electroluminescence from solution-processable hybrid OLEDs exploiting new iridium (III) complex containing benzoimidazophenanthridine ligand. *Dyes and Pigments*. 1 March 2020. Vol. 174. DOI 10.1016/j.dyepig.2019.108068.
46. QIAN, Yan, ZHANG, Xinwen, XIE, Linghai, QI, Dianpeng, CHANDRAN, Bevita K., CHEN,

Xiaodong and HUANG, Wei. Stretchable Organic Semiconductor Devices. *Advanced Materials* [online]. 1 November 2016. Vol. 28, no. 42, p. 9243–9265. [Accessed 11 May 2022]. DOI 10.1002/adma.201601278. Available from: https://onlinelibrary.wiley.com/doi/full/10.1002/adma.201601278

47. 9.18: Sigma and Pi Bonds - Chemistry LibreTexts. [online]. [Accessed 12 May 2022]. Available from: https://chem.libretexts.org/Bookshelves/Introductory_Chemistry/Introductory_Chemistry_(CK-12)/09%3A_Covalent_Bonding/9.18%3A_Sigma_and_Pi_Bonds
48. FLOWERS, PAUL, THEOPOLD, KLAUS and LANGLEY, RICHARD. *Chemistry 2e* [online]. 2002. [Accessed 12 May 2022]. ISBN 9781947172623. Available from: https://www.amazon.com/Chemistry-2e-Paul-Flowers-ebook-dp-B07T3FXQVS/dp/B07T3FXQVS/ref=mt_other?_encoding=UTF8&me=&qid=
49. THIYAGARAJAN, Manojkumar Dhanthala, BALIJAPALLI, Umamahesh, LEITONAS, Karolis, VOLYNIUK, Dmytro, SIMOKAITIENE, Jurate, KERUCKAS, Jonas, JATAUTIENĖ, Eglė, PATHAK, Madhvesh, IYER, Sathiyanarayanan Kulathu and GRAŽULEVIČIUS, Juozas Vidas. Human-eyes-friendly white electroluminescence from solution-processable hybrid OLEDs exploiting new iridium (III) complex containing benzoimidazophenanthridine ligand. *Dyes and Pigments*. 1 March 2020. Vol. 174, p. 108068. DOI 10.1016/j.dyepig.2019.108068.
50. ZIMMERMAN, James. Physical chemistry for the biosciences: Chang, Raymond. *Biochemistry and Molecular Biology Education*. 2005. Vol. 33, no. 5, p. 382–382. DOI 10.1002/bmb.2005.49403305383.
51. CLEAN ENERGY WIKI. The Polyene Series - CleanEnergyWIKI. [online]. 2011. [Accessed 13 May 2022]. Available from: http://cleanenergywiki.org/index.php?title=The_Polyene_Series
52. PLASSER, Felix. Chemical Quantum Images: - Molecular Graphics and Theoretical Chemistry -. [online]. 2013. [Accessed 13 May 2022]. Available from: http://chemical-quantum-images.blogspot.com/2013/04/band-gaps.html
53. CHOUDHURY, Bhaskar. *Organic light emitting devices (OLEDs) and Structurally integrated photoluminescence based chemical and biological sensors excited by OLEDs* [online]. Ames : Iowa State University, Digital Repository, 2005. [Accessed 15 May 2022]. Available from: https://lib.dr.iastate.edu/rtd/1723/
54. MANNA, Eeshita. *Enhanced light out-coupling of organic light emitting devices (OLEDs) using novel plastic substrates and improved performance of OLED-based photoluminescence sensing platform* [online]. Ames : Iowa State University, Digital Repository, 2017. [Accessed 15 May 2022]. Available from: https://lib.dr.iastate.edu/etd/15360/
55. LASSITER, Brian E. Tandem Organic Photovoltaics. [online]. 2013. [Accessed 15 May 2022]. Available from: https://www.researchgate.net/publication/295276580_Tandem_Organic_Photovoltaics/figures?lo=1
56. DEEN, M. Jamal. Organic Semiconductor Devices. In : *Wiley Encyclopedia of Electrical and Electronics Engineering*. John Wiley & Sons, Inc., 2014. p. 1–16.
57. SCHALLER, Chris P. 14.7: Fluorescence and Phosphorescence - Chemistry LibreTexts. *Chem LibreTexts* [online]. 2019. [Accessed 16 May 2022]. Available from: https://chem.libretexts.org/Bookshelves/Physical_and_Theoretical_Chemistry_Textbook_Maps/Map%3A_Physical_Chemistry_for_the_Biosciences_(Chang)/14%3A_Spectroscopy/14.7%3A_Fluorescence_and_Phosphorescence
58. VOLZ, Daniel, BAUMANN, Thomas, WALLESCH, Manuela and BRÄSE, Stefan. Late bloomers: copper complexes in organic LEDs. *SPIE Newsroom* [online]. 2014. [Accessed 31 December 2020]. DOI 10.1117/2.1201409.005617. Available from: https://www.researchgate.net/figure/Triplet-harvesting-and-singlet-harvesting-In-an-organic-LED-OLED-electrical-energy-is_fig1_267210174

59. YERSIN, Hartmut, RAUSCH, Andreas F., CZERWIENIEC, Rafał, HOFBECK, Thomas and FISCHER, Tobias. The triplet state of organo-transition metal compounds. Triplet harvesting and singlet harvesting for efficient OLEDs. *Coordination Chemistry Reviews*. 1 November 2011. Vol. 255, no. 21–22, p. 2622–2652. DOI 10.1016/j.ccr.2011.01.042.
60. EDINBURGH INSTRUMENTS. Jablonski Diagram | What is it? | Edinburgh Instruments. *Our Blog, Edinburgh Instruments* [online]. 2021. [Accessed 16 May 2022]. Available from: https://www.edinst.com/ko/blog/jablonski-diagram/
61. QUARANTA, Michela, BORISOV, Sergey M. and KLIMANT, Ingo. Indicators for optical oxygen sensors. *Bioanalytical Reviews* [online]. 1 December 2012. Vol. 4, no. 2–4, p. 115–157. [Accessed 16 May 2022]. DOI 10.1007/s12566-012-0032-y. Available from: https://pubmed.ncbi.nlm.nih.gov/23227132/
62. BALDO, M. A., ADACHI, C. and FORREST, S. R. Transient analysis of organic electrophosphorescence. II. Transient analysis of triplet-triplet annihilation. *Physical Review B - Condensed Matter and Materials Physics* [online]. 15 October 2000. Vol. 62, no. 16, p. 10967–10977. [Accessed 21 April 2022]. DOI 10.1103/PhysRevB.62.10967. Available from: https://journals.aps.org/prb/abstract/10.1103/PhysRevB.62.10967
63. Measuring Fluorescence and Phosphorescence Spectra | FLS1000. [online]. [Accessed 4 January 2022]. Available from: https://www.edinst.com/measuring-fluorescence-and-phosphorescence-spectra-at-low-temperature-using-the-fls1000-photoluminescence-spectrometer/
64. GODUMALA, Mallesham, CHOI, Suna, CHO, Min Ju and CHOI, Dong Hoon. Thermally activated delayed fluorescence blue dopants and hosts: from the design strategy to organic light-emitting diode applications. *Journal of Materials Chemistry C* [online]. 8 December 2016. Vol. 4, no. 48, p. 11355–11381. [Accessed 4 January 2022]. DOI 10.1039/C6TC04377A. Available from: https://pubs.rsc.org/en/content/articlehtml/2016/tc/c6tc04377a
65. GUPTA, Indarchand, INGLE, Avinash, PARALIKAR, Priti, PANDIT, Raksha, DA SILVA, Silvio Silvério and RAI, Mahendra. Bio-distribution and toxicity of noble metal nanoparticles in humans. In : *Metal Nanoparticles in Pharma* [online]. Springer, Cham, 2017. p. 469–482. [Accessed 30 September 2021]. ISBN 9783319637907. Available from: https://link.springer.com/chapter/10.1007/978-3-319-63790-7_21
66. FENG, Hai Tao, ZENG, Jiajie, YIN, Ping An, WANG, Xue Dong, PENG, Qian, ZHAO, Zujin, LAM, Jacky W.Y. and TANG, Ben Zhong. Tuning molecular emission of organic emitters from fluorescence to phosphorescence through push-pull electronic effects. *Nature Communications* [online]. 26 May 2020. Vol. 11, no. 1, p. 1–9. [Accessed 1 October 2021]. DOI 10.1038/s41467-020-16412-4. Available from: https://www.nature.com/articles/s41467-020-16412-4
67. ZHANG, Guoqing, PALMER, Gregory M., DEWHIRST, Mark W. and FRASER, Cassandra L. A dual-emissive-materials design concept enables tumour hypoxia imaging. *Nature Materials* [online]. 2009. Vol. 8, no. 9, p. 747–751. [Accessed 16 May 2022]. DOI 10.1038/nmat2509. Available from: https://pubmed.ncbi.nlm.nih.gov/19668206/
68. GODUMALA, Mallesham, CHOI, Suna, CHO, Min Ju and CHOI, Dong Hoon. *Thermally activated delayed fluorescence blue dopants and hosts: from the design strategy to organic light-emitting diode applications* [online]. 8 December 2016. The Royal Society of Chemistry. [Accessed 4 January 2022]. Available from: https://pubs.rsc.org/en/content/articlehtml/2016/tc/c6tc04377a
69. TOMKEVICIENE, Ausra, DABULIENĖ, Asta, MATULAITIS, Tomas, GUZAUSKAS, Matas, ANDRULEVICIENE, Viktorija, GRAZULEVICIUS, Juozas Vidas, YAMANAKA, Yuri, YANO, Yoshio and ONO, Toshikazu. Bipolar thianthrene derivatives exhibiting room temperature phosphorescence for oxygen sensing. *Dyes and Pigments*. 1 November 2019. Vol. 170, p. 107605. DOI 10.1016/j.dyepig.2019.107605.
70. YAO, Jingwen, XIAO, Shu, ZHANG, Shuai, SUN, Qian, DAI, Yanfeng, QIAO, Xianfeng,

YANG, Dezhi, CHEN, Jiangshan and MA, Dongge. High efficiency, low efficiency roll-off and long lifetime fluorescent white organic light-emitting diodes based on strategic management of triplet excitons: via triplet-triplet annihilation up-conversion and phosphor sensitization. *Journal of Materials Chemistry C* [online]. 8 May 2020. Vol. 8, no. 24, p. 8077–8084. [Accessed 9 May 2022]. DOI 10.1039/d0tc01622e. Available from: https://pubs.rsc.org/en/content/articlehtml/2020/tc/d0tc01622e

71. UOYAMA, Hiroki, GOUSHI, Kenichi, SHIZU, Katsuyuki, NOMURA, Hiroko and ADACHI, Chihaya. Highly efficient organic light-emitting diodes from delayed fluorescence. *Nature* [online]. 12 December 2012. Vol. 492, no. 7428, p. 234–238. [Accessed 30 September 2021]. DOI 10.1038/nature11687. Available from: https://www.nature.com/articles/nature11687
72. BAN, Xinxin, LIU, Yan, PAN, Jie, CHEN, Feng, ZHU, Aiyun, JIANG, Wei, SUN, Yueming and DONG, Yajie. Blocking exciton-quenching pathways in host and guest interfaces for high performance solution-processed TADF OLEDs with external quantum efficiency approaching 25%. *Organic Electronics*. 1 May 2020. Vol. 80, p. 105601. DOI 10.1016/j.orgel.2019.105601.
73. REGNAT, Markus, PERNSTICH, Kurt P. and RUHSTALLER, Beat. Influence of the bias-dependent emission zone on exciton quenching and OLED efficiency. *Organic Electronics*. 1 July 2019. Vol. 70, p. 219–226. DOI 10.1016/j.orgel.2019.04.027.
74. SHENG, Ren, YANG, Liping, LI, Asu, CHEN, Keming, ZHANG, Fujun, DUAN, Yu, ZHAO, Yi and CHEN, Ping. Highly efficient orange and white OLEDs based on ultrathin phosphorescent emitters with double reverse intersystem crossing system. *Journal of Luminescence*. 1 June 2022. Vol. 246, p. 118852. DOI 10.1016/j.jlumin.2022.118852.
75. LIN, Zesen, KABE, Ryota, NISHIMURA, Naohiro, JINNAI, Kazuya and ADACHI, Chihaya. Organic Long-Persistent Luminescence from a Flexible and Transparent Doped Polymer. *Advanced Materials* [online]. 1 November 2018. Vol. 30, no. 45, p. 1803713. [Accessed 21 October 2021]. DOI 10.1002/ADMA.201803713. Available from: https://onlinelibrary.wiley.com/doi/full/10.1002/adma.201803713
76. KABE, Ryota and ADACHI, Chihaya. Organic long persistent luminescence. *Nature 2017 550:7676* [online]. 2 October 2017. Vol. 550, no. 7676, p. 384–387. [Accessed 21 October 2021]. DOI 10.1038/nature24010. Available from: https://www.nature.com/articles/nature24010
77. DEEN, M. Jamal. Organic Semiconductor Devices. In : *Wiley Encyclopedia of Electrical and Electronics Engineering* [online]. John Wiley & Sons, Ltd, 2014. p. 1–16. [Accessed 11 May 2022]. Available from: https://onlinelibrary.wiley.com/doi/full/10.1002/047134608X.W3160.pub2
78. KAWABATA, Tokihisa and OHNO, Yoshi. Optical measurements of OLED panels for lighting applications. *Journal of Modern Optics* [online]. 1 August 2013. Vol. 60, no. 14, p. 1176–1186. [Accessed 2 May 2022]. DOI 10.1080/09500340.2013.806681. Available from: https://www.tandfonline.com/doi/abs/10.1080/09500340.2013.806681
79. CRAWFORD, Gregory Philip. *Flexible Flat Panel Displays*. John Wiley & Sons, 2005. ISBN 9780470870488.
80. YAHYA, M. and FADAVIESLAM, M. R. The effects of argon plasma treatment on ITO properties and the performance of OLED devices. *Optical Materials*. 1 October 2021. Vol. 120, p. 111400. DOI 10.1016/j.optmat.2021.111400.
81. SOMAN, Anjaly, M, Manuraj and UNNI, K. N.Narayanan. Addressing the efficiency roll-off in a fluorescent OLED by facile electron transport layer doping and carrier confinement. *Optical Materials*. 1 May 2018. Vol. 79, p. 413–419. DOI 10.1016/j.optmat.2018.03.053.
82. TSAO, Jeff Y. Light Emitting Diodes (LEDs) for General Illumination Roadmap. *Agenda* [online]. 2002. P. 112. [Accessed 18 April 2022]. Available from: https://www.researchgate.net/publication/237013114_Light_Emitting_Diodes_LEDs_for_General_Illumination-An_OIDA_Technology_Roadmap_Update
83. GHOSH, A. P., GERENSER, L. J., JARMAN, C. M. and FORNALIK, J. E. Thin-film

encapsulation of organic light-emitting devices. *Applied Physics Letters* [online]. 24 May 2005. Vol. 86, no. 22, p. 1–3. [Accessed 30 March 2022]. DOI 10.1063/1.1929867. Available from: https://aip.scitation.org/doi/abs/10.1063/1.1929867

84. VISSENBERG, M. C.J.M. and DE JONG, M. Theory of electric-field-induced photoluminescence quenching in disordered molecular solids. *Physical Review B - Condensed Matter and Materials Physics* [online]. 1 February 1998. Vol. 57, no. 5, p. 2667–2670. [Accessed 12 April 2022]. DOI 10.1103/PhysRevB.57.2667. Available from: https://journals.aps.org/prb/abstract/10.1103/PhysRevB.57.2667
85. INSTRUMENTS, Edinburgh, POSTS, Blog, ACTIVATED, Thermally and FLUORESCENCE, Delayed. TADF: What is Thermally Activated Delayed Fluorescence? - Physics World Buyers Guide. *IOP Publishing* [online]. 2018. P. 1–8. [Accessed 3 January 2021]. Available from: https://www.edinst.com/blog/tadf-thermally-activated-delayed-fluorescence/
86. SØNDERGAARD, Roar R., HÖSEL, Markus and KREBS, Frederik C. *Roll-to-Roll fabrication of large area functional organic materials* [online]. 1 January 2013. John Wiley & Sons, Ltd. [Accessed 10 May 2022]. Available from: https://onlinelibrary.wiley.com/doi/full/10.1002/polb.23192
87. KODEN, Mitsuhiro. OLED Fabrication Process. In : *OLED Displays and Lighting* [online]. John Wiley & Sons, Ltd, 2017. p. 103–116. [Accessed 9 May 2022]. Available from: https://onlinelibrary.wiley.com/doi/full/10.1002/9781119040477.ch6
88. YILBAS, Bekir Sami, AL-SHARAFI, Abdullah and ALI, Haider. Surfaces for Self-Cleaning. In : *Self-Cleaning of Surfaces and Water Droplet Mobility*. Elsevier, 2019. p. 45–98. ISBN 978-0-12-814776-4.
89. MISHRA, Abhilasha, BHATT, Neha and BAJPAI, A. K. Nanostructured superhydrophobic coatings for solar panel applications. In : *Nanomaterials-Based Coatings: Fundamentals and Applications*. Elsevier, 2019. p. 397–42. ISBN 9780128158845.
90. ZHANG, John X.J. and HOSHINO, Kazunori. Fundamentals of nano/microfabrication and scale effect. In : *Molecular Sensors and Nanodevices*. Academic Press, 2019. p. 43–111. ISBN 978-0-12-814862-4.
91. TSUJIMURA, Takatoshi. OLED Manufacturing Process. In : *OLED Displays* [online]. John Wiley & Sons, Ltd, 2012. p. 37–67. [Accessed 10 May 2022]. Available from: https://onlinelibrary.wiley.com/doi/full/10.1002/9781118173053.ch3
92. ANDERSSON, T. G., ANDREASSON, M., KLEMENT, U., LEE, C. B., PUJILAKSONO, B. and UDDIN, A. Preparation and characterization of the ITO surface and the Al/Alq3/ITO heterostructure for OLEDs. *Materials Science and Engineering B: Solid-State Materials for Advanced Technology*. 20 December 2007. Vol. 145, no. 1–3, p. 48–56. DOI 10.1016/j.mseb.2007.09.090.
93. JUNG, Sun Gyu, CHOI, Kyung Bok, PARK, Chan Hyuk, SHIM, Yong Sub, PARK, Cheol Hwee, PARK, Young Wook and JU, Byeong Kwon. Effects of Cl2 plasma treatment on stability, wettability, and electrical properties of ITO for OLEDs. *Optical Materials*. 1 July 2019. Vol. 93, p. 51–57. DOI 10.1016/j.optmat.2019.04.056.
94. DOS-SANTOS, PALOMA, LAYS. The Study of Thermally Activated Delayed Fluorescence Mechanism in Mono and Bimolecular Systems. *Thesis* [online]. 2018. [Accessed 12 April 2022]. Available from: https://www.semanticscholar.org/paper/The-study-of-thermally-activated-delayed-mechanism-Dos-Santos/efcd70c7f7581a348fd777b84cff6906dcbd48e5
95. WANG, X. J., ZHAO, J. M., ZHOU, Y. C., WANG, X. Z., ZHANG, S. T., ZHAN, Y. Q., XU, Z., DING, H. J., ZHONG, G. Y., SHI, H. Z., XIONG, Z. H., LIU, Y., WANG, Z. J., OBBARD, E. G., DING, X. M., HUANG, W. and HOU, X. Y. Enhancement of electron injection in organic light-emitting devices using an Ag/LiF cathode. *Journal of Applied Physics* [online]. 18 March 2004. Vol. 95, no. 7, p. 3828–3830. [Accessed 12 April 2022]. DOI 10.1063/1.1655676. Available from: https://aip.scitation.org/doi/abs/10.1063/1.1655676

96. DANIEL, DE SA PEREIRA, PRZEMYSLAW, DATA and MONKMAN, Andrew P. Methods of Analysis of Organic Light Emitting Diodes. *Display and Imaging* [online]. 15 November 2017. Vol. 2, no. May, p. 323–337. [Accessed 18 April 2022]. DOI 10.5281/ZENODO.3543463. Available from: https://zenodo.org/record/3543463
97. KUMAR, Brijesh, KAUSHIK, Brajesh Kumar and NEGI, Y. S. *Perspectives and challenges for organic thin film transistors: Materials, devices, processes and applications*. January 2014.
98. SCHLAF, R., PARKINSON, B. A., LEE, P. A., NEBESNY, K. W., JABBOUR, G., KIPPELEN, B., PEYGHAMBARIAN, N. and ARMSTRONG, N. R. Photoemission spectroscopy of LiF coated Al and Pt electrodes. *Journal of Applied Physics* [online]. 25 November 1998. Vol. 84, no. 12, p. 6729–6736. [Accessed 1 May 2022]. DOI 10.1063/1.369000. Available from: https://aip.scitation.org/doi/abs/10.1063/1.369000
99. LEITONAS, Karolis. *Developing of white hybrid organic light-emitting devices by solution-processing utilizing novel iridium (III) complexes: magistro darbas*. book. 2020. Kaunas : Kauno technologijos universitetas. Prieiga per eLABa – nacionalinė Lietuvos akademinė elektroninė biblioteka.
100. YOUNG, Ralph H., TANG, Ching W. and MARCHETTI, Alfred P. Current-induced fluorescence quenching in organic light-emitting diodes. *Applied Physics Letters* [online]. 30 January 2002. Vol. 80, no. 5, p. 874–876. [Accessed 28 April 2022]. DOI 10.1063/1.1445271. Available from: https://aip.scitation.org/doi/abs/10.1063/1.1445271
101. FAGNONI, Maurizio. Modern Molecular Photochemistry of Organic Molecules. By Nicholas J. Turro, V. Ramamurthy and Juan C. Scaiano. *Angewandte Chemie International Edition* [online]. 10 September 2010. Vol. 49, no. 38, p. 6709–6710. [Accessed 21 April 2022]. DOI 10.1002/anie.201003826. Available from: https://onlinelibrary.wiley.com/doi/full/10.1002/anie.201003826
102. BRITANNICA. Luminous intensity | physics | Britannica. [online]. 2020. [Accessed 1 May 2022]. Available from: https://www.britannica.com/science/luminous-intensity
103. COEHOORN, R., ZHANG, L., BOBBERT, P. A. and VAN EERSEL, H. Effect of polaron diffusion on exciton-polaron quenching in disordered organic semiconductors. *Physical Review B* [online]. 6 April 2017. Vol. 95, no. 13, p. 134202. [Accessed 9 May 2022]. DOI 10.1103/PhysRevB.95.134202. Available from: https://journals.aps.org/prb/abstract/10.1103/PhysRevB.95.134202
104. PARET, Dominique and CRÉGO, Pierre. Components. In : *Wearables, Smart Textiles and Smart Apparel* [online]. Elsevier, 2019. p. 203–259. [Accessed 4 May 2022]. ISBN 978-1-78548-293-9. Available from: https://linkinghub.elsevier.com/retrieve/pii/B9781785482939500131
105. GARCIA-BREIJO, Eduardo, PÉREZ, Berta Gómez Lor and COSSEDDU, Piero. *Organic Sensors: Materials and applications*. London : The Institution of Engineering and Technology, 2016. ISBN 9781849199865.
106. Dr. Dalius Gudeika - Google Scholar. [online]. [Accessed 9 February 2022]. Available from: https://scholar.google.ca/citations?user=PK44G5UAAAAJ&hl=en
107. GHASEMI, Melika, MAHMOUDI, Malek, GUDEIKA, Dalius, LIETONA, Karolis, SIMOKAITIENE, Jurate, DABULIENĖ, Asta, PANCHENKO, Alexander, MINAEV, Boris F., VOLYNIUK, Dmytro and GRAZULEVICIUS, Juozas Vidas. Isomerization dependent room-temperature phosphorescence, thermally activated delayed fluorescence and long persistent luminescence of organic hole-transporting materials with the selective potential for the application in electronic devices and optical s. . 2022. P. 36.
108. ZHOU, Yang, LI, Xinyao, HOU, Shili and XU, Jiaxi. Facile synthesis of dihydrochalcones via the AlCl 3-promoted tandem Friedel-Crafts acylation and alkylation of arenes with 2-alkenoyl chlorides. *Journal of Molecular Catalysis A: Chemical*. 1 December 2012. Vol. 365, p. 203–211. DOI 10.1016/j.molcata.2012.09.005.
109. MIYAURA, Norio, YAMADA, Kinji and SUZUKI, Akira. A new stereospecific cross-

coupling by the palladium-catalyzed reaction of 1-alkenylboranes with 1-alkenyl or 1-alkynyl halides. *Tetrahedron Letters*. 1 January 1979. Vol. 20, no. 36, p. 3437–3440. DOI 10.1016/S0040-4039(01)95429-2.
110. GHASEMI, Melika. *Semester Project 3 Research Article*. Kaunas, 2022.
111. TAPC for OLED Fabrication | CAS 58473-78-2 | Ossila. [online]. [Accessed 9 February 2022]. Available from: https://www.ossila.com/products/tapc
112. mCBP, 3,3′-Di(9H-carbazol-9-yl)-1,1′-biphenyl | 342638-54-4 | Ossila. [online]. [Accessed 9 February 2022]. Available from: https://www.ossila.com/products/mcbp?_pos=1&_sid=95ac497aa&_ss=r
113. Ir(ppy)3, Tris[2-phenylpyridine]iridium | 94928-86-6 | Ossila. [online]. [Accessed 9 February 2022]. Available from: https://www.ossila.com/products/irppy3?_pos=1&_sid=1b75075cd&_ss=r
114. TSPO1 | Sublimed >99% Purity, CAS 1286708-86-8 | Ossila. [online]. [Accessed 9 February 2022]. Available from: https://www.ossila.com/products/tspo1
115. TPBi, Suitable for OLED Devices | CAS 192198-85-9 | Ossila. [online]. [Accessed 9 February 2022]. Available from: https://www.ossila.com/products/tpbi?_pos=1&_sid=be2c23af5&_ss=r
116. Molybdic acid, MoO3 85% min, Thermo Scientific™ 100g Molybdic acid, MoO3 85% min, Thermo Scientific™ | Fisher Scientific. [online]. [Accessed 9 February 2022]. Available from: https://www.fishersci.no/shop/products/molybdic-acid-moo3-85-min-1/11468813
117. SYCH, Galyna, VOLYNIUK, Dmytro, BEZVIKONNYI, Oleksandr, LYTVYN, Roman and GRAZULEVICIUS, Juozas V. Dual Interface Exciplex Emission of Quinoline and Carbazole Derivatives for Simplified Nondoped White OLEDs. *Journal of Physical Chemistry C* [online]. 31 January 2019. Vol. 123, no. 4, p. 2386–2397. [Accessed 3 January 2021]. DOI 10.1021/acs.jpcc.8b09908. Available from: https://pubs.acs.org/doi/abs/10.1021/acs.jpcc.8b09908
118. DUVENHAGE, Mart Mari, NTWAEABORWA, Martin, VISSER, Hendrik G., SWARTS, Pieter J., SWARTS, Jannie C. and SWART, Hendrik C. Determination of the optical band gap of Alq3 and its derivatives for the use in two-layer OLEDs. *Optical Materials*. 1 April 2015. Vol. 42, p. 193–198. DOI 10.1016/j.optmat.2015.01.008.
119. ARELLANO, U., WANG, J. A., TIMKO, M. T., CHEN, L. F., PAREDES CARRERA, S. P., ASOMOZA, M., GONZÁLEZ VARGAS, O. A. and LLANOS, M. E. Oxidative removal of dibenzothiophene in a biphasic system using sol-gel FeTiO2 catalysts and H2O2 promoted with acetic acid. *Fuel*. 15 June 2014. Vol. 126, p. 16–25. DOI 10.1016/j.fuel.2014.02.028.
120. TANAKA, Hiromitsu, TOKITO, Shizuo, TAGA, Yasunori and OKADA, Akane. Novel hole-transporting materials based on triphenylamine for organic electroluminescent devices. *Chemical Communications*. January 1996. No. 18, p. 2175–2176. DOI 10.1039/cc9960002175.
121. ANDRULEVICIENE, Viktorija, LEITONAS, Karolis, VOLYNIUK, Dmytro, SINI, Gjergji, GRAZULEVICIUS, Juozas Vidas and GETAUTIS, Vytautas. TADF versus TTA emission mechanisms in acridan and carbazole-substituted dibenzo[a,c]phenazines: Towards triplet harvesting emitters and hosts. *Chemical Engineering Journal*. August 2021. Vol. 417, p. 127902. DOI 10.1016/j.cej.2020.127902.
122. HIRATA, Shuzo and HIRATA, S. Recent Advances in Materials with Room-Temperature Phosphorescence: Photophysics for Triplet Exciton Stabilization. *Advanced Optical Materials*. September 2017. Vol. 5, no. 17, p. 1700116. DOI 10.1002/ADOM.201700116.
123. YAMAZAKI, Masahiro. Industrialization and application development of cyclo-olefin polymer. *Journal of Molecular Catalysis A: Chemical*. 2004. Vol. 213, no. 1, p. 81–87. DOI 10.1016/j.molcata.2003.10.058.
124. NISHIMURA, Naohiro, LIN, Zesen, JINNAI, Kazuya, KABE, Ryota and ADACHI, Chihaya. Many Exciplex Systems Exhibit Organic Long-Persistent Luminescence. *Advanced Functional Materials*. 2020. Vol. 30, no. 22. DOI 10.1002/adfm.202000795.

125. KABE, Ryota and ADACHI, Chihaya. Organic long persistent luminescence. *Nature* [online]. 2 October 2017. Vol. 550, no. 7676, p. 384–387. [Accessed 21 October 2021]. DOI 10.1038/nature24010. Available from: https://www.nature.com/articles/nature24010
126. SWORAKOWSKI, Juliusz. How accurate are energies of HOMO and LUMO levels in small-molecule organic semiconductors determined from cyclic voltammetry or optical spectrosco. *Synthetic Metals*. January 2018. Vol. 235, p. 125–130. DOI 10.1016/j.synthmet.2017.11.013.
127. TSUNG, K. K. and SO, S. K. Advantages of admittance spectroscopy over time-of-flight technique for studying dispersive charge transport in an organic semiconductor. *Journal of Applied Physics*. October 2009. Vol. 106, no. 8, p. 083710. DOI 10.1063/1.3251409.
128. TYUTNEV, Andrey P., SAENKO, Vladimir S., POZHIDAEV, Evgenii D. and KOLESNIKOV, Vladislav A. Verification of the dispersive charge transport in a hydrazone: polycarbonate molecularly doped polymer. *Journal of Physics Condensed Matter*. 2009. Vol. 21, no. 11. DOI 10.1088/0953-8984/21/11/115107.
129. HOFBECK, Thomas and YERSIN, Hartmut. The triplet state of fac-Ir(ppy)3. *Inorganic Chemistry*. October 2010. Vol. 49, no. 20, p. 9290–9299. DOI 10.1021/ic100872w.
130. ZHANG, Y. Q., ZHONG, G. Y. and CAO, X. A. Concentration quenching of electroluminescence in neat Ir (ppy)3 organic light-emitting diodes. *Journal of Applied Physics*. October 2010. Vol. 108, no. 8, p. 083107. DOI 10.1063/1.3504599.
131. VIPIN, C K, SHUKLA, Atul, RAJEEV, Kavya, HASAN, Monirul, LO, Shih Chun, NAMDAS, Ebinazar B, AJAYAGHOSH, Ayyappanpillai and UNNI, K. N.Narayanan. White Organic Light-Emitting Diodes from Single Emissive Layers: Combining Exciplex Emission with Electromer Emission. *Journal of Physical Chemistry C*. 2021. Vol. 125, no. 41, p. 22809–22816. DOI 10.1021/acs.jpcc.1c06323.
132. GIEBINK, N. C., D'ANDRADE, B. W., WEAVER, M. S., MACKENZIE, P. B., BROWN, J. J., THOMPSON, M. E. and FORREST, S. R. Intrinsic luminance loss in phosphorescent small-molecule organic light emitting devices due to bimolecular annihilation reactions. *Journal of Applied Physics*. 2008. Vol. 103, no. 4. DOI 10.1063/1.2884530.
133. LEE, Jaesang, JEONG, Changyeong, BATAGODA, Thilini, COBURN, Caleb, THOMPSON, Mark E. and FORREST, Stephen R. Hot excited state management for long-lived blue phosphorescent organic light-emitting diodes. *Nature Communications*. May 2017. Vol. 8, no. 1, p. 1–9. DOI 10.1038/ncomms15566.
134. TOMKEVICIENE, Ausra, MATULAITIS, Tomas, GUZAUSKAS, Matas, ANDRULEVICIENE, Viktorija, VOLYNIUK, Dmytro and GRAZULEVICIUS, Juozas Vidas. Thianthrene and acridan-substituted benzophenone or diphenylsulfone: Effect of triplet harvesting via TADF and phosphorescence on efficiency of all-organic OLEDS. *Organic Electronics*. July 2019. Vol. 70, p. 227–239. DOI 10.1016/j.orgel.2019.04.025.
135. KIM, Kwon Hyeon and KIM, Jang Joo. Origin and Control of Orientation of Phosphorescent and TADF Dyes for High-Efficiency OLEDs. *Advanced Materials*. October 2018. Vol. 30, no. 42, p. 1705600. DOI 10.1002/adma.201705600.
136. MINAEV, Boris F. Ab initio study of the ground state properties of molecular oxygen. *Spectrochimica Acta - Part A: Molecular and Biomolecular Spectroscopy*. April 2004. Vol. 60, no. 5, p. 1027–1041. DOI 10.1016/S1386-1425(03)00334-2.
137. (PDF) Quantum-chemical investigation of the mechanisms of the photosensitization, luminescence, and quenching of singlet1Δg oxygen in solutions | Boris Minaev - Academia.edu. .
138. BORISOV, Sergey M., ZENKL, Gunter and KLIMANT, Ingo. Phosphorescent platinum(II) and palladium(II) complexes with azatetrabenzoporphyrinss new-red laser diode-compatible indicators for optical oxygen sensing. *ACS Applied Materials and Interfaces*. February 2010. Vol. 2, no. 2, p. 366–374. DOI 10.1021/am900932z.